C-X BOND FORMATION WITH TRIDENTATE NACNAC BASED PYRIDINE-IMINE LIGANDS AND STUDY OF A TETRADENTATE DIIMINE REDOX NON-INNOCENT LIGAND

A Dissertation

Presented to the Faculty of the Graduate School

of Cornell University

In Partial Fulfillment of the Requirements for the Degree of

Doctor of Philosophy

by

Wesley Daniel Morris

August 2014

C-X BOND FORMATION WITH TRIDENTATE NACNAC BASED PYRIDINE-IMINE LIGANDS AND STUDY OF A TETRADENTATE DIIMINE REDOX NON-INNOCENT LIGAND

Wesley Daniel Morris, Ph. D.

Cornell University 2014

First row transition metals are attractive candidates for catalysis because they are much more abundant, cheaper, and less toxic than their 2nd and 3rd row congeners. Unfortunately, these first row metals typically promote one electron (radical) processes instead of the two electron transformations observed in oxidation/reduction and bond breaking/forming reactions. One way around this is to use redox non-innocent ligands that have the capacity to store electrons and then release them over the course of the catalytic cycle to limit the oxidation state changes that occur at the metal center. The goal of this work was to expand the scope of redox non-innocent ligands in development of new catalytic processes.

A tridentate ligand was synthesized that contained a 2-pyridine methylamine arm on a nacnac ligand backbone. Deprotonation at the methylene position formed a new redox non-innocent ligand that was stable only in the bis-reduced form chelated to Fe(II). The neutral ligand was prone to intramolecular cyclization via C-N bond formation to form a new pyrimidine ring structure while the monoanionic ligand was prone to reductive coupling with formation of a new carbon-carbon bond. This system showed a strong preference for maintaining a ferrous state of iron with C-C or C-N bond formation observed when the redox noninnocent ligand was in its neutral or mono-anionic form.

A tetradentate ligand was synthesized with diimine and ortho-phenylenediamine functionalities that could exist in 5 different oxidation states from neutral to tetraanionic, which should support group transfer reactivity. The ligand was installed on iron and manganese to form standard M^{+2} coordination compounds. The corresponding chromium compound showed a different electronic structure consistent with a reduced ligand. Remarkably, it was shown calculationally to have an S=1 ligand antiferromagnetically coupled to a high spin Cr^{2+} metal center. Cyclic voltammetric measurements exhibited two reversible one-electron ligand reductions as well as three quasi-reversible oxidations consistent with 1 metal based oxidation and two ligand based oxidations.

BIOGRAPHICAL SKETCH

Wesley grew up in Murrysville, Pennsylvania under the wonderful guidance of his parents, Peter and Carol Morris and older brother Christopher Morris. After graduating from Franklin Regional Senior High School in 2005 with an interest in pursuing further studies in a science and technology field unknown to him at the time. He choose to attend Virginia Polytechnic Institute and State University (Virginia Tech) because it would allow for study any scientific field that sparked his interest. Following freshman orientation, Wes decided he wanted to play Ultimate Frisbee and spend extra time studying Chemistry. Playing Frisbee with VT Burn he attended tournaments all over the east coast with favorites in Las Vegas, NV, Baton Rouge, LA, and Boone, NC.

Wes spent the summer of 2007 at Colorado State University exploring the mountains and working as an REU student with Amy Prieto on the synthesis of ternary phase change materials via chemical vapor deposition. The next summer he traveled to Livermore, CA to work with Ross Williams analyzing uranium and plutonium isotope ratios in bulk environmental samples. While an undergraduate at Virginia Tech, Wesley worked with Webster Santos on the organic synthesis of small molecules for cancer therapeutics. After graduation in May 2009 Wes headed to Ithaca, NY to study organometallic chemistry at Cornell University.

Upon arrival at Cornell University he quickly found that the Wolczanski group was a good match for his chemistry interests and love for beer. His graduate studies focused on the application of redox non-innocence to first row transition metals. In his first year, Wes met another graduate student named Anna Greenswag whom he has had the pleasure to get to know better since they started dating 4.5 years ago. After graduation, Wes will spend some time traveling in Australia before starting a postdoc studying proton couple electron transport with Jim Mayer at Yale University.

Dedicated to Mom and Dad whose unwavering love and support have made this work possible.

ACKNOWLEDGMENTS

First and foremost I would like to thank my advisor, Pete Wolczanski, for his patience and guidance over the last 4 years. I would also like to thank my other committee members, Prof. Geoff Coates and Prof. William Dichtel, for helpful discussions and advice over the years. Prof. Kyle Lancaster has been a tremendous resource for intellectual discussion and a friend who is always willing to throw down to blow off some steam. Thanks go to Emil Lobkovsky for his help with X-Ray crystallography despite not always giving me the structure I wanted. Considerable credit goes to Karsten Meyer and his group for help with Mössbauer spectroscopy, elemental analysis, and SQUID. DFT and multireference calculations performed by Tom Cundari provided significant insight into the molecules synthesized in the following pages.

I would like to thank all the former Wolczanski group members who have helped to train me and provide guidance even after they had left Cornell. Brenda, Emily, Elliott, and Erika; I am forever grateful. I want to thank my classmate Valerie Williams for being such a wonderful labmate and for putting up with sitting next to me for all these years. I hope one day I can match your enthusiasm and work ethic as both are truly inspiring. I feel exceptionally blessed to have met my other labmate Brian Lindley whose optimism and positive attitude will surely be missed. Some of my favorite moments in grad school involved sitting with Brian and filling countless hood sashes with crazy molecules we wanted to make. I wish you the best as you finish up in the next year or so. To Brian Jacobs, Spencer Heins, and Ala'aeddeen Swidan: it has been great getting to know you all and I wish you the best as you travel down the bumpy road that is graduate school. Times will be tough but just take a break to go home, and try to tackle the problem with fresh eyes in the morning.

All my other classmates have contributed to my graduate school experience whether it was lending me chemicals or helping to collect data and for that I am very thankful. I would like to thank Kenneth Hernandez in the Abruña for help in acquiring air free cyclic voltammetry and for putting up with my ignorant questions about electrochemistry.

A very special thanks goes out to Anna Greenswag. We have come a long way over the last few years but your endless love and words of confidence have helped me in ways I cannot even begin to describe. I wasn't always there to help you through the tough times but you never turned your back on me and for that I am forever grateful.

I want to thank my parents for always being an attentive ear over the ups and downs and for always leaving clean sheets on the bed in case a trip back to Murrysville was needed to clear the mind. Big thanks to my older brother Chris who has been a role model to me ever since we were little kids.

Lastly I want to thank all the Ithacans I have known over the years who have been wonderful friends and distractions from the sheltered life of a chemistry graduate student. These folks include the many Frisbee teams over the years (The Shake, Bermuda, and Townies) as well as the chemistry department staff including Josh Wakeman, Dave Neish, and Larry Stull who were always quick to fix all the problems in the lab.

TABLE OF CONTENTS

LIST OF FIGURES

LIST OF TABLES

LIST OF SCHEMES

CHAPTER 1

Reactivity Studies of Titanium Oxo Clusters $(Me\text{-}Cp)_6Ti_6O_{8-x}Cl_x$ (x = 0, 2)

I. Introduction

One conceivable way to circumvent the one electron chemistry associated with first row transition metals is to use clusters containing multiple metal centers. Single electrons provided by different metal centers could be used for catalysis thereby limiting the number of oxidation state changes any one metal must undergo. Biology is full of examples that use metal cofactors to bring together the necessary electrons and substrates in order to catalyze important processes. The iron-molybdenum cofactor of nitrogenase brings together 8 electrons and 8 protons to convert atmospheric dinitrogen to ammonia and dihydrogen.[1,2] The oxygen evolving complex of photosystem II oxidizes water to dioxygen using a manganese- and oxygen-containing active site.[3,4] Nature has found a way to use the one electron chemistry of first row transition metals to its favor. While the different states of the manganese ions are not fully understood, it is thought that the clustered ions undergo complex sequential one electron oxidations prior to the oxidation of water.

Polynuclear clusters bearing excess electrons may behave in an analogous fashion to some of these biological active sites.[5] Caulton's initially discovery showed that treatment of $Cp_2Ti(CO)_2$ ($Cp = \eta^5\text{-}C_5H_5$) with H_2 produced methane and a new, blue, diamagnetic solid.[6] Structure determination by X-Ray diffraction showed the novel cluster $Cp_6Ti_6O_8$ in which the Ti atoms make up the points of an octahedron and each of the triangular faces contains a μ-3 oxide.[7] The Ti atoms make up a $Ti^{III}_2Ti^{IV}_4$ core in which the two electrons are paired in a symmetric a_{1g} molecular orbital.[8] Years

later, Bottomley found that he could synthesize $Cp_6Ti_6O_8$ in high yields with the addition of water to $Cp_2Ti(CO)_2$.[9]

Expanding the scope of this chemistry Floriani developed an alternate synthesis allowing for higher yields and greater functionalization.[10] They reduced (R-Cp)$TiCl_3$ (R-Cp = η^5-RC_5H_4, R = H, Me) to compounds of the type $(R\text{-}Cp)_6Ti_6O_{8-x}Cl_x$ (R = H, Me; x = 0, 2, 4). The formal oxidation states for the titanium ions in $(R\text{-}Cp)_6Ti_6O_6Cl_2$ are $Ti^{III}_4Ti^{IV}_2$ resulting in 4 cluster electrons, again affording a diamagnetic ground state while $(R\text{-}Cp)_6Ti_6O_4Cl_4$ is paramagnetic. To study the reaction chemistry of these systems, the clusters derived from Me-Cp were chosen for reasons of increased solubility and additional useful NMR handles. Initial studies focused on the $(Me\text{-}Cp)_6Ti_6O_8$ (**1**) and $(Me\text{-}Cp)_6Ti_6O_6Cl_2$ (**2**) clusters due to their ease of synthesis and diamagnetic nature, which would make characterization of reactivity more readily monitored.

II. Results and Discussion

A. Synthesis of [(Me-Cp)TiCl(μ_2-O)]$_4$, 4 .

Hydrolysis of (Me-Cp)$TiCl_3$ (**3**) in refluxing acetone cleanly provides the tetrameric Ti(IV) [(Me-Cp)TiCl(μ_2-O)]$_4$ (**4**) as a bright yellow, crystalline, solid that precipitates from solution (Scheme 1.1).[10–12] The piano-stool **3** was made in one step from Li(Me-Cp) and $TiCl_4$ in toluene and could be easily purified by sublimation[13] or continuous extraction with hot pentane. If the bis-tetrahydrofuran adduct, $TiCl_4(THF)_2$, was used as a Ti precursor, the dominant product was $(Me\text{-}Cp)_2TiCl_2$.

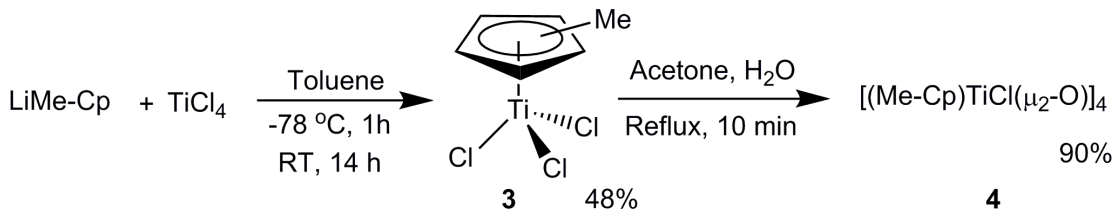

Scheme 1.1. Synthesis of $[(Me\text{-}Cp)TiCl(\mu_2\text{-}O)]_4$, (**4**).

B. Synthesis of $(Me\text{-}Cp)_6Ti_6O_6Cl_2$ (2)

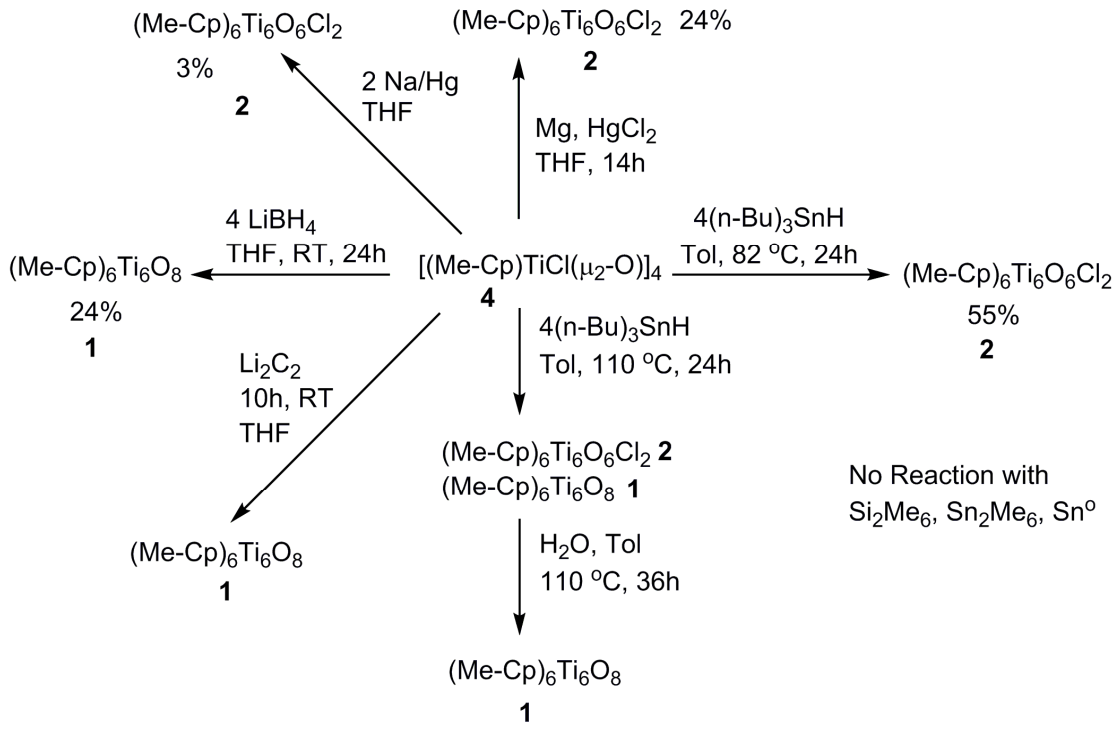

Scheme 1.2. Synthetic routes towards $(Me\text{-}Cp)_6Ti_6O_6Cl_2$ (**2**) and $(Me\text{-}Cp)_6Ti_6O_8$ (**1**).

The literature preparation for $(Me\text{-}Cp)_6Ti_6O_6Cl_2$ (**2**) calls for treatment of tetramer, **4**, with $(n\text{-}Bu)_3SnH$ in refluxing toluene to give a dark blue solution that yields crystalline **2** upon cooling.[10] Exhaustive attemps to duplicate this procedure yielded either mixtures of products or no observable reaction. Attempts were made to synthesize **2** using other reducing agents and those results are summarized in Scheme

1.2. After extensive experimentation, $(n\text{-}Bu)_3SnH$ was found to be the best reducing agent for this reaction, but required a lower temperature of 82 ^{o}C to give exclusively the dichloride cluster, **2**.

C. Synthesis of $(Me\text{-}Cp)_6Ti_6O_8$ (1)

Following the synthesis set forth by Floriani, **2** was easily converted to **1** with the addition of water and heating to 110 ^{o}C in toluene. This proved to be a convenient method for converting mixtures of **2** and **1** to pure $(Me\text{-}Cp)_6Ti_6O_8$ (**1**).

D. Reactivity of hexanuclear titanium clusters

Having established successful routes to **1** and **2**, an investigation into their reactivity was initiated. A rather exhaustive array of reagents showed no promising reactivity towards either compound. We suspected **2** would provide the most reactivity because of its propensity to convert to the likely more thermodynamically stable **1**.

Unfortunately all of the attempted transormations yielded mixtures of unidentifiable products. Reactions with dichloride, **2**, often showed the fully oxidized cluster, **1**, and when heating was necessary to initiate any reaction, the tetramer (**4**) was the major product. Minor products were hard to identify because ^{1}H NMR only provided a 2:2:3 ratio of resonances corresponding to the cyclopentadienyl groups which offered little insight into the chemical structure.

E. Cyclic Voltammetry of $(Me\text{-}Cp)_6Ti_6O_8$ (1) & $(Me\text{-}Cp)_6Ti_6O_6Cl_2$ (2)

The delocalized cluster electrons of **1** and **2** could plausibly be used reversibly to catalyze other transformations with small molecules, so cyclic voltammetry (CV) was utilized to probe the oxidation/reduction chemistry of the clusters. Figure 1.1 shows two reversible redox processes for **1** at -1.8 V and -2.8 V (vs Ag/Ag^{+})

suggesting the stability of both a one and two electron reduced speices. The inset of Figure 1.1 shows that with continued cycling beyond -3 V, any electrochemical process loses its reversibility suggesting any reduced species is not stable on longer timescales.

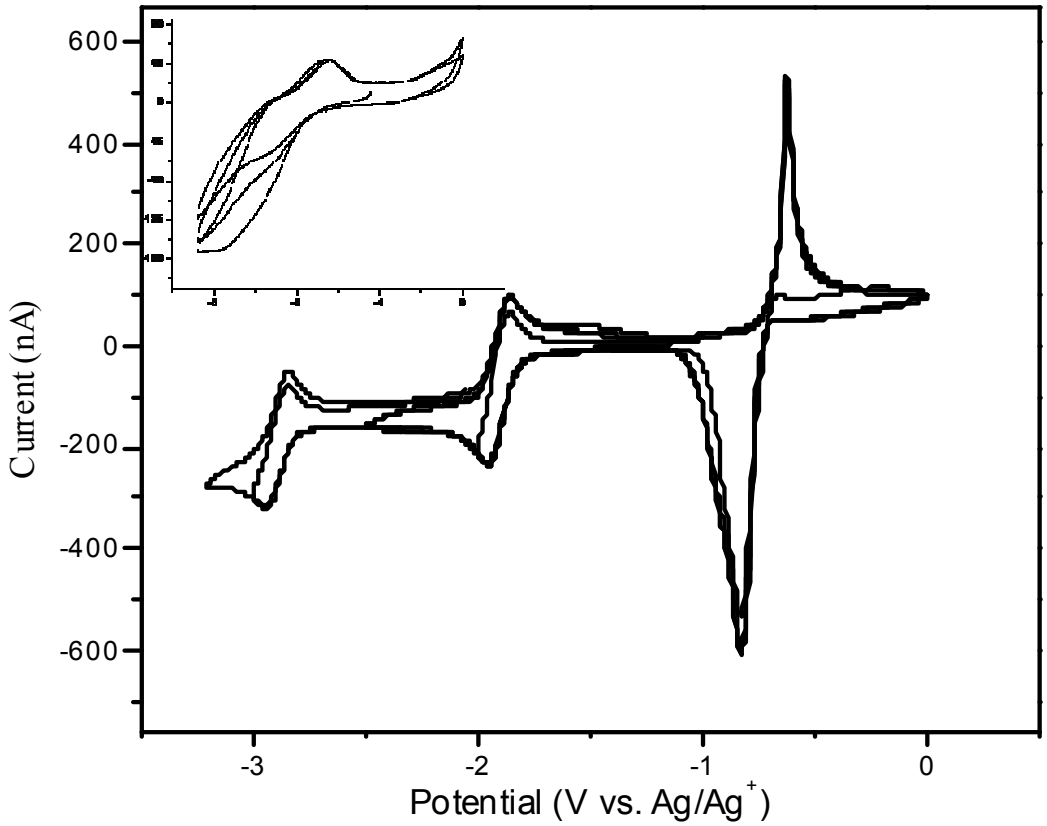

Figure 1.1. CV of $(Me\text{-}Cp)_6Ti_6O_8$ (**1**) (c = 0.75 mM) in THF/0.1 M TBAP at rt at 50 mV s^{-1}.

The CV for **2** showed a significantly different electrochemical response as shown in Figure 1.2. Upon initial cycling in the reductive direction (black line) there was no response, but after cycling oxidatively past ~0 V an anodic current is observed. The second sweep in the reductive direction (red line) shows significant change in the signal as several reductions now become apparent. Continued cycling

(Figure 1.2 B) shows many redox processes not present in initial scans, indicating these signals do not arise from **2** and may show the electrochemistry of decomposition products. In both the CV for **1** and **2** the sharp signal at -0.9 V is not well understood and could indicate a surface process involving deposition on the electrode. For (Me-Cp)$_6$Ti$_6$O$_6$Cl$_2$ (**2**) (Figure 1.2), the sharp cathodic response at -0.9 V does not scale with any other redox process, supporting the hypothesis that this signal is a result of a deleterious process in the system.

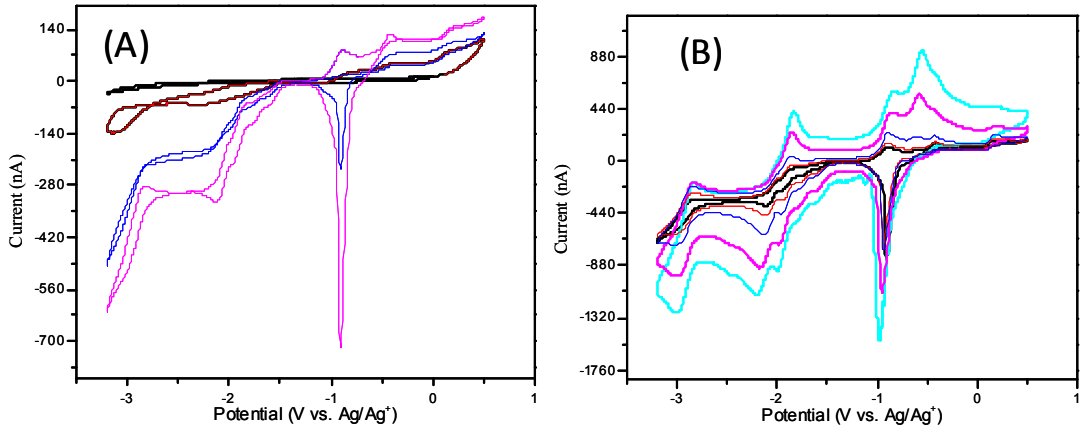

Figure 1.2. CV of (Me-Cp)$_6$Ti$_6$O$_6$Cl$_2$ (**2**) (c = 0.75 mM) in THF/0.1 M TBAP at rt at 50 mV s^{-1} at early cycles (A) and after continued cycling (B).

III. Conclusions

Titanium oxo clusters (Me-Cp)$_6$Ti$_6$O$_8$ (**1**) and (Me-Cp)$_6$Ti$_6$O$_6$Cl$_2$ (**2**) were sythnesized reproducibly through modified literature procedures. Reactivity studies on **1** and **2** showed no clean reactivity which halted any further investigation into these systems.

IV. Experimental

A. General Considerations

All manipulations were performed using either glovebox or high-vacuum techniques. Hydrocarbon and ethereal solvents were dried over sodium and vacuum transferred from sodium benzophenone ketyl (3-4 mL tetraglyme/L were added to hydrocarbons). Benzene-d_6 was sequentially dried over sodium and stored over sodium. All glassware was oven dried at 165 ^{o}C before use. Li(Me-Cp) was synthesized according to literature procedures.[14]

^{1}H and ^{13}C NMR spectra were obtained on Varian 300 MHz (Mercury) and 400 MHz (INOVA) spectrometers. ^{1}H NMR and ^{13}C NMR shifts are referenced to benzene-d_6 (^{1}H, δ 7.16 ppm; ^{13}C 128.39 ppm) and chloroform-d (^{1}H, δ 7.26 ppm; ^{13}C 77.16 ppm). Cyclic voltammograms were recorded in THF solution ~1mM concentration using tetrabutylammonium perchlorate (0.1 M) as supporting electrolyte with a 3 mm glassy-carbon working electrode, Pt-wire counter electrode, and Ag/Ag^{+} reference electrode. The cyclic voltammetry experiments were referenced to the ferrocene$^{0/+}$ redox couple at +0.683V.

B. Synthesis

*Methyl-cyclopentadienyltitanium trichloride (**3**).* To a slurry of Li(Me-Cp) (9.81 g, 114 mmol) in toluene (400 mL) at -78 ^{o}C was added $TiCl_4$ (25.9 g, 137 mmol) via syringe under Ar. The reaction was warmed to room temperature giving a dark red solution. After stirring for 14 h at ambient temperature, the toluene was removed under vacuum. The solid was placed in a soxhlet thimble and continuously extracted for 24 hr resulting in an orange solution and orange precipitate. Cooling the filtrate

and filtering yielded 12.7 g (48 %) orange Me-CpTiCl$_3$ (**3**). ^{1}H NMR (C_6D_6, 300 MHz, 295 K, δ): 5.99 (m, 2H, Cp-*H*), 5.87 (m, 2H, Cp-*H*), 1.82 (s, 3H, Cp-C*H*$_3$).

*[(Me-Cp)TiCl(μ$_2$-O)]$_4$ (**4**).* (Me-Cp)TiCl$_3$ (**3**) (12.7 g, 54.3 mmol) was dissolved in 94 mL acetone under air. Water was added dropwise until a bright yellow solid had precipitated from. The yellow solid was collected by filtration and dried under reduced pressure yielding 8.7 g (90%) of the desired product. ^{1}H NMR (C_6D_6, 300 MHz, 295 K, δ): 6.41 (m, 2H, Cp-*H*), 6.29 (m, 2H, Cp-*H*), 2.25 (s, 3H, Cp-C*H*$_3$).

*(Me-Cp)$_6$Ti$_6$O$_6$Cl$_2$ (**2**).* A 150 mL bomb was charged with [(Me-Cp)TiCl(μ$_2$-O)]$_4$ (**4**) (1.0 g, 1.4 mmol) and 20 mL toluene. Under argon (n-Bu)$_3$SnH (1.63 g, 5.60 mmol) was added and the solution degassed. The reaction was heated at 85 ^{o}C for 20 hr generating a dark blue solution. After degassing the solution it was cooled to -35 ^{o}C overnight. The dark blue product was collected on a glass frit and washed with diethyl ether (480 mg, 55 %). ^{1}H NMR (C_6D_6, 300 MHz, 295 K, δ): 6.34 (m, 2H, Cp-*H*), 5.96 (m, 2H, Cp-*H*), 2.50 (s, 3H, Cp-C*H*$_3$).

*(Me-Cp)$_6$Ti$_6$O$_8$ (**1**).* A 60 mL bomb was charged with (Me-Cp)$_6$Ti$_6$O$_8$ (**1**) (500 mg, 0.538 mmol), 12 mL Toluene, and 10 μL water. The reaction was heated in a 110 ^{o}C oil bath for 36 h resulting in a dark royal purple color. Upon cooling the reaction is degassed and cooled to -35 ^{o}C for 3 d. After this time 225 mg (47%) purple microcrystalline solid was isolated by filtration. ^{1}H NMR (C_6D_6, 300 MHz, 295 K, δ): 5.94 (m, 2H, Cp-*H*), 5.77 (m, 2H, Cp-*H*), 2.25 (s, 3H, Cp-C*H*$_3$).

REFERENCES

(1) Burgess, B. K.; Lowe, D. J. *Chem. Rev.* **1996**, *96*, 2983–3012.

(2) Eady, R. R. *Chem. Rev.* **1996**, *96*, 3013–3030.

(3) McEvoy, J. P.; Brudvig, G. W. *Chem. Rev.* **2006**, *106*, 4455–4483.

(4) Yachandra, V. K.; Sauer, K.; Klein, M. P. *Chem. Rev.* **1996**, *96*, 2927–2950.

(5) Bottomley, F. *Polyhedron* **1992**, *11*, 1707–1731.

(6) Huffman, J. C.; Stone, J. G.; Krusell, W. C.; Caulton, K. G. *J. Am. Chem. Soc.* **1977**, *99*, 5829–5831.

(7) Bottomley, F.; Paez, D. E.; White, P. S. *J. Am. Chem. Soc.* **1982**, *104*, 5651–5657.

(8) Bottomley, F.; Grein, F. *Inorg. Chem.* **1982**, *21*, 4170–4178.

(9) Bottomley, F.; Drummond, D. F.; Egharevba, G. O.; White, P. S. *Organometallics* **1986**, *5*, 1620–1625.

(10) Carofiglio, T.; Floriani, C.; Roth, A.; Sgamellotti, A.; Rosi, M.; Chiesi-Villa, A.; Rizzoli, C. *J. Organomet. Chem.* **1995**, *488*, 141–154.

(11) Skapski, A. C.; Troughton, P. G. H.; Sutherland, H. H. *Chem. Commun. Lond.*

(12) Gorsich, R. D. *J. Am. Chem. Soc.* **1960**, *82*, 4211–4214.

(13) Lucas, C. R.; Green, M. L. H.; Taylor, B. H.; Tebbe, F. N. In *Inorganic Syntheses*; Basolo, F., Ed.; John Wiley & Sons, Inc.: Hoboken, NJ, USA, 1976; Vol. 16, pp. 237–240.

(14) Beachley, O. T.; Pazik, J. C.; Glassman, T. E.; Churchill, M. R.; Fettinger, J. C.; Blom, R. *Organometallics* **1988**, *7*, 1051–1059.

Chapter 2

Synthetic Efforts Toward Catalysis with a Tridentate Pyridine-Imine Ligand

I. Introduction

Pincer ligands comprise a diverse class used in a range of catalytic processes because the ease in which steric and electronic factors can be tuned makes them ideal candidates for catalytic screenings. A pincer ligand is tridentate and planar, binding in a meridional fashion with donors that are typically neutral phosphorous or nitrogen containing groups although anionic carbon, nitrogen, phosphorous, and oxygen donors are also found. Some typical pincer ligands are shown in Figure 2.1.

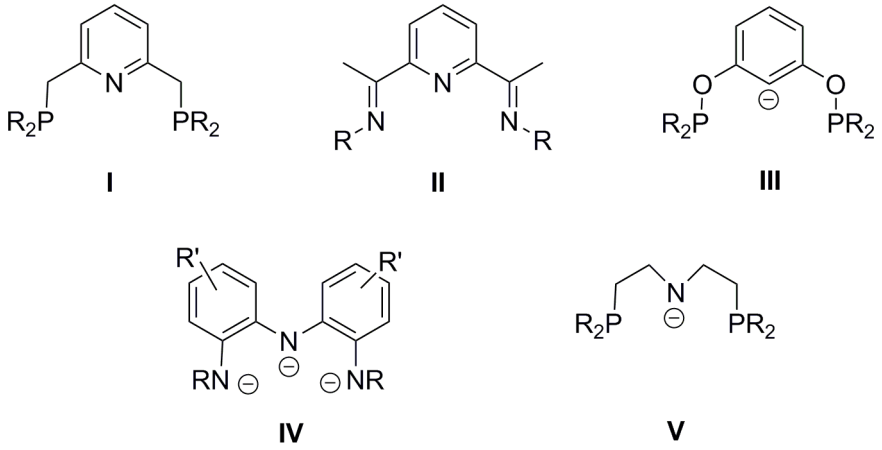

Figure 2.1. Examples of pincer ligands used in catalysis.

Studies of these systems have shown very diverse scopes of chemistry. One theme is the redox non-innocent systems (Figure 1.1; II & IV) made popular by Chirik[1,2] and Heyduk[3,4], respectively. While the effect of redox non-innocence in catalysis is not well understood, it has been proposed that shuttling electrons to and from the ligand may aid in catalysis by limiting the oxidation state changes occurring at the metal center.

Metal-ligand cooperativity has also been invoked in catalysis using pincer ligands as Milstein has used PNP pincer complexes (Figure 1.1; I) in hydrogenations, an example of which is shown in Scheme 1.1.[5] Here, the dearomatization of the pyridine ring upon deprotonation leaves an alkene which is later used to accept a hydrogen in a 1,3-addition. As in redox non-innocence, the ligand helps support minimal oxidation state at the metal, but there is no transfer of electrons as the metal center remains in the +2 oxidation state over the whole catalytic cycle.

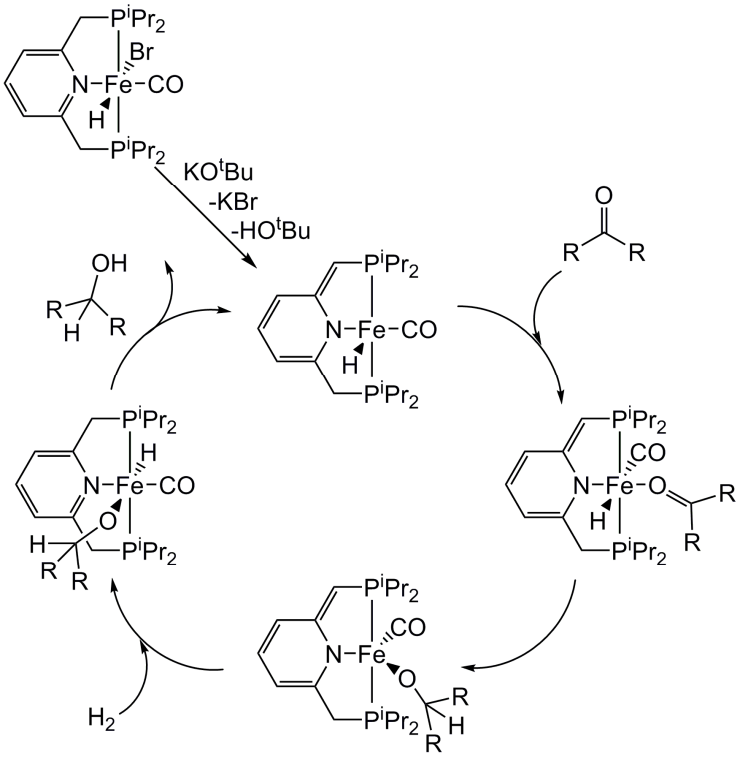

Scheme 2.1. Example of metal-ligand cooperativity in the reduction of a ketone to a secondary alcohol.

Having not had success installing a stable pyridine imine (PI) on other systems a ligand that could combine both redox non-innocence and metal-ligand cooperativity was sought. A modular ligand was deemed desirable that could be easily functionalized with little modification of synthetic protocol. Figure 1.2 illustrates a

ligand with 4 available redox states between the pyridine imine and o-phenylenediamine that offers a potential wide range of redox noninnocent supported reactivity. It was also envisioned that the imine could be used to accept a proton in reactions involving ligand cooperativity (Scheme 1.1). This and other reactivity was explored.

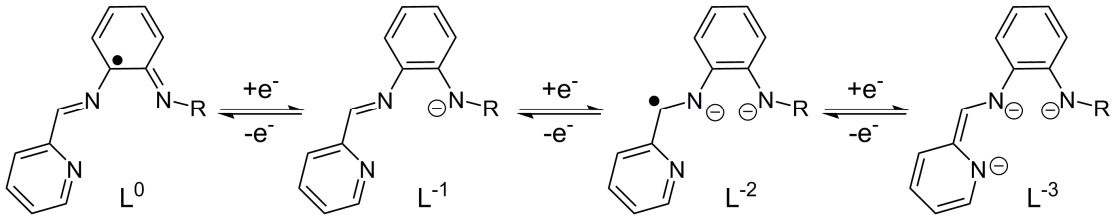

Figure 2.2. Oxidation states available to tridentate ligand.

II. Results and Discussion

A. Ligand Syntheses.

1. Synthesis of Substituted Anilines.

The anilines for this project were made primarily from literature procedures with modest modifications.[6–8] 1-Fluoro-2-nitrobenze made a versatile starting material for this chemistry (Scheme 2.1) as the nitro group helped polarize the F-C_{aryl} making it susceptible to substitution with many primary amines. Bulky, 2,6-disubstituted anilines required very high temperatures for the reaction to proceed, and excess aniline was required to act as a base for HF formed. The reaction required the addition of KF and would not proceed with added bases such as Na_2CO_3. Aliphatic amines reacted under milder conditions and due to their ease of removal can be used in vast excess. Reduction of the nitro group proved easy in all cases. as hydrogenation with catalytic Raney Ni produced the substituted aniline in >90% yield and without the need for any further purification.[9]

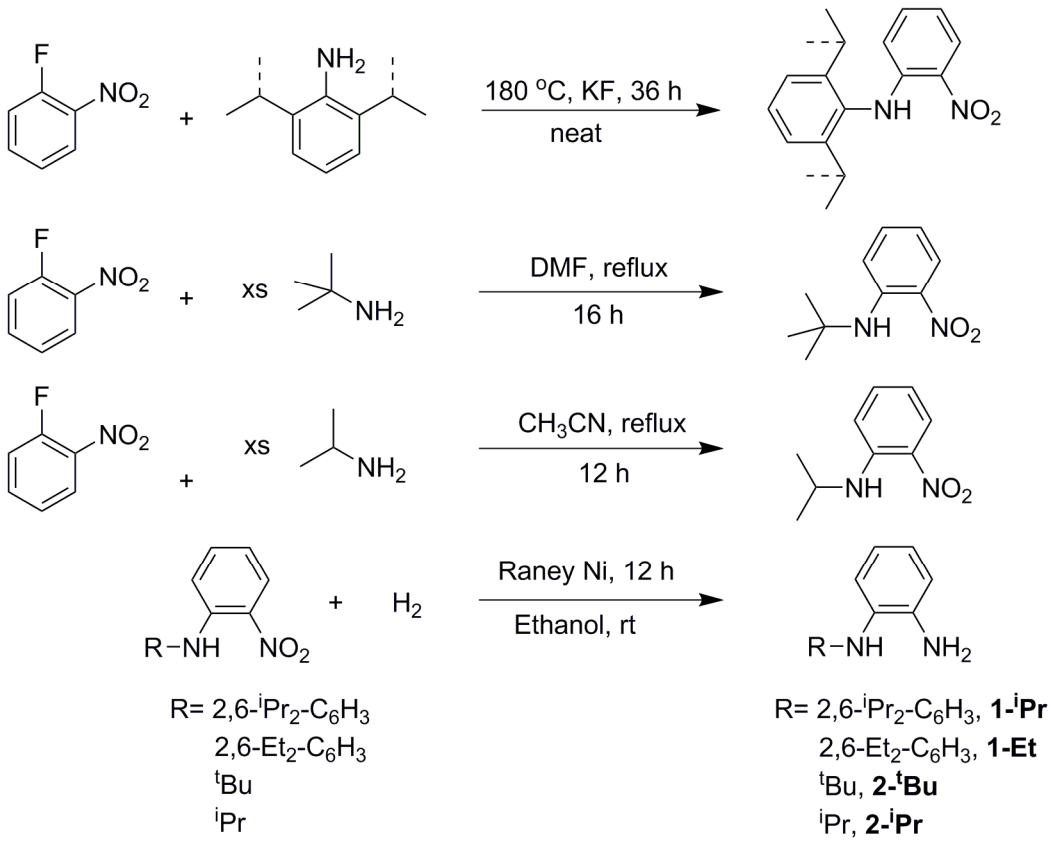

Scheme 2.2. Synthesis of N-substituted diaminobenzene ligand precursors

2. Condensations with 2-carbonylpyridines

The imino-pyridine target compound was first synthesized in the condensation of N-(2-aminophenyl)-2,6-diisopropylaniline (**1-^{i}Pr**) with 2-pyridinecarboxaldehyde (Scheme 2.2). This reaction cleanly made imine **3-^{i}Pr** in quantitative yield and workup only required filtering to remove the drying agent. The 2,6-diethylphenyl derivative **3-Et** was synthesized just as easily, but care must be taken to limit the reaction time. At extended reaction times (monitored by ^{1}H NMR), resonances corresponding to unidentified side products were observed.

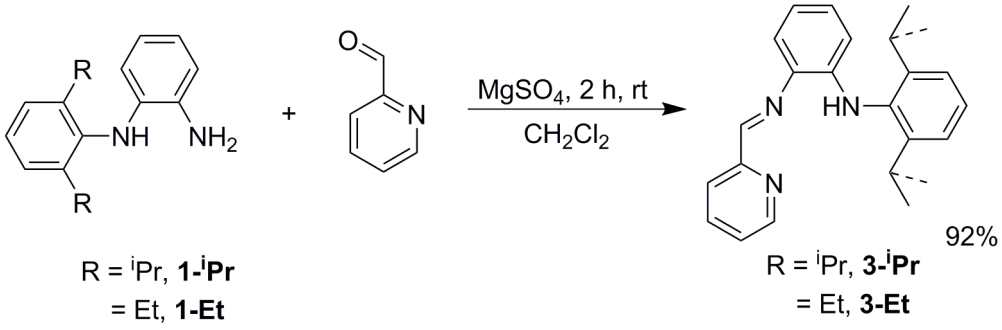

Equation 2.1.

Reactions of the aliphatic substituted anilines with 2-pyridinecarboxaldehyde quickly and cleanly cyclize intramolecularly to make new benzimidazoles **4-^{i}Pr, 4-^{t}Bu** along with other unidentified products (Scheme 2.3).[10] It is likely that the increased nucleophilicity and decreased sterics associated with the aliphatic substituted anilines allowed this cyclization to take place. The cyclization was confirmed by 2D NMR spectroscopy. In the condensation of aliphatic aniline **2-^{i}Pr** with 2-pyridinecarboxaldehyde, there is a heteronuclear multiple-bond correlation spectroscopy (HMBC) cross peak showing a correlation of the ^{i}Pr methine with the carbon derived from the aldehyde. The upfield (~6 ppm) chemical shift of the proton in the 5-membered ring was also indicative of cyclization.

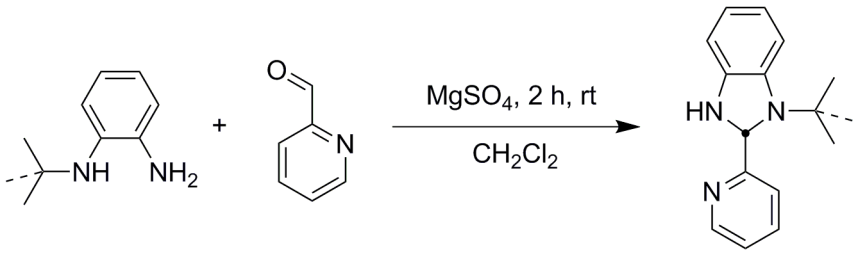

Equation 2.2.

Attempts to condense 2-aminoanilines with pyridylketones resulted in mixtures of products as these reactions typically required heating which provided more favorable conditions for cyclization.

B. Metallation of Ligands

1. Reactions of M[N(TMS)$_2$](THF) with 3-^{i}Pr; Synthesis of 5-M

The acidic proton on **3-^{i}Pr** makes metallation with known metal bis-amides very easy, as the internal base deprotonates the ligand, and the byproduct, HMDS, is readily removed under vacuum. Upon addition of C_6H_6 to a flask containing M[N(TMS$_2$)]$_2$(THF)$_x$ (M = Cr, x = 2; M = Fe, Co x = 1) and **3-^{i}Pr** (Equation 2.3), the solution becomes intensely colored. Stirring overnight ensured complete reaction, and filtering and isolation of the pure compounds showed that all were paramagnetic species. A summary of the results is shown in Table 2.1.

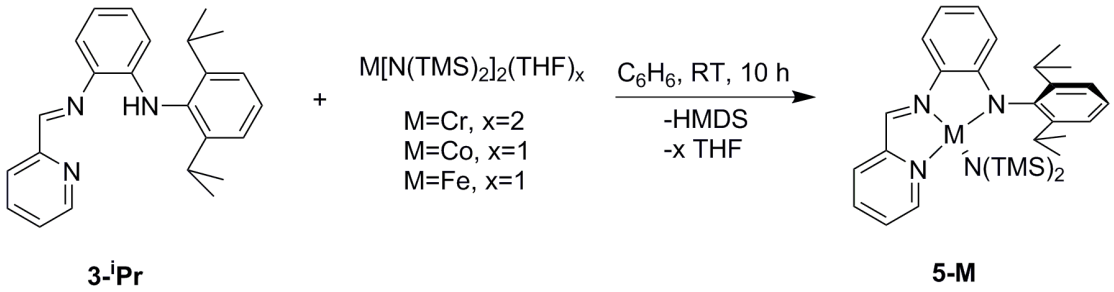

3-^{i}Pr **5-M**

Equation 2.3.

Table 2.1. Yield, color, and magnetic moment of Metal-amide compounds

Compound	Yield (%)	Color	μ_{eff} (μ_B)[a]
5-Cr	64	Burgundy	4.7
5-Fe	70	Blue-Green	5.0
5-Co	85	Green	4.4

[a]Solution Evans measurement in C_6D_6

5-Cr is a burgundy solid that was isolated in 64% overall yield. Determination of the room temperature magnetic moment by Evans method[11,12] gave a μ_{eff} of 4.7 μ_B, consistent with high spin S=2 Cr(II). Isolated in 70% yield as a dark blue solid, **5-Fe** is an Fe(II) S = 2 system with a room temperature magnetic moment of 5.0 μ_B. Green, **5-Co**, has a μ_{eff} of 4.4 μ_B consistent with S=3/2 Co(II) center with a large amount of spin orbit coupling.[13]

2. Salt metathesis routes to metal halide compounds 6-M (M = Ni, Fe)

Deprotonation of **3-^{i}Pr** with LiHMDS showed instantaneous production of a dark green solution, and assay of the reaction mixture by ^{1}H NMR showed very complicated NMR spectra owing to some sort of decomposition. The anion formed may be nucleophilic enough to induce cyclization as was seen for the aliphatic anilines (Scheme 2.3).

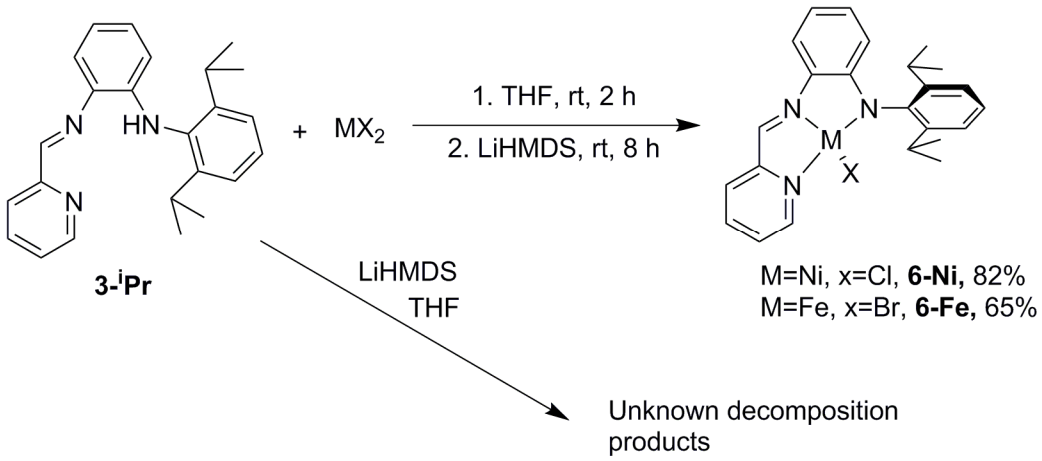

Scheme 2.1 Metallation via salt metathesis.

Salt metathesis proved to be a viable route towards synthesis of metal-halide compounds **6-M** (M = Ni, Fe). Complexing the protonated ligand to the metal prior to deprotonation ensured that once deprotonated the metal will already be in place to

prevent cyclization. **6-Fe** is a dark blue solid that affords a paramagnetically shifted and broadened NMR spectrum. No magnetic data was collected for **6-Fe** but it is expected to be a high spin Fe(II) S = 2 system like the Fe-N(TMS)$_2$ analogue, **5-Fe**. Synthesis of **6-Ni** with $NiCl_2$ (dried over thionyl chloride) showed a significant amount of free ligand. This led to a search for a better, anhydrous, starting material, so when $NiCl_2$(DME) was used, red, diamagnetic, **6-Ni** was isolated in 82% yield. The diamagnetism of **6-Ni** was expected for a pseudo square planar Ni(II) d^8 compound.

3. Reaction of 3-^{i}Pr with $Me_2Fe(PMe_3)_4$

Treatment of **3-^{i}Pr** with Karsch's $Me_2Fe(PMe_3)_4$ in C_6D_6 instantly formed a dark grey paramagnetic solution consistent with assignment as the iron (II) methyl compound **10**. Addition of H_2 to a J. Young tube containing **10** showed loss of resonances corresponding to **10** over 3 hours with no new major resonances. IR of the reaction showed no metal-hydride stretch. Ethylene showed no insertion or polymerization reactivity with **10** until elevated temperatures showed decomposition with formation of solids, presumably iron metal.

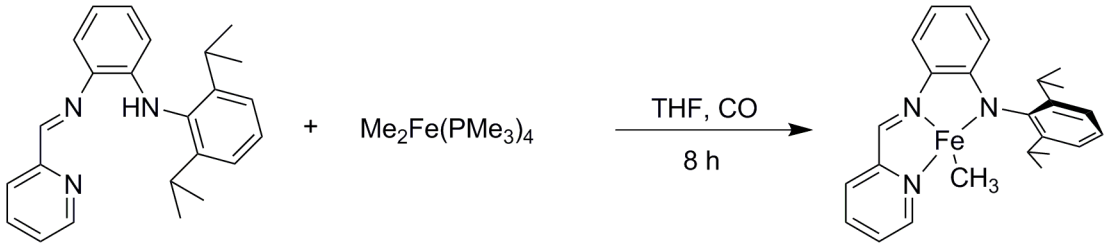

3-^{i}Pr **10**

Equation 2.4.

C. UV/VIS spectra of 4-coordinate compounds

1. UV/VIS of 6-Fe and 6-Ni

The intense colors shown by these compounds prompted investigation of their electronic structure with UV/VIS spectroscopy. The spectra are dominated by transitions with large extinction coefficients so are assigned as charge transfer transitions. It has not been determined whether the bands correspond to ligand to metal (LMCT), metal to ligand (MLCT), or intraligand (ILCT) charge transfers or is inclusive.

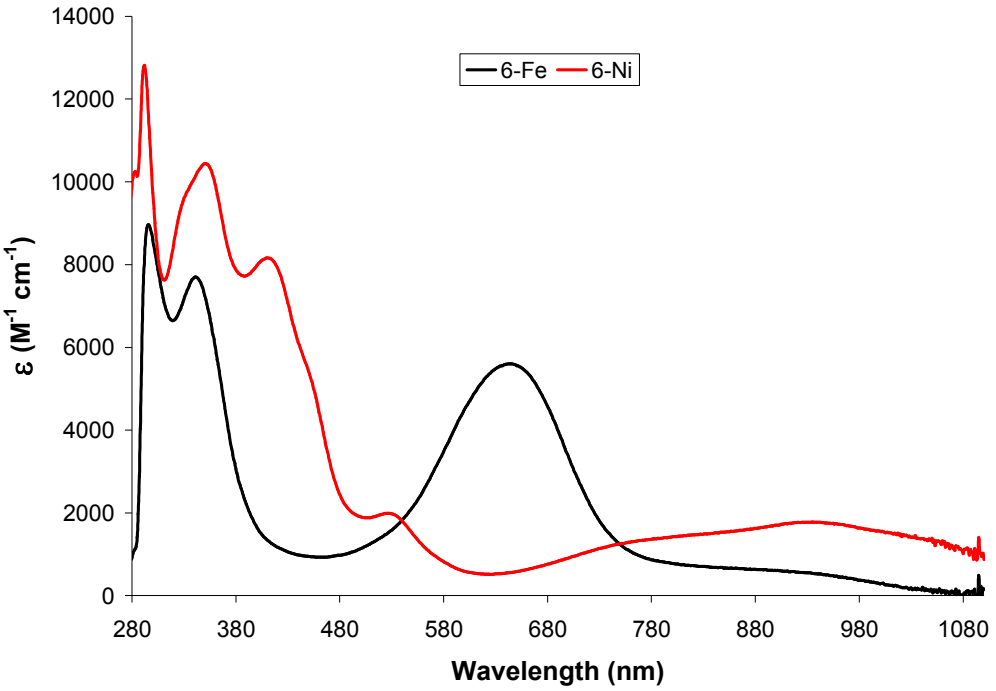

Figure 2.3. UV/VIS of **6-Fe** (black) and **6-Ni** (red) in THF.

The UV/VIS spectrum of **6-Ni** displayed three high energy band with large extinction coefficients at 291 nm ($\varepsilon \sim 13000\ cm^{-1}$), 347 nm ($\varepsilon \sim 10000\ cm^{-1}$), and 407 nm ($\varepsilon \sim 8000\ cm^{-1}$). Additional, less intense, features were observed at 524 nm ($\varepsilon \sim$

2000 cm^{-1}) and 924 nm ($\varepsilon \sim 1700\ cm^{-1}$). The absorbance spectrum of **6-Fe** also showed three bands with large extinction coefficients. Analogous to **6-Ni**, two high energy bands were noted at 294 nm ($\varepsilon \sim 9000\ cm^{-1}$) and 339 nm ($\varepsilon \sim 8000\ cm^{-1}$) while the low energy band was red shifted to 640 nm ($\varepsilon \sim 6000\ cm^{-1}$).

A qualitative d-orbital splitting diagram for **6-Ni** is shown in Figure 2.4. As a low spin d^8 species, nickel is likely in a pseudo square planar environment consistent with the d-orbital splitting diagram shown on the left of Figure 2.4. On the right is a simplified, qualitative diagram showing the origins of different electronic transitions expected in the UV/VIS spectrum. The intense transitions observed are due to charge transfer (CT) transitions but they cannot be assigned to any particular type without further experimentation or calculations. Hidden underneath the more intense CT bands are the d-d transitions which become more allowed at the lower symmetry present in **6-M** (M = Fe, Ni), but are expected to have extinction coefficients <1000 $M^{-1}cm^{-1}$.

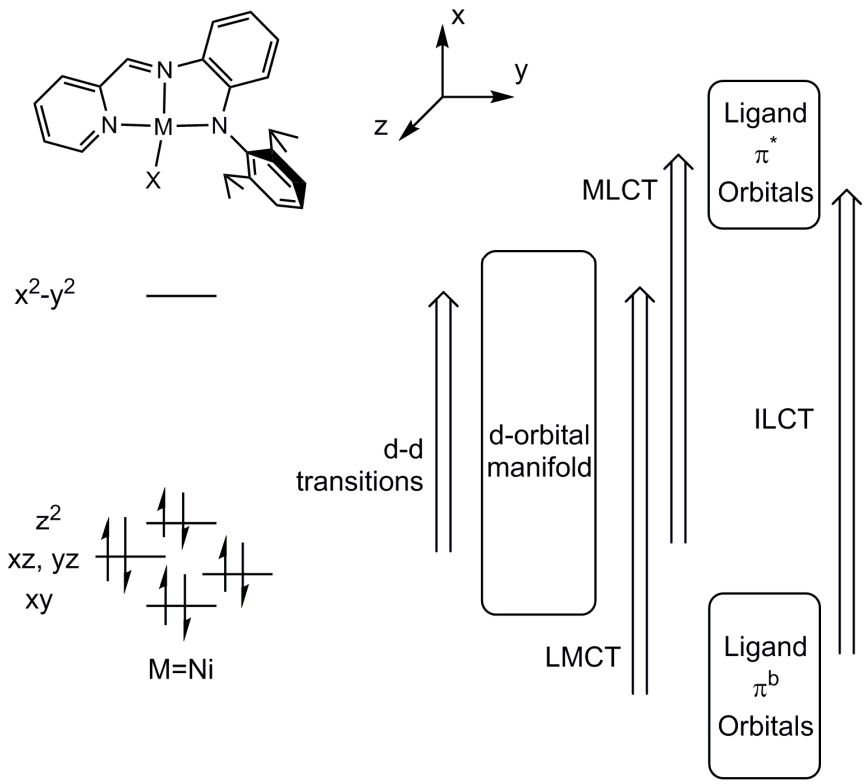

Figure 2.4. d-orbital splitting diagram of **6-Ni** (left), and qualitative picture showing origin of possible electronic transitions.

2. UV/VIS spectra of 5-M (M = Cr, Fe, Co)

The UV/VIS absorption spectrum of the 4-coordinate metal amide compounds (**5-**M, M = Cr, Fe, Co) are also dominated by intense charge transfer (CT) transitions. All three compounds share several features including the two high energy bands and a band at lower energy. A small shoulder was observed at 426 nm ($\varepsilon \sim 4000$ cm^{-1}) on the high energy features of **5-Co**. **5-Cr** displayed bands of similar intensity that are red shifted to 472 nm and 528 nm with extinction coefficients of 5000 $M^{-1}cm^{-1}$ and 4000 $M^{-1}cm^{-1}$, respectively. Again, any d-d transitions were not observed as they are less intense than the CT bands observed. The remaining features are summarized in Table 2.2.

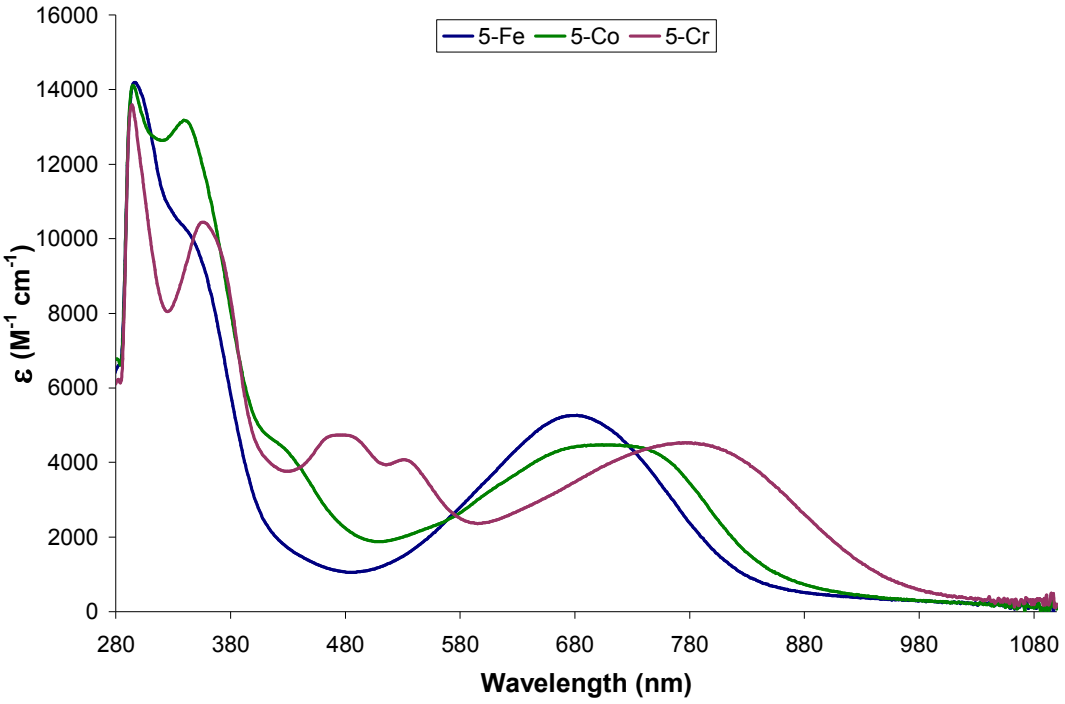

Figure 2.5. UV-VIS spectra of **5-Fe** (blue), **5-Co** (green) and **5-Cr** (purple) in THF.

Table 2.2. UV/VIS data for 5-M (M = Cr, Fe, Co).

5-Cr		**5-Fe**		**5-Co**	
λ (nm)	ε (M^{-1} cm^{-1})	λ (nm)	ε (M^{-1} cm^{-1})	λ (nm)	ε (M^{-1} cm^{-1})
293	13000	295	13000	294	14000
352	10000	340	10000	336	13000
472	5000	676	5000	426	4000
528	4000			710	4500
774	4500				

D. Reactivity of 4-coordinate compounds

1. Reactions of 6-Fe

With **6-Fe** in hand the exchange of halide with more reactive functional groups was sought. Reductions were attempted in the presence of coordinating ligands as a way to remove the halide and open up a fourth coordination site on the metal for reactivity. Exhaustive attempts to reduce **6-Fe** resulted in formation of unidentified

products. Neither Na/Hg, KC_8, $Mg/HgCl_2$, nor $Zn/HgCl_2$ cleanly reduced the metal halide, even when trimethylphosphine was added in excess during reduction attempts to coordinate with the reduced metal center. The sterics associated with the isopropyl groups on the ligand may have prevented phosphine binding, but reductions in the presence of excess CO or N_2 showed a complex mixture of products in the ^{1}H NMR spectrum and no stretch in the IR expected for a bound carbonyl or N_2. It is possible that reduction to M(I) reduces the pyridine-imine leaving radical character on the ligand. Prior results have shown that mono-reduced PI fragments are prone to intermolecular carbon-carbon bond formation, but reaction mixtures were never quenched to determine the fate of the organic fragments after the reaction.[14–16]

Salt metathesis reactions were also attempted to try to substitute more reactive groups for the halide. Treatment of **6-Fe** with alkyl (neopentyl, methyl) lithium reagents resulted in intractable products. Reaction of **6-Fe** with sodium ethoxide showed decomposition and attempts to make an iron hydride with $LiHBEt_3$ showed decomposition with no evidence of an iron hydride stretch in the IR spectrum.

2. Reactions of 6-Ni

As was the case with the **6-Fe**, **6-Ni** was not successfully reduced using standard M^0 reduction conditions, and little experimentation was done to determine what other anionic ligands would be stable in place of the chloride. In an attempt to synthesize a nickel hydride, **6-Ni** was treated with $LiHBEt_3$. The maroon solid displayed a diamagnetic ^{1}H NMR (Figure 2.6) consistent with a saturated ligand backbone and formation of **7**. In the NMR a new set of doublets was observed at 3.20 ppm and 2.60 ppm corresponding to a diasteriotopic set of methylene protons

consistent with reduction of the imine. The fourth coordination site on nickel is plausibly occupied by a bound THF molecule.

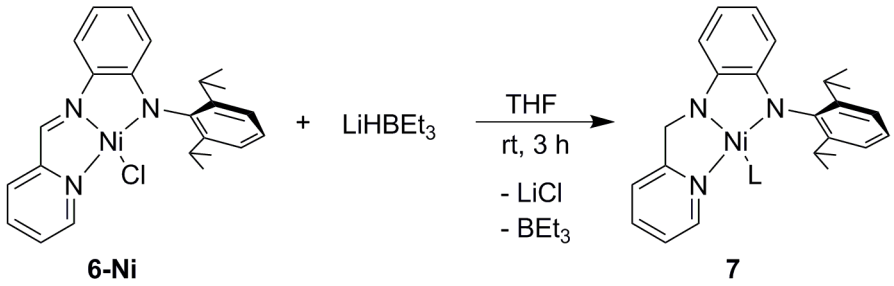

6-Ni **7**

Equation 2.5.

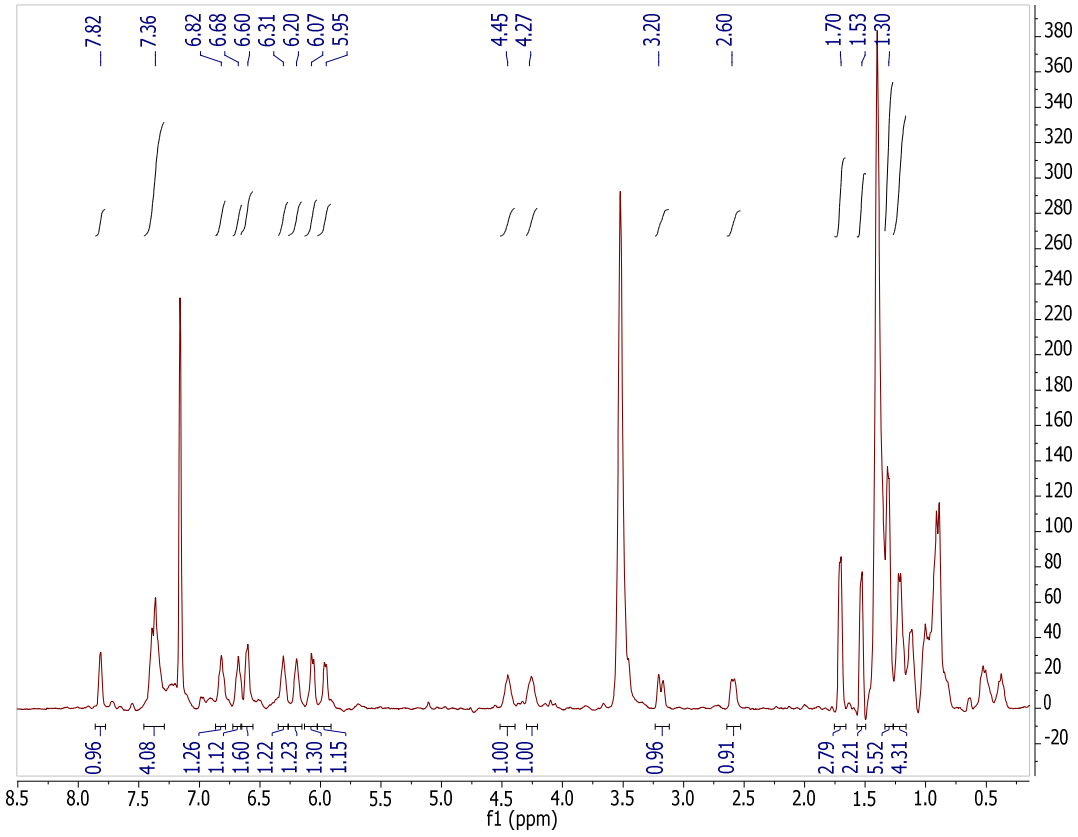

Figure 2.6. ^{1}H NMR spectrum of the crude reaction mixture showing formation of **7**.

3. Reactions of 5-M (M = Cr, Fe, Co).

Metal ligand cooperation was explored in performing 1,3-additions across the unsaturated ligand backbone and metal center. Treatment of the metal amides with dihydrogen showed no reaction up until decomposition at temperatures in excess of 110 ^{o}C. 1,3-addition of H_2 across the metal and imine was not observed so the saturated ligand was synthesized independently.

E. Chemistry of the Reduced 3-coordinate Ligand (8).

1. Ligand Synthesis: Reduction of 3-^{i}Pr to 8.

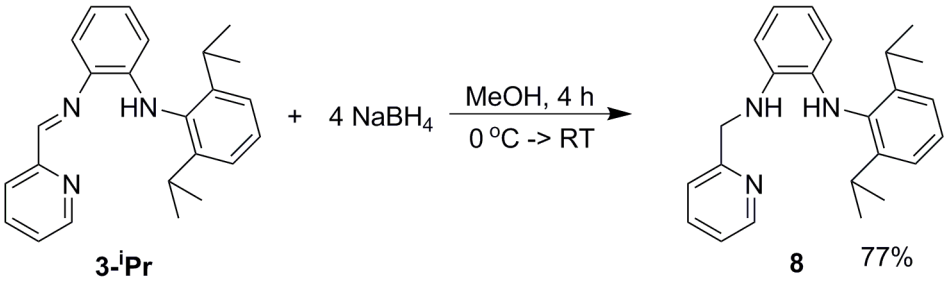

Equation 2.6.

Reduction of **3-^{i}Pr** was performed with standard conditions using sodium borohydride in methanol (Figure 2.6).[17] The reaction was followed by watching the intense orange color of **3-^{i}Pr** disappear, and saturated ligand **8** was synthesized as a white solid in 77% yield.

2. Metallation of 8.

Treatment of **8** with $Fe[N(TMS)_2]_2(THF)$ under an atmosphere of CO produced the bis-(CO) iron(II) compound **9** (Equation 2.7) whose spectrum showed a brown diamagnetic solid. IR showed two CO stretches at 1984 and 1919 cm^{-1}, consistent with other Fe(II) species. Attempts to install this ligand on other metal complexes proved fruitless. Sterics likely prevented binding of PMe_3, and

incorporation of other L type ligands in the reaction such as N_2 and 2-butyne did not allow for formation of a stable compound.

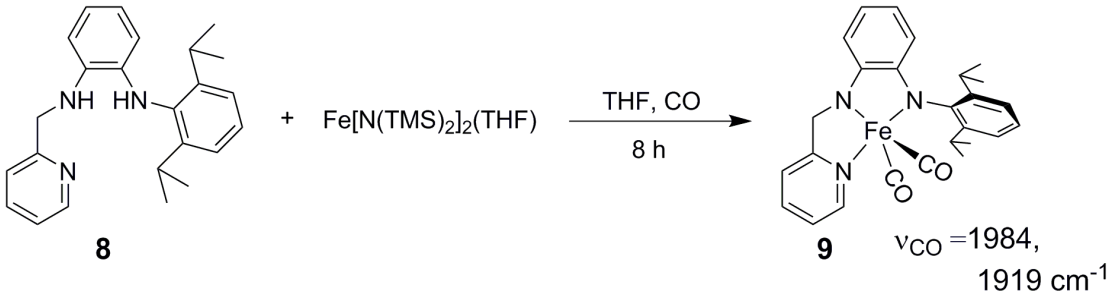

Equation 2.7.

III. Conclusions

Despite some synthetic complications a new ligand bearing a pyridine imine functionality was prepared. Redox non-innocence was not observed and did not assist in supporting any reactive metal centers. All other attempted reactions showed only mixtures of products with several factors limiting clean reactivity.

The ligand itself has been shown to be unstable with respect to cyclization, and pushing electron density onto the ligand may help facilitate this process. Additionally, sterics of the 2,6-diisopropyl group may limit what can bind to the coordinatively unsaturated metal center. The chemistry of this system was not entirely explored due to the limited reactivity observed.

IV. Experimental

A. General Considerations

All manipulations were performed using either glovebox or high-vacuum techniques unless otherwise indicated. Hydrocarbon and ethereal solvents were dried over sodium and vacuum transferred from sodium benzophenone ketyl (3-4 mL

tetraglyme/L were added to hydrocarbons). Benzene-d_6 was sequentially dried over sodium and stored over sodium metal. All glassware was oven dried at 165 ^{o}C before use.

$Cr[N(TMS)_2]_2(THF)_2$,[18] $Mn[N(TMS)_2]_2(THF)$,[19] $Fe[N(TMS)_2]_2(THF)$,[20] $Co[N(TMS)_2]_2(THF)$,[21] $NiCl_2(DME)$,[22] $FeMe_2(PMe_3)_4$[23] were prepared by literature procedures. ^{1}H and ^{13}C NMR spectra were obtained on Varian 300 MHz (Mercury) and 400 MHz (INOVA) spectrometers. ^{1}H NMR and ^{13}C NMR shifts are referenced to benzene-d_6 (^{1}H, δ 7.16 ppm; ^{13}C 128.39 ppm), tetrahydrofuran-d_8 (^{1}H, δ 3.58 ppm; ^{13}C 67.21 ppm), and chloroform-d (^{1}H, δ 7.26 ppm; ^{13}C 77.16 ppm).

B. Synthesis

N-(2-nitrophenyl)-2,6-diisopropylaniline. To a flask containing 2,6-diisopropylaniline (8.0 g, 45 mmol) was added 1-fluoro-2-nitrobenzene (3.2 g, 22 mmol) and potassium fluoride (2.0 g, 34 mmol). The bright orange mixture was heated to 180 °C with stirring for 48 h. The reaction was cooled and added to water (50 mL). The aqueous layer was extracted with methylene chloride (3 x 50 mL) and dried over sodium sulfate. Volatiles were removed under vacuum. Any remaining aniline and 1-fluoro-2-nitrobenzene were removed by distillation (60-80 °C, 0.1 mTorr). The product was crystallized from absolute ethanol to yield orange prisms (3.3 g, 11 mmol, 49%). ^{1}H NMR ($CDCl_3$, 400 MHz, 295K, δ): 9.21 (s, 1H, N*H*), 8.23 (d, J = 9 Hz, 1H), 7.38 (m, 1H), 7.27 (m, 3H), 6.68 (m, 1H), 6.38 (d, J=9 Hz, 1H), 3.04 (sept, J=7 Hz, 2H), 1.18 (d, J = 7 Hz, 6H), 1.11 (d, J = 7Hz, 6H).

*N-(2-aminophenyl)-2,6-diisopropylaniline (**1-^{i}Pr**).* N-(2-nitrophenyl)-2,6-diisopropylaniline (3.3 g, 11 mmol) was dissolved in an EtOAc/EtOH (75/25) mixture

and Raney Nickel (1.5 g in H_2O) was added. The flask was placed under vacuum and H_2 (1 atm) was placed over the reaction. The reaction was stirred (and additional H_2 placed over the solution) until the dark orange color dissipates. Raney Nickel is removed by filtration and the solvent is removed under vacuum to yield a pure dark purple solid (2.9 g, 11 mmol, 96%). ^{1}H NMR ($CDCl_3$, 300 MHz, 295K): δ 7.23 (m, 3H), 6.79 (d, J = 8 Hz, 1H), 6.71 (m, 1H), 6.64 (m, 1H), 6.19 (d, J = 8 Hz, 1H), 4.90 (s, 1H, N*H*), 3.57 (s, 2H, NH_2), 3.06 (sept, J = 7 Hz, 2H), 1.14 (s, 12H).

N-(2-nitrophenyl)-2,6-diethylaniline. The procedure was the same as the synthesis of N-(2-nitrophenyl)-2,6-diisopropylaniline but with 2,6-diethylaniline (21.15 g, 142 mmol) and 1-fluoro-2-nitrobenzene (8.0 g, 57 mmol). The product was isolated via vacuum distillation (140 ^{o}C, 0.1 mTorr) as an orange oil (8.0 g, 52%). ^{1}H NMR ($CDCl_3$, 400 MHz, 295K, δ): 9.23 (s, 1H, N-*H*), 8.22 (d, J = 8 Hz, 1H, arylC-*H*), 7.28 (m, 2H), 7.22 (m, 2H), 6.68 (t, J = 8 Hz, 1H, arylC-*H*), 6.38 (d, J = 8 Hz, 1H, arylC-*H*), 2.54 (m, 4H, -CH_2-), 1.14 (t, J = 8 Hz, -CH_3).

*N-(2-aminophenyl)-2,6-diethylaniline (**1-Et**).* N-(2-nitrophenyl)-2,6-diethylaniline (8.0 g, was dissolved in 125 mL ethanol and 2 g Raney Ni (slurry in H_2O) added. Hydrogen (1 atm) was placed over the reaction and stirred at room temperature until the dark orange color no longer persisted. The reaction was degassed and filtered and solvent removed under vacuum to leave N-(2-aminophenyl)-2,6-diethylaniline (**1-Et**) as a dark red solid (6.8 g, 96%). ^{1}H NMR ($CDCl_3$, 400 MHz, 295K, δ): 7.15 (s, 3H), 6.76 (m, 2H), (6.63, t, J = 8 Hz, 1H), 6.22 (d, J = 8 Hz, 1H), 4.88 (s, 1H, -N*H*-), 3.61 (s, 2H, -NH_2), 2.52 (m, 4H, -CH_2-), 1.15 (t, J = 7 Hz, -CH_3).

*N^1-(2,6-diisopropylphenyl)-N^2-(2-pyridylimino)phenylenediamine (**3-^{i}Pr**).* N-(2-aminophenyl)-2,6-diisopropylaniline (**1-^{i}Pr**) (0.50 g, 1.9 mmol) was dissolved in 10 mL methylene chloride and $MgSO_4$ (1.1 g, 9.3 mmol) was added. 2-pyridinecarboxaldehyde (200 mg, 1.9 mmol) was dissolved in 2 mL methylene chloride and added dropwise resulting in a bright orange solution. The reaction was stirred for 2h before filtered and solvent was removed under vacuum leaving a viscous orange oil of the imine (606 mg, 1.7 mmol, 91%). ^{1}H NMR ($CDCl_3$, 300 MHz, 295, δ): 8.83 (s, 1H), 8.72 (d, J = 5 Hz, 1H), 8.25 (d, J = 8 Hz, 1H), 7.81 (m, 1H), 7.36 (m, 1H), 7.30 (m, 1H), 7.24 (m, 3H), 7.03 (m, 1H), 6.71 (m, 1H), 6.59 (s, 1H, N*H*), 6.23 (d, J = 8 Hz, 1H), 3.25 (sept, J = 7 Hz, 2H), 1.17 (m, 12H). ^{13}C {^{1}H} NMR ($CDCl_3$, 100 MHz, 295 K): δ 156.91, 155.19, 149.73, 147.88, 144.32, 136.63, 135.77, 134.36, 128.95, 127.38, 124.89, 123.86, 121.22, 117.17, 116.72, 111.93, 28.42, 24.84, 23.14.

*N^1-(2,6-diethylphenyl)-N^2-(2-pyridylimino)phenylenediamine (**3-Et**).* A 1 mL solution of 2-pyridinecarboxaldehyde (390 mg, 3.7 mmol) in CH_2Cl_2 was added dropwise to a slurry containing N-(2-aminophenyl)-2,6-diethylaniline (**1-Et**) (0.88 g, 3.7 mmol) and $MgSO_4$ (1.32 g, 11 mmol) in 10 mL CH_2Cl_2. The reaction immediately turned bright yellow and was left to stir at room temperature for 1 h. After this time the reaction was filtered and solvent removed under vacuum leaving a sticky orange solid (1.1 g, 92%). ^{1}H NMR ($CDCl_3$, 400 MHz, 295K, δ): 8.81 (s, 1H, imineC-*H*), 8.72 (d, J = 5 Hz, 1H), 8.25 (d, J = 8 Hz, 1H), 7.80 (t, J = 8 Hz, 1H), 7.36 (m, 1H), 7.21 (m, 4H), 7.02 (t, J = 8 Hz, 1H), 6.71 (t, J = 8 Hz, 1H), 6.63 (s, 1H, -N*H*-), 6.22 (d, J = 8 Hz, 1H), 2.64 (m, 4H, -CH_2), 1.17 (t, J = 7 Hz, -CH_3). ^{13}C {^{1}H} NMR ($CDCl_3$,

125 MHz, 295K): δ 156.86, 155.15, 149.71, 143.58, 142.99, 137.34, 136.62, 134.61, 128.94, 126.83, 126.72, 124.89, 121.25, 117.29, 116.73, 111.83, 24.90, 14.97.

N-(2-nitrophenyl)-tert-butylamine. To a solution of 1-fluoro-2-nitrobenzene (5.0 g, 35 mmol) in 75 mL DMF was added tert-butylamine (13.0 g, 177 mmol). The reaction was heated to reflux with stirring under argon. After stirring for 16 h the bright orange solution was poured over brine (250 mL) and extracted with ethyl acetate (4 x 50 mL). Volatiles were removed under vacuum and excess DMF was removed by vacuum distillation at 60 ^{o}C (0.1 mTorr) leaving N-(2-nitrophenyl)-tert-butylamine (6.2 g, 90 %) as an intensely colored orange oil. ^{1}H NMR ($CDCl_3$, 400 MHz, 295 K, δ): 8.41 (s, 1H, N-*H*), 8.18 (m, 1H), 7.37 (m, 1H), 7.10 (m, 1H), 6.59 (m, 1H), 1.51 (s, 9H, -C(C*H*$_3$)$_3$).

*N-(2-aminophenyl)-tert-butylamine (**2-^{t}Bu**).* To a solution of N-(2-nitrophenyl)-tert-butylamine (11.6 g, 59.7 mmol) in 100 mL ethanol was added Raney Ni (2.5 g slurry in water). The solution was degassed and 1 atm H_2 was placed over solution. The solution was left to stir at room temperature until the intense orange color had gone away at which point the Raney Ni was removed by filtration. Volatiles were removed under vacuum leaving N-(2-aminophenyl)-tert-butylamine (**2-^{t}Bu**) (9.0 g, 92 %) as a dark red oil. ^{1}H NMR ($CDCl_3$, 400 MHz, 295 K, δ): 6.92 (m, 1H), 6.74 (m, 3H), 3.60 (s, 2H, -N*H*$_2$), 2.72 (s, 1H, -N*H*-), 1.30 (s, 9H, -C(C*H*$_3$)$_3$).

N-(2-nitrophenyl)-isopropylamine. Isopropylamine (29.3 g, 500 mmol), 1-fluoro-2-nitrobenzene (7.0 g, 50 mmol), and potassium carbonate (4.80 g, 34.7 mmol) were combined in 56 mL acetonitrile. The reaction was heated to reflux in air. After stirring overnight the solution was bright orange. The reaction was cooled to room

temperature, filtered, and volatiles were removed under vacuum. To the orange oil was added 60 mL water and 50 mL ethyl acetate. The organic layer was isolate and the aqueous layer extracted with ethyl acetate (2 x 30 mL). Combined organics fractions were dried over sodium sulfate, filtered, and volatiles removed leaving N-(2-nitrophenyl)-isopropylamine (8.6 g, 96%) as a bright orange oil. ^{1}H NMR ($CDCl_3$, 400 MHz, 295 K, δ): 8.16 (m, 1H), 8.02 (s, 1H, -N*H*-), 7.41 (m, 1H), 6.60 (m, 1H), (sept, J = 7 Hz, 1H, -C*H*-$(CH_3)_2$), 1.33 (d, J = 7 Hz, 6H, -CH(C*H*$_3)_2$).

*N-(2-aminophenyl)-isopropylamine (**2-^{i}Pr**).* In a flask containing N-(2-nitrophenyl)-isopropylamine (8.6 g, 48 mmol) and 75 mL ethanol was added Raney Nickel (2.5 g slurry in water). The solution was placed under vacuum and 1 atm H_2 was placed over the solution. The solution was stirred at room temperature, adding more H_2 as necessary. When the bright orange color of the solution had dissipated, the reaction was degassed before filtering to remove any remaining Raney Nickel. Volatiles were removed under vacuum to leave N-(2-aminophenyl)-isopropylamine (**2-^{i}Pr**) (6.52 g, 91 %) as a dark red oil. ^{1}H NMR ($CDCl_3$, 400 MHz, 295 K, δ): 6.81 (m, 1H), 6.67 (m, 3H), 3.59 (sept, J = 6 Hz, 1H, -C*H*-$(CH_3)_2$), 3.29 (s, 2H, -N*H*$_2$), 3.18 (s, 1H, -N*H*-), 1.23 (d, J = 6 Hz, 6H, -CH(C*H*$_3)_2$).

*(bis-trimethylsilylamide) chromium N^1-(2,6-diisopropylpehnyl)-N^2-(2-pyridylimino)phenylenediamine (**5-Cr**).* To a 50 mL flask charged with **3-^{i}Pr** (518 mg, 1.45 mmol) and $C[N(TMS)_2]_2(THF)_2$ (750 mg, 1.45 mmol) at -78 ^{o}C was added 25 mL benzene. The flask was allowed to warm to ambient temperature and the deep red solution was stirred for 14 h. The solution was filtered, washed until colorless, and concentrated. **5-Cr** was isolated as a burgundy solid by filtering in diethyl ether (530

mg, 64%). ^{1}H NMR (C_6D_6, 400 MHz, 295 K, δ): 51.78 ($\nu_{1/2}$ = 3000 Hz, 14H), 35.97 ($\nu_{1/2}$ = 850 Hz, 1H), 10.24 ($\nu_{1/2}$ = 260 Hz, 2H), 5.10 ($\nu_{1/2}$ = 1240 Hz, 18H), -7.69 ($\nu_{1/2}$ = 750 Hz, 1H), -27.17 ($\nu_{1/2}$ = 500 Hz, 1H), -46.45 ($\nu_{1/2}$ = 760 Hz, 1H), -53.15 ($\nu_{1/2}$ = 1100 Hz, 1H). μ_{eff} (Evans): 4.7 μ_B.

*(bis-trimethylsilylamide) iron N^1-(2,6-diisopropylphenyl)-N^2-(2-pyridylimino)phenylenediamine (**5-Fe**).* To a 25 mL flask charged with **3-^{i}Pr** (260 mg, 0.727 mmol) and Fe[N(TMS)$_2$](THF) (326 mg, 0.727 mmol) at -78 ^{o}C was added 10 mL benzene. The reaction was warmed and the intense blue/green solution was stirred at ambient temperature for 16 h. Volatiles were removed under vacuum and 15 mL diethyl ether was added. The solution was filtered, washed, and concentrated. **5-Fe** was collected as a dark blue solid by filtering in cold hexanes (290 mg, 70%). ^{1}H NMR (C_6D_6, 400 MHz, 295 K, δ): 124.25 ($\nu_{1/2}$ = 510 Hz, 1H), 57.06 ($\nu_{1/2}$ = 210 Hz, 1H), 52.52 ($\nu_{1/2}$ = 220 Hz, 1H), 51.51 ($\nu_{1/2}$ = 87 Hz, 1H), 44.12 ($\nu_{1/2}$ = 72 Hz, 1H), 29.62 ($\nu_{1/2}$ = 67 Hz, 1H), 18.36 ($\nu_{1/2}$ = 72 Hz, 1H), 13.23 ($\nu_{1/2}$ = 36 Hz, 2H), 11.14 ($\nu_{1/2}$ = 90 Hz, 6H), 0.89 ($\nu_{1/2}$ = 270 Hz, 18H), -26.55 ($\nu_{1/2}$ = 55 Hz, 1H), -30.26 ($\nu_{1/2}$ = 115 Hz, 6H), -31.82 ($\nu_{1/2}$ = 46 Hz, 1H), -34.39 ($\nu_{1/2}$ = 540 Hz, 1H). μ_{eff} (Evans): 4.9 μ_B.

*(bis-trimethylsilylamide) iron N^1-(2,6-diisopropylphenyl)-N^2-(2-pyridylimino)phenylenediamine (**5-Co**).* To a 25 mL flask charged with **3-^{i}Pr** (364 mg, 1.02 mmol) and Co[N(TMS)$_2$](THF) (460 mg, 1.02 mmol) at -78 ^{o}C was added 20 mL benzene. The reaction was warmed and the intense green solution was stirred at ambient temperature for 16 h. Volatiles were removed under vacuum and 15 mL diethyl ether was added. The solution was filtered, washed, and concentrated. **5-Co**

was collected as a dark green solid by filtering in cold pentane (500 mg, 85%). ^{1}H NMR (C_6D_6, 400 MHz, 295 K, δ): 126.58 ($\nu_{1/2}$ = 140 Hz, 1H), 83.39 ($\nu_{1/2}$ = 85, 1H), 72.01 ($\nu_{1/2}$ = 125 Hz, 1H), 49.25 ($\nu_{1/2}$ = 640 Hz, 1H), 46.97 ($\nu_{1/2}$ = 76 Hz, 1H), 44.03 ($\nu_{1/2}$ = 37 Hz, 1H), 42.87 ($\nu_{1/2}$ = 65 Hz, 2H), 27.62 ($\nu_{1/2}$ = 57 Hz, 6H), 11.94 ($\nu_{1/2}$ = 68 Hz, 1H), -3.32 ($\nu_{1/2}$ = 57 Hz, 1H), -11.95 ($\nu_{1/2}$ = 37 Hz, 1H), -12.73 ($\nu_{1/2}$ = 105 Hz, 6H), -14.53 ($\nu_{1/2}$ = 144 Hz, 18H), -22.52 ($\nu_{1/2}$ = 68 Hz, 1H). μ_{eff} (Evans): 4.4 μ_B.

*N^1-(2,6-diisopropylphenyl)-N^2-(2-pyridylimino)phenylenediamine iron bromide (**6-Fe**).* A 4 dram scintillation vial was charged with **3-^{i}Pr** (338 mg, 0.945 mmol) and $FeBr_2(THF)_2$ (340 mg, 0.945 mmol) and 7 mL THF was added. The deep red solution was stirred at room temperature for 2 hours before LiHMDS (158 mg, 0.945 mmol) was added. The intense blue solution was stirred 12 h and filtered. The blue solid was triturated with benzene and the solid was collected by filtration from benzene (302 mg, 65%). ^{1}H NMR (THF- d_8, 400 MHz, 295 K, δ): 86.21 ($\nu_{1/2}$ = 160 Hz, 1H), 47.57 ($\nu_{1/2}$ = 190 Hz, 1H), 44.63 ($\nu_{1/2}$ = 75 Hz, 1H), 32.07 ($\nu_{1/2}$ = 65 Hz, 2H), 28.97 ($\nu_{1/2}$ = 150 Hz, 1H), 23.25 ($\nu_{1/2}$ = 190 Hz, 1H), 20.66 ($\nu_{1/2}$ = 1000 Hz, 1H), 10.68 ($\nu_{1/2}$ = 270 Hz, 1H), 9.60 ($\nu_{1/2}$ = 90 Hz, 6H), 7.28 ($\nu_{1/2}$ = 45 Hz, 1H), -6.10 ($\nu_{1/2}$ = 200 Hz, 6H), -9.18 ($\nu_{1/2}$ = 121 Hz, 1H), -22.54 ($\nu_{1/2}$ = 60 Hz, 1H).

*N^1-(2,6-diisopropylphenyl)-N^2-(2-pyridylimino)phenylenediamine nickel chloride (**6-Ni**).* A 4 dram scintillation vial was charged with **3-^{i}Pr** (515 mg, 1.44 mmol) and $NiCl_2$(DME) (446 mg, 1.44 mmol) and 7 mL THF was added. The resulting red solution was stirred 2 hours before LiHMDS (241 mg, 1.44 mmol) was added producing a deep red solution. After stirring for 12 h at ambient temperature,

the reaction was filtered and concentrated. Benzene was added and the red solid collected by filtration (530 mg, 82%). ^{1}H NMR (C_6D_6, 400 MHz, 295 K, δ): 8.14 (m, 1H), 7.25 (m, 3H), 6.30 (m, 3H), 5.85 (m, 3H), 5.66 (d, J = 9 Hz, 1H), 5.57 (m, 1H), 4.65 (sept, J = 7 Hz, 2H), 1.83 (d, J = 7 Hz, 6H), 1.40 (d, J = 7 Hz, 6H). ^{13}C {^{1}H} NMR (C_6D_6, 125 MHz, 295 K): δ 166.27, 158.48, 152.77, 146.64, 144.18, 142.79, 139.38, 134.91, 133.23, 128.35, 126.13, 124.75, 123.88, 117.60, 117.24, 112.79, 29.22, 24.85, 24.53.

N^1-(2,6-diisopropylphenyl)-N^2-(2-pyridylmethyl)phenylenediamine nickel (7). A 10 mL flask was charged with **6-Ni** (30 mg, 0.067 mmol) and 2 mL THF. Lithium superhydride (0.073 mL, 0.073 mL) was added at -78 ^{o}C as a 1.0 M solution in THF. The solution immediately turned black in color which changed to maroon after 1 h at room temperature. After stirring overnight at ambient temperature solvent was removed. A crude ^{1}H NMR spectrum was acquired and showed resonances consistent with ligand reduction and formation of **7** in modest yield. Poor resolution of the NMR spectrum precluded formal assignment. ^{1}H NMR (C_6D_6, 400 MHz, 295 K): δ 7.82 (1H), 7.36 (1H), 6.82 (1H), 6.68 (1H), 6.60 (1H), 6.31 (1H), 6.20 (1H), 6.07 (1H), 5.95 (1H), 4.45 (1H), 4.27 (1H), 3.20 (1H), 2.60 (1H), 1.70 (3H), 1.53 (1H), 1.30 (3H), 1.22 (3H).

*NMR scale synthesis of N^1-(2,6-diisopropylphenyl)-N^2-(2-pyridylimino)phenylenediamine iron methyl (**10**).* A small vial was charged with **3-^{i}Pr** (11 mg, 0.031 mmol) and $FeMe_2(PMe_3)_4$ (12 mg, 0.031 mmol). 0.5 mL C_6D_6 was added and the solution instantly turned dark purple. After 30 min the reaction was filtered into a J. Young tube and reaction progress was monitored by ^{1}H NMR

spectroscopy. After 40 minutes complete conversion was observed to a new paramagnetic product (**10**). ^{1}H NMR (C_6D_6, 400 MHz, 295 K, δ): 99.91 ($\nu_{1/2}$ = 300 Hz, 1H), 65.93 ($\nu_{1/2}$ = 94 Hz, 1H), 50.62 ($\nu_{1/2}$ = 125 Hz, 1H), 42.22 ($\nu_{1/2}$ = 230 Hz, 12H), 31.08 ($\nu_{1/2}$ = 60 Hz, 1H), 28.08 ($\nu_{1/2}$ = 100 Hz, 1H), 23.11 ($\nu_{1/2}$ = 50 Hz, 1H), 19.14 ($\nu_{1/2}$ = 460 Hz, 1H), 16.22 ($\nu_{1/2}$ = 75 Hz, 1H), 14.09 ($\nu_{1/2}$ = 75 Hz, 1H), 4.50 ($\nu_{1/2}$ = 115 Hz, 3H), -1.26 ($\nu_{1/2}$ = 180 Hz, 3H), -25.38 ($\nu_{1/2}$ = 115 Hz, 1H), -40.69 ($\nu_{1/2}$ = 100 Hz, 1H).

*N^1-(2,6-diisopropylphenyl)-N^2-(2-pyridylmethyl)phenylenediamine (**8**).* To a 50 mL flask charged with **3-^{i}Pr** (750 mg, 2.10 mmol) and sodium borohydride (317 mg, 8.39 mmol) was added 13 mL methanol at 0 ^{o}C. The ice bath was allowed to slowly warm to room temperature. After 4 h stirring the solution was cloudy and the bright orange color of **3-^{i}Pr** had dissipated. Residual sodium borohydride was quenched with water then 1 M HCl. The aqueous layer was extracted with dichloromethane and the organic layer was washed with brine and dried over sodium sulfate. Solvent was removed under vacuum leaving a white solid (580 mg, 77%). ^{1}H NMR ($CDCl_3$, 400 MHz, 295 K, δ): 8.68 (d, J = 5 Hz, 1H), 7.99 (m, 1H), 7.65 (d, J = 8 Hz, 1H), 7.50 (m, 1H), 7.22 (m, 3H), 6.66 (m, 3H), 6.24 (d, J = 7 Hz), 4.82 (s, 2H), 3.12 (sept, J = 7 Hz, 2H), 1.21 (m, 6H), 1.08 (m, 6H).

*N^1-(2,6-diisopropylphenyl)-N^2-(2-pyridylmethyl)phenylenediamine iron dicarbonyl (**9**).* A 10 mL round bottom flask was charged with $Fe[N(TMS)_2]_2(THF)$ (37 mg, 0.083 mmol) and **reduced ligand** (30 mg, 0.083 mmol). THF (3mL) was frozen over the solid and 1 atm CO was placed over the solution. The reaction was warmed to room temperature and the grey solution is stirred 8 h. Volatiles were

removed and the solid was triturated with benzene to remove residual THF. Assay of the reaction by ^{1}H NMR spectroscopy revealed 1 diamagnetic product. ^{1}H NMR (C_6D_6, 400 MHz, 295 K, δ): 7.88 (m, 1H), 7.31 (m, 1H), 7.24 (m, 1H), 7.08 (m, 1H), 6.96 (m, 1H), 6.75 (m, 1H), 6.57 (m, 1H), 6.26 (m, 1H), 6.02 (m, 1H), 4.65 (s, 2H, -C*H*$_2$-), 3.13 (sept, J = 7 Hz, -C*H*-$(CH_3)_2$), 1.48 (d, J = 7 Hz, -C*H*$_3$), 1.03 (d, J = 7 Hz, -C*H*$_3$). IR (C_6D_6): ν_{CO} = 1984 cm^{-1}, 1919 cm^{-1}.

REFERENCES

(1) Bart, S. C.; Lobkovsky, E.; Chirik, P. J. *J. Am. Chem. Soc.* **2004**, *126*, 13794–13807.

(2) Tondreau, A. M.; Atienza, C. C. H.; Weller, K. J.; Nye, S. A.; Lewis, K. M.; Delis, J. G. P.; Chirik, P. J. *Science* **2012**, *335*, 567–570.

(3) Zarkesh, R. A.; Ziller, J. W.; Heyduk, A. F. *Angew. Chem. Int. Ed.* **2008**, *47*, 4715–4718.

(4) Munhá, R. F.; Zarkesh, R. A.; Heyduk, A. F. *Inorg. Chem.* **2013**, *52*, 11244–11255.

(5) Langer, R.; Leitus, G.; Ben-David, Y.; Milstein, D. *Angew. Chem. Int. Ed.* **2011**, *50*, 2120–2124.

(6) Zhang, P.; Terefenko, E. A.; Bray, J.; Deecher, D.; Fensome, A.; Harrison, J.; Kim, C.; Koury, E.; Mark, L.; McComas, C. C.; Mugford, C. A.; Trybulski, E. J.; Vu, A. T.; Whiteside, G. T.; Mahaney, P. E. *J. Med. Chem.* **2009**, *52*, 5703–5711.

(7) Xia, C.; Kwong, R.; Rayabarapu, D.; Ma, B. Phosphorescent Emitters. US2010141127 (A1), June 10, 2010.

(8) Jaekel, S.; Murfin, S.; Taylor, S.; Aicher, B.; Kelter, A.-R.; Coulter, T. Thienopyrimidines for Pharmaceutical Compositions. WO2006136402 (A1), December 28, 2006.

(9) Benington, F.; Shoop, E. V.; Poirier, R. H. *J. Org. Chem.* **1953**, *18*, 1506–1510.

(10) G. Smith, J.; Ho, I. *Tetrahedron Lett.* **1971**, *12*, 3541–3544.

(11) Evans, D. F. *J. Chem. Soc. Resumed* **1959**, 2003–2005.

(12) Bain, G. A.; Berry, J. F. *J. Chem. Educ.* **2008**, *85*, 532.

(13) Carlin, R. L. *Magnetochemistry*; Springer-Verlag: New York, 1986.

(14) Morris, W. D.; Wolczanski, Peter T.; Sutter, Jorg; Meyer, Karsten; Cundari, Thomas R.; Lobkovsky, Emil B. *Inorg. Chem.* **2014**.

(15) De Angelis, S.; Solari, E.; Gallo, E.; Floriani, C.; Chiesi-Villa, A.; Rizzoli, C. *Inorg. Chem.* **1996**, *35*, 5995–6003.

(16) Franceschi, F.; Solari, E.; Scopelliti, R.; Floriani, C. *Angew. Chem. Int. Ed.* **2000**, *39*, 1685–1687.

(17) Billman, J. H.; Diesing, A. C. *J. Org. Chem.* **1957**, *22*, 1068–1070.

(18) Horvath, B.; Strutz, J.; Horvath, E. G. *Z. Für Anorg. Allg. Chem.* **1979**, *457*, 38–50.

(19) Horvath, B.; Moeseler, R.; Horvath, E. G. *Z. F□r Anorg. Allg. Chem.* **1979**, *450*, 165–177.

(20) Olmstead, M. M.; Power, P. P.; Shoner, S. C. *Inorg. Chem.* **1991**, *30*, 2547–2551.

(21) Bryan, A. M.; Long, G. J.; Grandjean, F.; Power, P. P. *Inorg. Chem.* **2013**, *52*, 12152–12160.

(22) Ward, L. G. L.; Pipal, J. R. In *Inorganic Syntheses*; Cotton, F. A., Ed.; John Wiley & Sons, Inc.: Hoboken, NJ, USA, 1972; Vol. 13, pp. 154–164.

(23) Karsch, H. H. *Chem. Ber.* **1977**, *110*, 2699–2711.

CHAPTER 3

Iron and Chromium Complexes Containing Tridentate Chelates Based on Nacnac and Imino- and Methyl-Pyridine Components: Triggering C-X Bond Formation[‡]

I. Introduction

Carbon-carbon bond formation has been observed with ligands that contain the 2-azaallyl functionality. Transition metal complexes bearing the smif (smif = di-2-pyridyl-2-azaallyl) ligand have exhibited ligand centered reactivity reminiscent of nucleophilic as well as singlet diradical character. A rationale for this reactivity can be seen in Figure 3.1 with the expansion of the wave function of the CNC non-bonding orbital. The diradical portion is responsible for the dimerization of (smif)FeN(TMS)$_2$ in the solid state while the ionic component explains the nucleophilic behavior observed in the reaction of (smif)$_2$Fe with isocyanates (Figure 3.2).[1–3]

[‡] Reproduced with permission from: Morris, W. D.; Wolczanski, P. T.; Sutter, J.; Meyer, K.; Cundari, T. R.; Lobkovsky, E. B. *Inorg. Chem.* **2014,** *Accepted.*

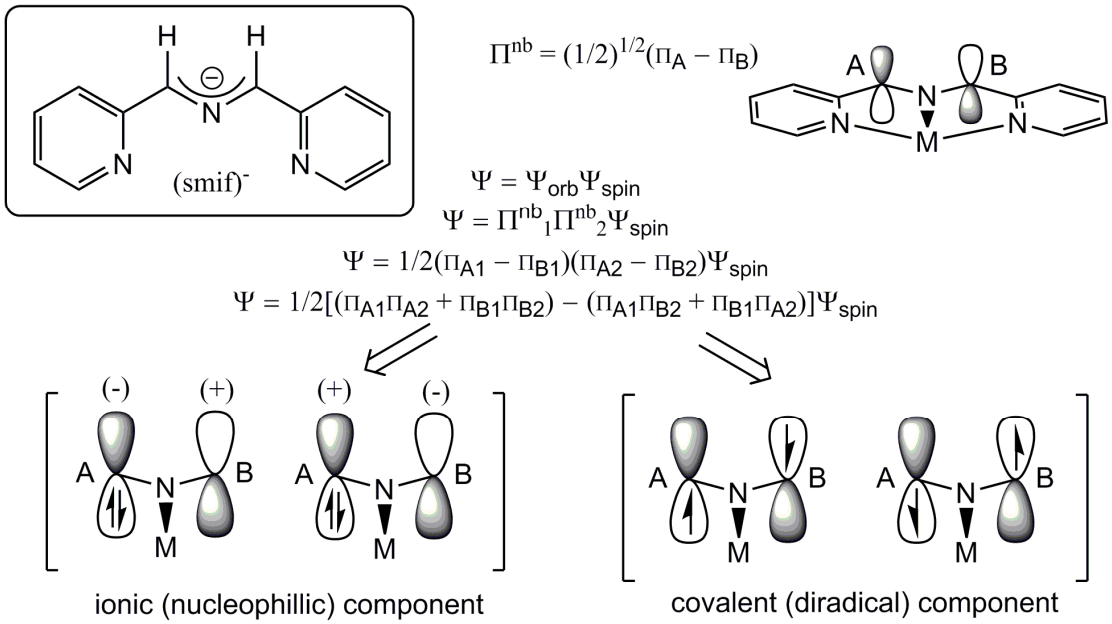

Figure 3.1. Expansion of the orbital component of the smif CNC backbone. Orbitals are denoted (A & B) and electrons (1 & 2).

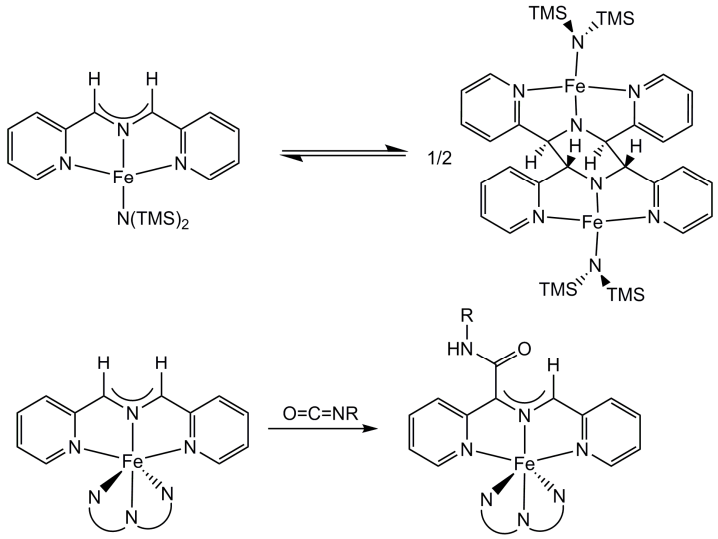

Figure 3.2. Dimerization of (smif)FeN(TMS)$_2$ in the solid state and reaction of (smif)$_2$Fe with an organic isocyanate.

Deprotonation of the diimine ligand of {Me$_2$C(CH=NCH$_2$py)}M (M = Cr, Co, Ni) with dibasic metal precursor resulted in formation of 3 new carbon-carbon bonds. Initial deprotonation forms transient azaallyls which can couple as shown in Scheme

3.1 to form three new bonds in one step.[4] The lower pKa of the benzilic proton allows for a more facile deprotonation to be realized.[5–7]

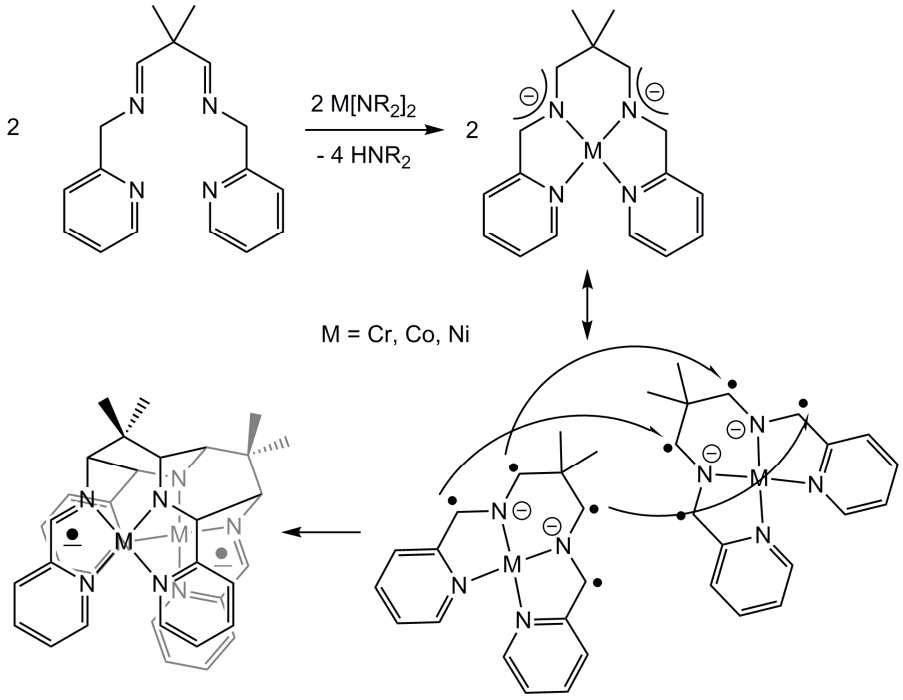

Scheme 3.1. 3 Carbon-carbon bonds formed via radical coupling of putative azaallyls (M = Cr, Co, Ni).

A new nacnac framework was envisioned with incorporation of 2-(aminomethyl)pyridine groups as precursors to azaallyls (Figure 3.3). Instead of observing C-C coupling via azaallyls, new coordination compounds were observed bearing a redox non-innocent ligand. The bis-phosphine {nacnac(CH_2py)(CHpy)}Fe(PR_2R')$_2$ (**A**, PR_2R' = PMe_3, PMe_2Ph) and mono-phosphine {nacnac(CH_2py)(CHpy)}Fe(PR_2R') (**B**, PR_2R' = PMe_2Ph, PPh_3) compounds were observed bearing a ligand that acted as a 2 electron reservoir.[8] Oxidative reactivity at the metal did not show that the 2 ligand electrons could be shuttled back onto the metal, supposedly due to a coordinatively saturated metal center. It was envisioned that replacement of one of the 2-(aminomethyl)pyridine arms

with a substituted aniline would open up a coordination site to reactivity, while retaining the redox non-innocence imparted by the ligand (**C**).

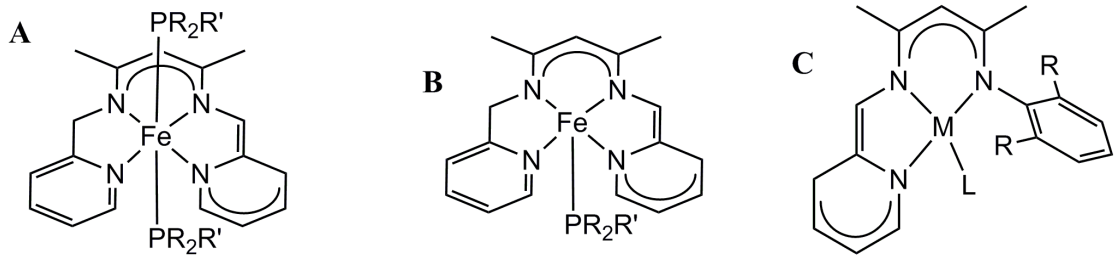

Figure 3.3. Nacnac containing redox non-innocent compounds.

II. Results and Discussion

A. Ligand Synthesis

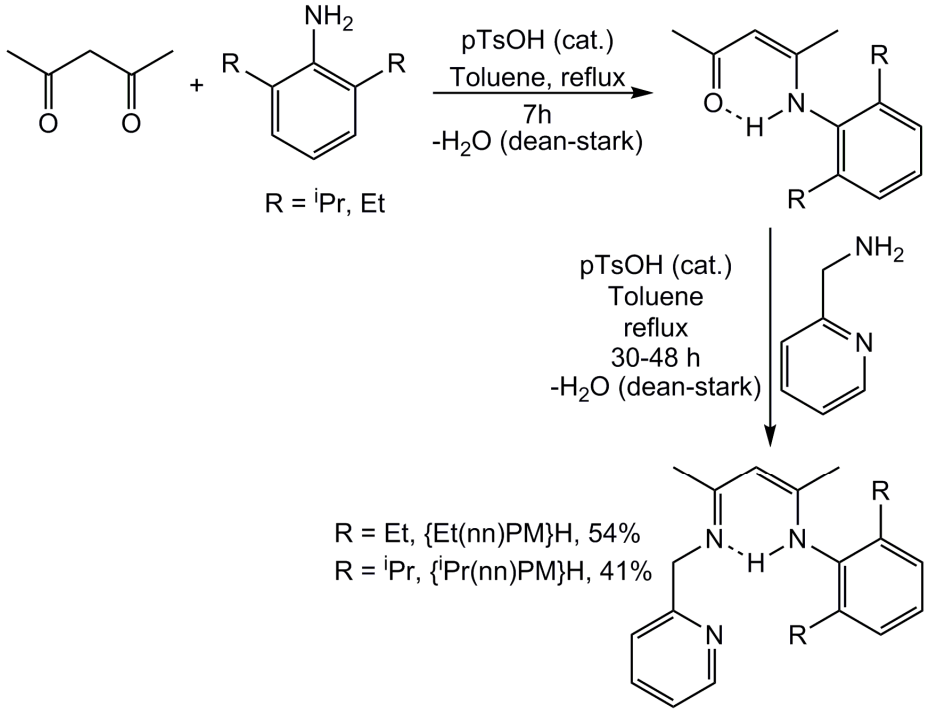

Scheme 3.2. Ligand Synthesis of {R(nn)PM}H, R = Et, iPr.

The tridentate, nacnac based ligands were synthesized through condensation routes according to literature procedures (Scheme 3.2).[9] The isopropyl derivative, {^{i}Pr(nn)PM}H, was crystallized from hot hexanes in 41% yield and the ethyl derivative, {Et(nn)PM}H, was vacuum distilled as an orange oil in 54% yield. Condensation of the respective aniline must be done prior to condensation with 2-picolyamine.

B. Metallation of Ligands

1. Syntheses using M[N(TMS)$_2$](THF)$_x$ (M = Cr, x = 2; M = Fe, Co, x = 1)

Treatment of {^{i}Pr(nn)PM}H with metal bis-amide precursors produced 4-coordinate{^{i}Pr(nn)PM}MN(TMS)$_2$ (**1-M^{iPr}**, M = Cr, Fe) derivatives as maroon and yellow solids, respectively, in good yield (Equation 3.1). The less bulky {Et(nn)PM}H was metallated with Fe and Co to form {Et(nn)PM}MN(TMS)$_2$ (**1-M^{Et}**, M = Fe, Co) as yellow and green solids. Evans magnetic measurements of the 4-coordinate amide compounds showed all to be high spin M(II). **1-Fe^{iPr}**, **1-Fe^{Et}**, and **1-Co^{Et}** had magnetic moments of 5.3 μ_B, 5.3 μ_B, and 4.5 μ_B respectively, which are higher than the spin only value due to spin-orbit coupling, and **1-Cr^{iPr}** exhibited the spin only value of 4.9 μ_B.

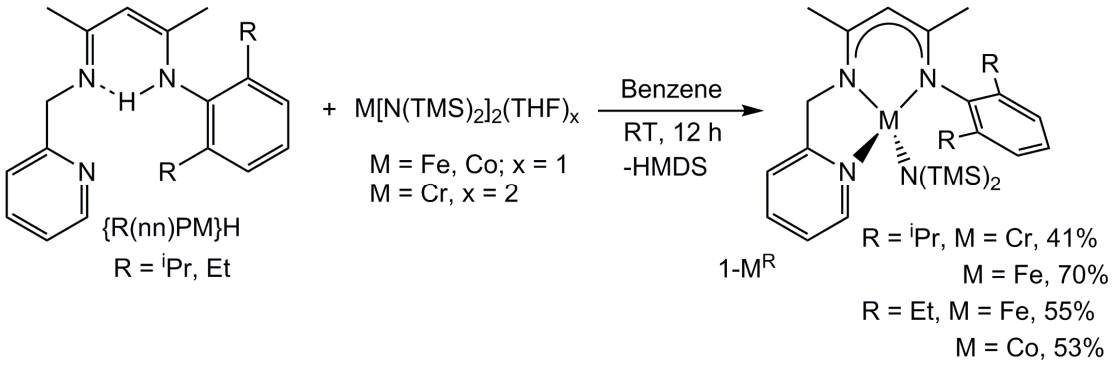

Equation 3.1.

2. Synthesis via salt metathesis

Deprotonation of {R(nn)PM}H with $LiN(TMS)_2$ afforded {R(nn)PM}Li, which produced bright green {R(nn)PM}FeBr (**2-Fe^{R}**) upon treatment with $FeBr_2$ in THF (Scheme 3.3). **2-Fe^{Et}** and **2-Fe^{iPr}** were both shown to be high spin ferrous species by Evans method measurements (5.4 μ_B and 5.0 μ_B respectively). Alkylation of **2-Fe^{R}** with neopentyllithium produced orange iron alkyls {R(nn)PM}Fe^{neo}Pe (R = ^{i}Pr, Et; **3-Fe^{R}**) as high spin ferrous (μ_{eff} = 5.2, **3-Fe^{iPr}**; 5.1, **3-Fe^{Et}**) solids in modest yield.

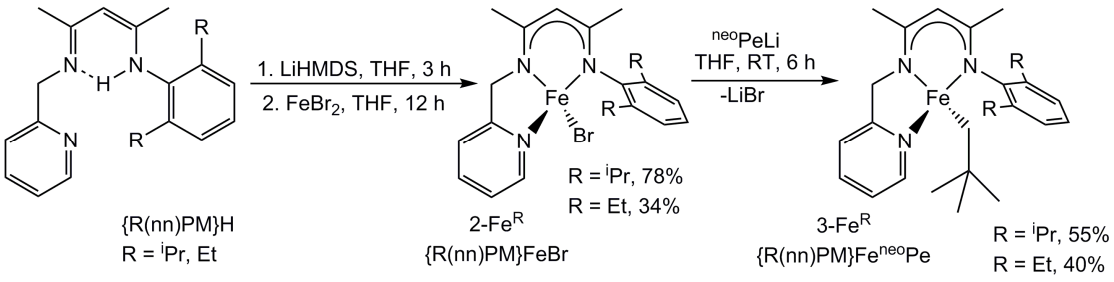

Scheme 3.3. Synthesis of **2-Fe^{R}** and **3-Fe^{R}**.

C. Mössbauer spectra of 1-Fe^{iPr}, 2-Fe^{iPr}, and 3-Fe^{iPr}

Zero field Mössbauer[10] spectra were recorded at 80 K for **1-Fe^{iPr}**, **2-Fe^{iPr}**, and **3-Fe^{iPr}** and the spectra are shown in Figure (3.4). The spectra for the amide and bromide differ very little with isomer shifts of 0.77 mm/s and 0.79 mm/s, respectively, and quadrupole splittings of 1.02 mm/s. The similarity in this data suggests complementary geometry and donor properties between amide and bromide. A significant difference was observed in **3-Fe^{iPr}**, which exhibited an isomer shift of 0.58 mm/s and quadrupole splitting of 1.20 mm/s. The lower isomer shift is consistent with a greater field strength and shorter bonds imposed by the alkyl donor, and the larger quadrupole splitting shows greater asymmetry in electron density about iron indicating deviation towards a square planar environment.

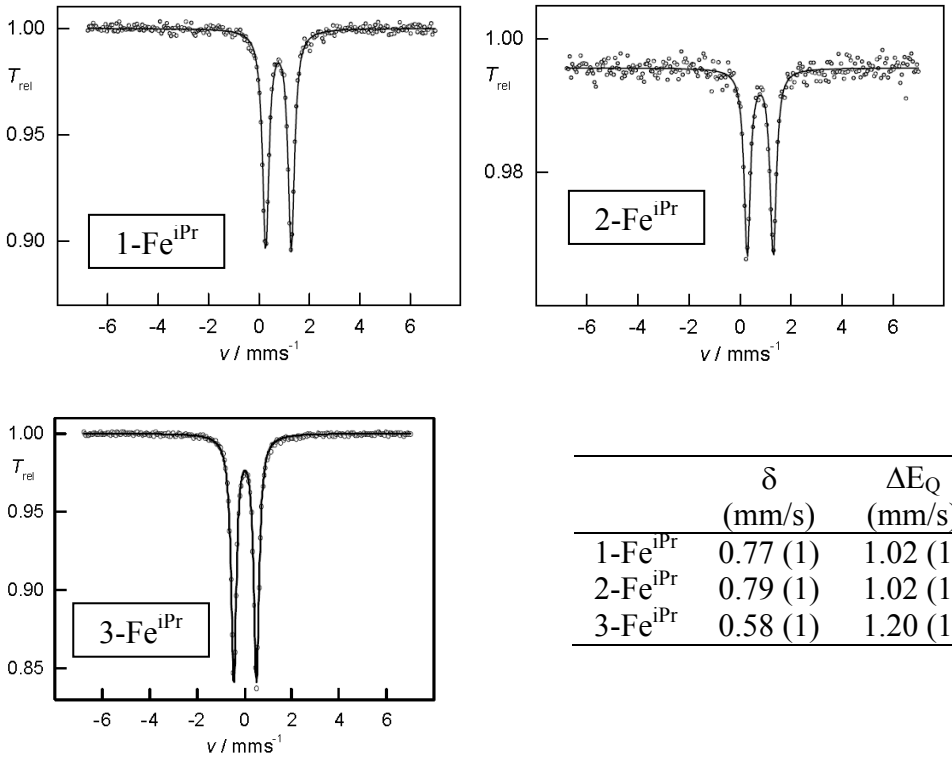

	δ (mm/s)	ΔE_Q (mm/s)	Γ_{FWHM} (mm/s)
1-Fe^{iPr}	0.77 (1)	1.02 (1)	0.30 (1)
2-Fe^{iPr}	0.79 (1)	1.02 (1)	0.28 (1)
3-Fe^{iPr}	0.58 (1)	1.20 (1)	0.27 (1)

Figure 3.4. Mössbauer spectra for **1-Fe^{iPr}**, **2-Fe^{iPr}**, and **3-Fe^{iPr}**.

D. Crystal Structures of {R(nn)PM}MN(TMS)$_2$ (1-M^R; R = ^{i}Pr, M = Fe, Cr; R = Et, M = Co) and {^{i}Pr(nn)PM}FeBr (2-Fe^{iPr}).

Pertinent interatomic distances are given in Table 3.1, and the molecular views are shown in Figure 3.5. The core M-N distances are all within expected ranges with the amides being the shortest bonds and the M-N$_{pyr}$ distance being longer as the weakest donor. Going from **1-Cr^{iPr}** to **1-Fe^{iPr}** to **1-Co^{Et}** the M-N bonds compress following the decrease in covalent radius. The nacnac backbone is symmetric in each compound with d(C2-C3) and d(C3-C4) measuring between 1.39-1.41 Å and d(N1-C2) and d(C4-N2) measuring 1.31-1.34 Å.

Table 3.1. Pertinent interatomic distances (Å) and angles (^{o}) for {R(nn)PM}MN(TMS)$_2$ (**1-M^R**; R = ^{i}Pr, M = Cr, Fe; R = Et, M = Co) and {^{i}Pr(nn)PM}FeBr (**2-Fe^{iPr}**).

	1-Cr^{iPr}	**1-Fe^{iPr}**	**1-Co^{Et}**	**2-Fe^{iPr}**
M-N1	2.076(2)	2.029(2)	1.974(2)	2.007(2)
M-N2	2.045(2)	2.036(2)	1.978(2)	2.030(2)
M-N3	2.120(2)	2.201(2)	2.108(2)	2.127(2)
N-N4/Br	2.071(2)	1.967(2)	1.955(2)	2.4146(3)
N1-C6	1.447(2)	1.446(3)	1.435(3)	1.446(2)
N1-C2	1.337(2)	1.333(3)	1.334(3)	1.335(2)
C2-C3	1.399(3)	1.407(4)	1.401(4)	1.403(2)
C3-C4	1.393(3)	1.393(4)	1.401(4)	1.404(3)
C4-N2	1.331(2)	1.313(4)	1.324(3)	1.320(2)
N2-C18/C16	1.464(2)	1.458(4)	1.452(4)[a]	1.459(2)
C18/C16-C19/C17	1.493(3)	1.495(5)	1.495(4)[a]	1.511(3)
C19/C17-N3	1.343(2)	1.344(3)	1.354(3)[a]	1.341(2)
N4-Si(avg)	1.706(7)	1.708(14)	1.708(2)	
N1-M-N2	90.07(6)	90.08(9)	93.41(9)	92.19(6)
N1-M-N3	156.06(6)	131.56(8)	125.83(9)	141.39(6)
N1-M-N4/Br	106.15(6)	121.89(8)	117.18(9)	111.22(4)
N2-M-N3	78.49(6)	76.87(9)	79.20(9)	78.02(6)
N2-M-N4/Br	152.25(6)	130.84(9)	122.85(9)	145.73(4)
N3-M-N4/Br	93.06(6)	100.56(8)	111.30(9)	96.16(4)

[a]For 1-Co^{Et}, N2-C16, C16-C17, N3-C17 are the corresponding distances.

Table 3.2.	Select crystallographic and refinement data for {R(nn)PM}MN(TMS)$_2$ (R = ^{i}Pr, M = Cr, **1-Cr^{iPr}**; Fe, **1-Fe^{iPr}**; R = Et, M = Co, **1-Co^{Et}**), {^{i}Pr(nn)PM}FeBr (**2-Fe^{iPr}**), and {^{i}Pr(nn)PM}Fe(CO^{neo}Pe)CO (**4-Fe^{iPr}**).				
	1-Cr^{iPr}	**1-Fe^{iPr}**	**1-Co^{Et}**	**2-Fe^{iPr}**	**4-Fe^{iPr}**
formula	$C_{29}H_{48}N_4Si_2Cr$	$C_{29}H_{48}N_4Si_2Fe$	$C_{27}H_{44}N_4Si_2Co$	$C_{23}H_{30}N_3BrFe$	$C_{30}H_{41}N_3O_2Fe$
form wt	560.89	564.74	539.77	484.26	531.51
space gp	P1bar	P1bar	$P2_1/c$	$P2_1/c$	P1bar
Z	2	2	4	4	2
a, Å	11.0716(8)	8.7885(6)	11.9196(4)	12.2363(6)	9.1288(7)
b, Å	11.5269(8)	11.7993(8)	16.2443(5)	11.8702(6)	10.9934(8)
c, Å	15.1284(11)	15.8560(10)	15.5843(5)	15.9743(8)	15.2486(12)
α, deg	91.882(4)	98.584(4)	90	90	85.922(3)
β, deg	109.554(3)	96.286(4)	94.9870(10)	101.9250(10)	88.695(3)
χ, deg	117.60(3)	100.285(4)	90	90	69.620(3)
V, Å^3	1570.97(19)	1583.96(18)	3006.10(17)	2270.2(2)	1430.99(19)
$\rho_{calc.}$ g cm^{-3}	1.186	1.184	1.193	1.417	1.234
m, mm^{-1}	0.464	0.575	0.671	2.437	0.557
temp, K	173(2)	173(2)	193(2)	183(2)	193(2)
λ, Å	0.7103	0.7103	0.7103	0.7103	0.7103
R indices[a,b] [I>2σ(I)	R_1 = 0.0380 wR_2 = 0.0839	R_1 = 0.0456 wR_2 = 0.1269	R_1 = 0.0378 wR_2 = 0.0842	R_1 = 0.0280 wR_2 = 0.0727	R_1 = 0.0348 wR_2 = 0.0920
R Indices[a,b] (all data)	R_1 = 0.0597 wR_2 = 0.0931	R_1 = 0.0731 wR_2 = 0.1418	R_1 = 0.0609 wR_2 = 0.0947	R_1 = 0.0382 wR_2 = 0.0770	R_1 = 0.0469 wR_2 = 0.0984
GOF[c]	1.027	1.034	1.011	1.037	1.067

[a] $R_1 = \Sigma||F_o|-|F_c||/ \Sigma|F_o|$. [b] $wR_2 = [\Sigma w(|F_o| - |F_c|)^2/ SwF_o^2]^{1/2}$. [c] GOF (all data) = $[\Sigma w(|F_o| - |F_c|)^2/ (n-p)]^{1/2}$
n = number of independent reflections, p=number of parameters

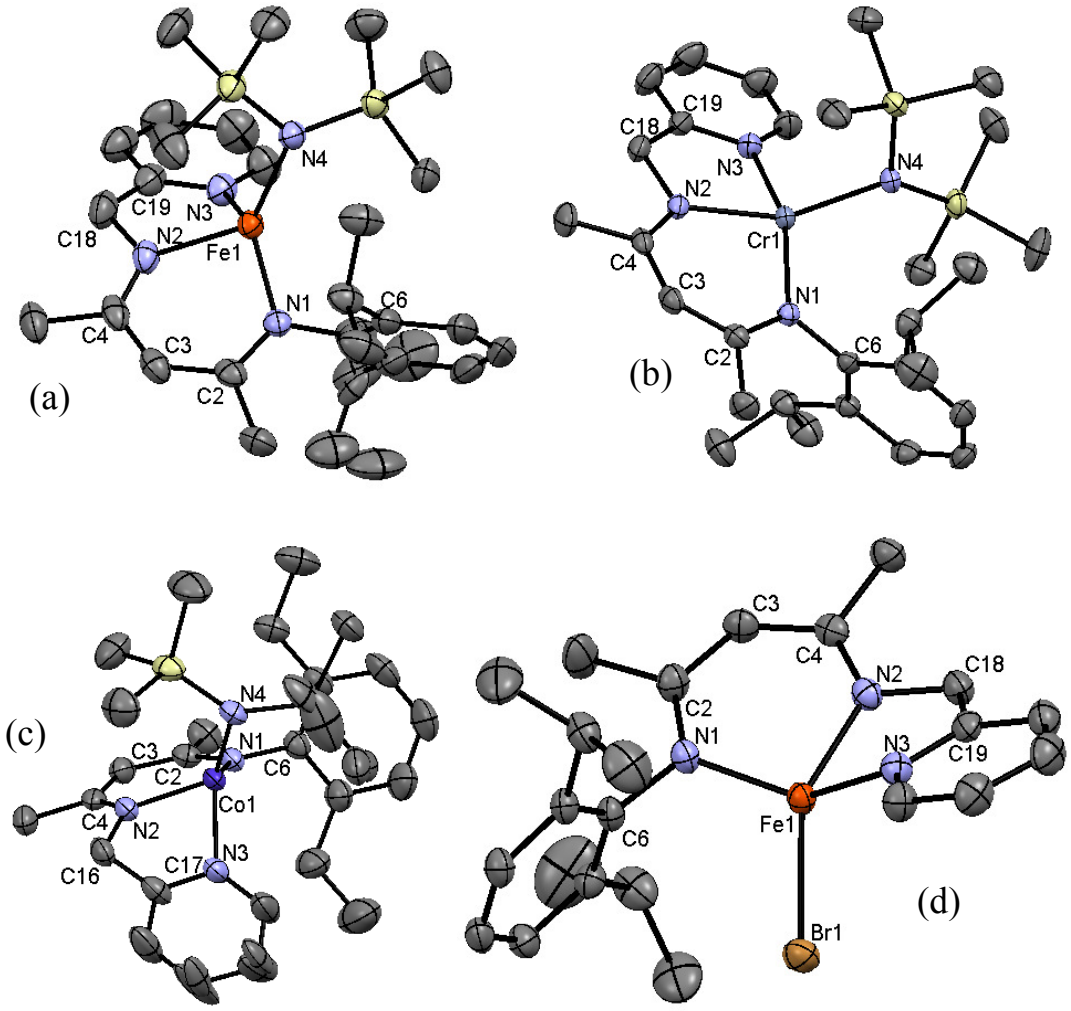

Figure 3.5. Molecular views of (a){^{i}Pr(nn)PM}FeN(TMS)$_2$ (**1-Fe^{iPr}**); (b) {^{i}Pr(nn)PM}CrN(TMS)$_2$ (**1-Cr^{iPr}**); (c) {Et(nn)PM}CoN(TMS)$_2$ (**1-Co^{Et}**), and (d) {^{i}Pr(nn)PM}FeBr (**2-Fe^{iPr}**).

The varying tetrahedral distortion is most pronounced in comparison of the core N1-M-N3 and N2-M-N4 bond angles. The N1-M-N3$_{(py)}$ angle decreases from 156.06^{o} to 131.56^{o} to 125.83^{o} from **1-Cr^{iPr}** to **1-Co^{Et}** with chromium displaying the greatest degree of planarity and cobalt exhibiting the greatest distortion towards tetrahedral. The N2-M-N4 shows similar distortions with angles of 152.25^{o}, 130.84^{o}, and 122.85^{o} for **1-Cr^{iPr}**, **1-Fe^{iPr}**, and **1-Co^{Et}** respectively.

Angular overlap methods were used to quantify the ligand field stabilization attained by each compound through the distortions described above.[11,12] The symmetry adapted linear combinations of the four nitrogen donors make up the sigma bonding orbitals and are stabilized by a total of -4 e_σ. Destabilized by a total energy of 4 e_σ, the d-orbital manifold will manifest sigma antibonding character and the placement of electrons in those orbitals will dictate the net stabilization (Fig. 3.6). Treatment of the electronic stabilization by angular overlap methods required a coordinate axis, so the bite angle (~90°) and planarity enforced by the nacnac backbone made the M-N1 and M-N2 vectors reasonable axis. The methods work in this case under the assumptions that all donors are equal, that π interactions can be ignored, and that the bond distances are equal and give rise to equal overlap with all the ligands.

The geometry associated with {^{i}Pr(nn)PM}CrN(TMS)$_2$ (**1-Cr^{iPr}**) affords the greatest amount of stabilization for d^4 systems because the high energy d_{x2-y2} orbital contributes most of the antibonding character and remains unoccupied. Only minor energetic differences were noted in the structural preferences for compounds with higher d electron counts. The structure of {Et(nn)PM}CoN(TMS)$_2$ (**1-Co^{Et}**) gave the lowest energy for the d^6 species but the sterics imposed by the isopropyl groups of **1-Fe^{iPr}** may prevent convergence to that geometry. Shorter metal-ligand bond distances in **1-Fe^{iPr}** and **1-Co^{Et}** compared to **1-Cr^{iPr}** place an increasing prejudice on steric factors over electronic factors in determining geometry. **1-Co^{Et}** has the shortest metal-ligand bonds and the distorted tetrahedral geometry grants relief of steric repulsions from the compressing of bonds.

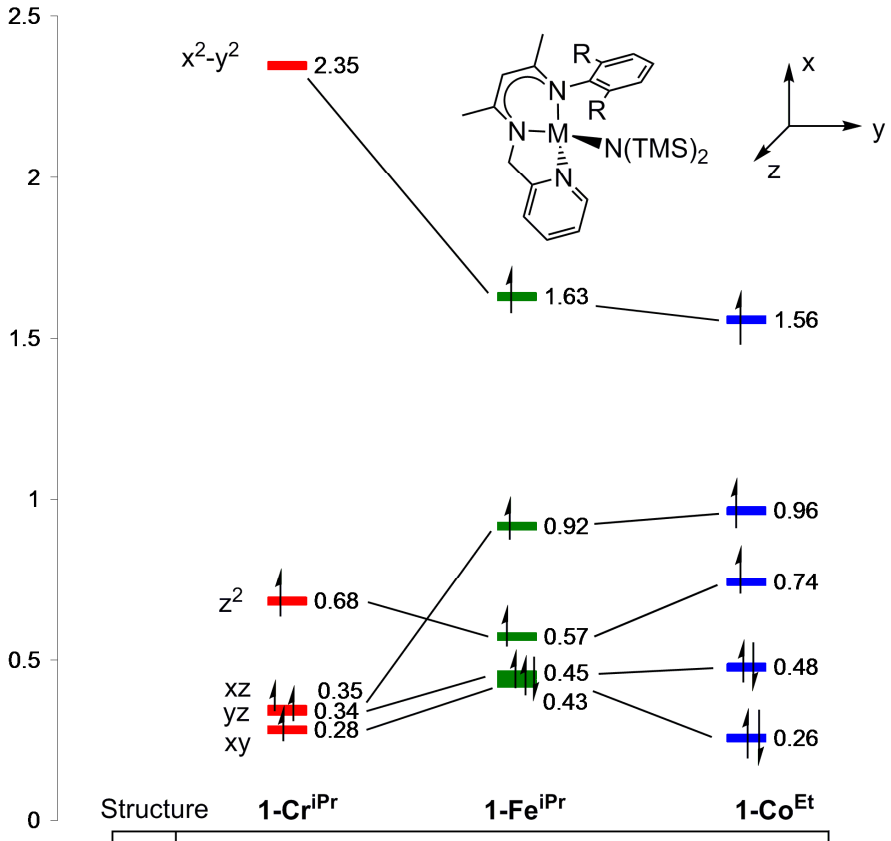

Structure		1-Cr^{iPr}	1-Fe^{iPr}	1-Co^{Et}
d-count	4	-6.35	-5.63	-5.56
	5	-4.00	-4.00	-4.00
	6	-3.72	-3.57	-3.74
	7	-3.38	-3.12	-3.26

Figure 3.6. d-orbital splitting diagrams for **1-Cr^{iPr}**, **1-Fe^{iPr}**, and **1-Co^{Et}** from angular overlap methods. The net stabilization for different d-counts and geometries are calculated and shown below the respective diagram.

D. Carbonylation of {Et(nn)PM}FeN(TMS)$_2$ (1-Fe^{Et}), {^{i}Pr(nn)PM}FeN(TMS)$_2$ (1-Fe^{iPr}), {^{i}Pr(nn)PM}Fe^{neo}Pe (3-Fe^{iPr}).

1. Synthesis of {R(nn)PI}Fe(CO)$_2$ (R = ^{i}Pr, Et) and {^{i}Pr(nn)PI}Fe(CO^{neo}Pe)CO

Previous studies on {PM(nn)PM}FeN(TMS)$_2$ have shown that HN(TMS)$_2$ loss can be triggered with addition of strong L donors such as PMe$_3$ and CO.[8] Treatment of benzene solutions of **1-Fe^{Et}** and **1-Fe^{iPr}** with excess CO resulted in a color change

from yellow to deep red after heating for 8 h at 60°C (Eq. 3.2). Loss of HMDS was observed with formation of a diamagnetic product characterized as {R(nn)PI}Fe(CO)$_2$ (**5-Fe^{R}**, R = Et, ^{i}Pr). The infrared spectrum showed two terminal CO stretches at 1910 and 1971 cm^{-1} for **5-Fe^{iPr}** and two stretches at 1909 and 1960 cm^{-1} for **5-Fe^{Et}**. Attempts to induce the 1,3-elimination with other L-type ligands (PMe_3, pyridine, 2-2'-bypridine, olefins, alkynes, etc.) were unsuccessful.[13,14]

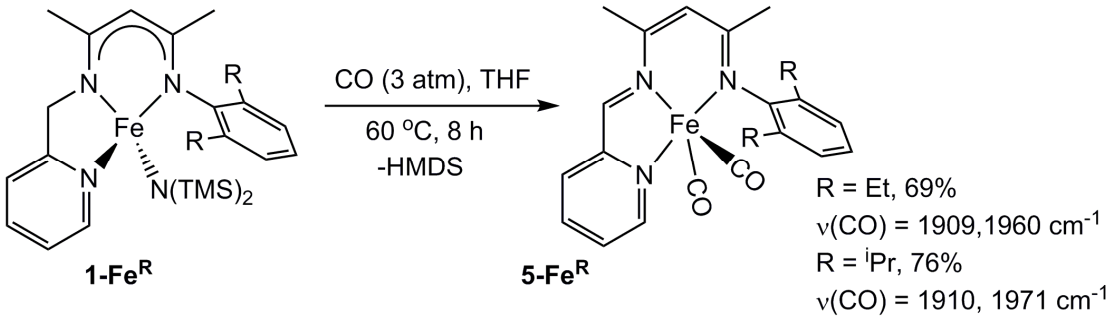

Equation 3.2

Carbonylation of {^{iPr}(nn)PM}Fe^{neo}Pe (**3-Fe^{iPr}**) did not induce 1,3-elimination of neopentane but instead CO inserted into the Fe-alkyl bond to produce {^{i}Pr(nn)PI}Fe(CO^{neo}Pe)CO (**4-Fe-^{iPr}**) in 87% yield (Eq. 3.3). The infrared spectrum exhibits a terminal CO stretch at 1906 cm^{-1} and a stretch at 1638 cm^{-1} corresponding to the newly formed acyl. 1,3-elimination of HMDS from **1-Fe^{R}** was more facile than elimination of ^{neo}PeH from **3-Fe^{iPr}** because binding of CO forces the amide of **1-Fe^{R}** into the apical position and positions the lone pair of the amide adjacent to the proton of the methylene arm, enabling deprotonation.

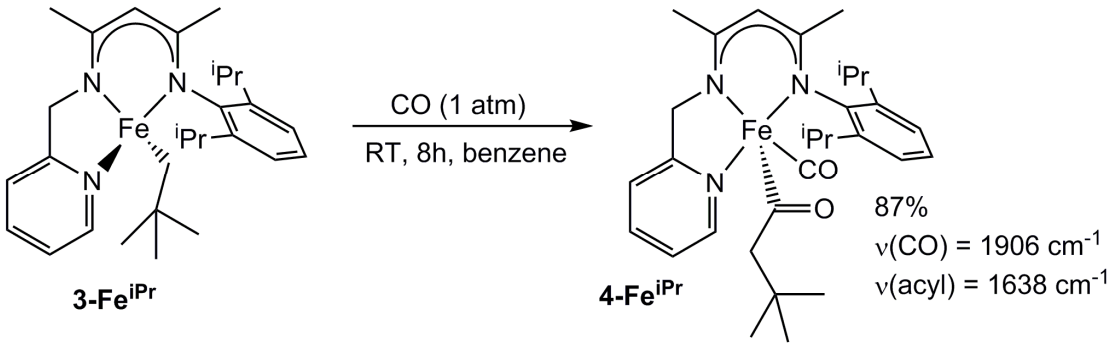

3-Fe^{iPr} **4-Fe^{iPr}**

Equation 1.3

2. Mössbauer spectra of 4-Fe^{iPr} and 5-Fe^{Et}

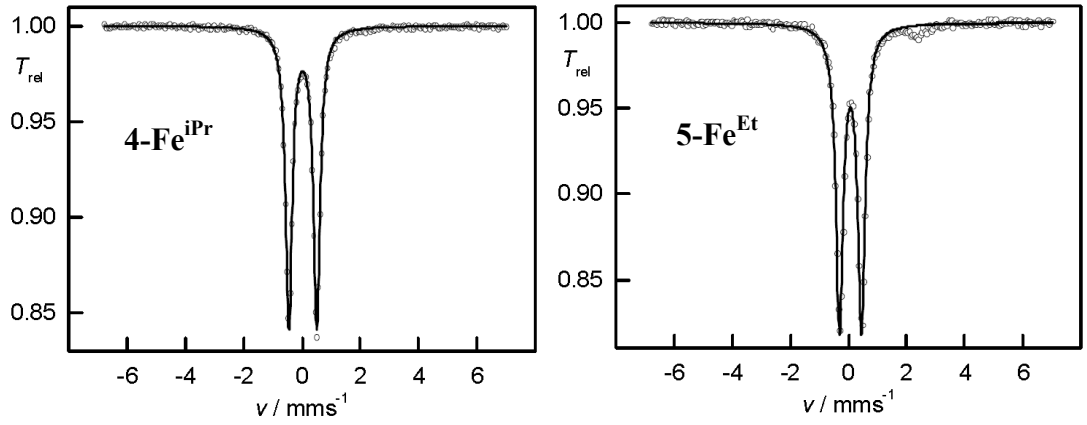

δ (mm/s)	0.03(1)	0.07(1)
ΔE_Q (mm/s)	0.96(1)	0.75(1)
Γ_{FWHM} (mm/s)	0.28(1)	0.30(1)

Figure 3.7. Mössbauer spectra of **4-Fe^{iPr}** (left) and **5-Fe^{Et}** (right).

The zero field Mössbauer spectrum of {^{i}Pr(nn)PM}Fe(CO^{neo}Pe)CO (**4-Fe^{iPr}**) exhibits an isomer shift of δ 0.03(1) mm/s (Figure 3.7), which is low compared to the other Fe(II) compounds presented here and shows a greater amount of covalency consistent with shorter bonds about iron. The ΔE_Q of 0.96(1) mm/s reveals greater asymmetry in the electron density around iron, in concert with a pseudo square

pyramidal geometry. The Mössbauer spectrum of {Et(nn)PI}Fe(CO) (**5-Fe^{Et}**) is similar to that of **4-Fe^{iPr}** with an isomer shift of δ 0.07(1) mm/s and ΔE_Q of 0.75(1) mm/s. The lower isomer shift is consistent with the shorter bonds and greater covalency of **5-Fe^{Et}** in comparison to **1-Fe^{iPr}** and **2-Fe^{iPr}**. The lower quadrupole splitting of **5-Fe^{Et}** indicates greater symmetry about the pseudo square pyramidal metal center in comparison to **4-Fe^{iPr}**.

The Mössbauer spectrum of **5-Fe^{Et}** offers little insight into the formal oxidation state of the metal center as the low isomer shift (δ 0.07) is in the range of the formally Fe^0 compounds, $Fe(CO)_5$ and $Fe(CO)_4PPh_3$.[15–17] However, the nacnac and acyl anions confirm that **4-Fe^{iPr}** is Fe(II) despite the low isomer shift. Increased covalency and shorter bond lengths must be responsible for the lower isomer shift of **4-Fe^{iPr}** and **5-Fe^{Et}** and an unambiguous oxidation state assignment cannot be made from Mössbauer data alone.[18,19] An analogous compound, {nn(PM)(PI)}FeCO, has been shown to have an isomer shift of δ 0.14 mm/s despite assignment as Fe(II) by crystallographic and computational methods.[8]

3. Structural studies of {^{i}Pr(nn)PM}Fe(CO^{neo}Pe)CO (4-Fe^{iPr}) & {^{i}Pr(nn)PI}Fe(CO)$_2$ (5-Fe^{iPr})

The structure of diamagnetic **4-Fe^{iPr}** was confirmed by single crystal X-Ray diffraction and the molecular view is shown in Figure 3.8. The molecule is square pyramidal with the nacnac(PM) and carbonyl ligands occupying the square plane and the neopentyl acyl ligand in the apical position. The core angles about iron vary between 82.05^o and 101.21^o with deviations from ideal (90^o) attributed to geometric constraints enforced by the molecular structure of the ligand. Within the nacnac

backbone, the bond distances are symmetric, and the metal ligand bond distances are all expectedly shorter in **4-Fe^{iPr}** in comparison to the high spin structures of **1-Fe^{iPr}** and **2-Fe^{iPr}**. Strong π-backbonding is noted in the d(Fe-C_{CO}) (1.754 Å) and d(C_{CO}-O) (1.154 Å) and is consistent with the strong covalency observed in the Mössbauer parameters.

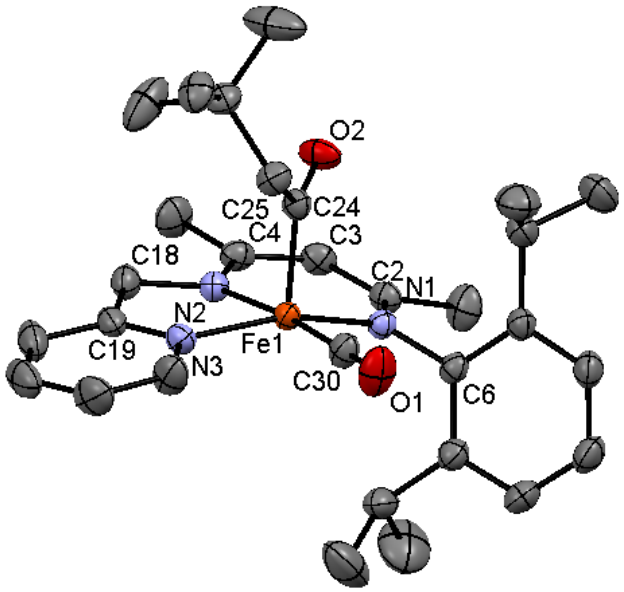

Figure 3.8. Molecular view of {^{i}Pr(nn)PM}Fe(CO^{neo}Pe)CO (**4-Fe^{iPr}**). Selected interatomic distances (Å) and angles (^{o}): Fe-N1, 1.938(2); Fe-N2, 1.926(2); Fe-N3, 1.971(2); Fe-C24, 1.908(2); Fe-C30, 1.754(2); N1-C2, 1.332(2); C2-C3, 1.396(2); C3-C4, 1.385(2); N2-C4, 1.331(2); N2-C18, 1.459(2);C18-C19, 1.486(2); N3-C19, 1.343(2); C24-O2, 1.211(2); C30-O1, 1.154(2); C24-C25, 1.528(2); N1-Fe-N2, 92.16(5); N1-Fe-N3, 162.07(5); N1-Fe-C24, 101.21(5); N1-Fe-C30, 92.82(5); N2-Fe-N3, 82.05(5); N2-Fe-C24, 92.96(5); N2-Fe-C30, 173.07(5); N3-Fe-C24, 96.05(5); N3-Fe-C30, 91.77(6); C24-Fe-C30, 90.79(6); Fe-C24-O2, 116.8(2); Fe-C30-O1, 175.2(2).

The structure of {^{i}Pr(nn)PI}Fe(CO)$_2$ (**5-Fe^{iPr}**, Figure 3.9) was determined by X-Ray crystallography and displays pseudo square pyramidal geometry. The structure of **5-Fe^{iPr}** closely resembles the structure of **4-Fe^{iPr}** with shorter metal-ligand bonds than {^{i}Pr(nn)PM}FeX (X = N(TMS)$_2$, **1-Fe^{iPr}**; Br, **2-Fe^{iPr}**) and Fe-C bonds of 1.779(2) Å and 1.766(2) Å.

Table 3.3. Selected crystallographic and refinement data for {^{i}Pr(nn)PI}Fe(CO)$_2$ (**5-Fe^{iPr}**), {κ^2-N,N-pyrim-pyr}Cr(CO)$_4$ (**6-Cr^{iPr}**), {^{i}Pr(nn)CHpy}$_2$Fe$_2$Cl$_2$ (**7-Fe^{iPr}**), {[Et(nn)CHpy]$_2$} (**8-Fe^{Et}**), and {^{i}Pr(nn)CHpy}$_2$(FeN=CPh$_2$)$_2$.

	5-Fe^{iPr}	**6-Cr^{iPr}**	**7-Fe^{iPr}**	**8-Fe^{Et}**	**9-Fe^{iPr}**
formula	$C_{25}H_{29}N_3O_2Fe$	$C_{39}H_{41}N_3O_4Cr$	$C_{52}H_{64}N_6Cl_2Fe$	$C_{42}H_{50}N_6Fe$	$C_{72}H_{78}N_8O_2Fe_2$
form wt	459.36	667.75	955.69	694.73	1167.12
space gp	P1bar	P1bar	$P2_1/c$	$Pna2_1$	Pbca
Z	2	2	4	4	4
a, Å	8.9026(5)	9.6836(7)	19.371(7)	19.624(2)	18.765(4)
b, Å	9.0638(6)	13.1687(9)	17.597(6)	11.6891(14)	15.7753(3)
c, Å	15.4509(10)	14.8173(10)	16.506(6)	16.0964(17)	21.2437(5)
α, deg	90.636(2)	97.047(2)	90	90	90
β, deg	103.810(2)	102.152(3)	102.446(8)	90	90
χ, deg	110.307(2)	107.505(2)	90	90	90
V, Å^3	11294.41(12)	1726.2(2)	5494(3)	3692.4(7)	6289.5(2)
$\rho_{calc.}$ g cm^{-3}	1.351	1.285	1.155	1.250	1.233
m, mm^{-1}	0.694	0.376	0.662	0.447	0.510
temp, K	173(2)	173(2)	173(2)	173(2)	183(2)
Å	0.71073	0.71073	0.71073	0.71073	0.71073
R indices[a,b] [I>2σ(I)]	$R_1 = 0.0272$ $wR_2 = 0.0754$	$R_1 = 0.0320$ $wR_2 = 0.0868$	$R_1 = 0.0391$ $wR_2 = 0.0896$	$R_1 = 0.0463$ $wR_2 = 0.0722$	$R_1 = 0.0420$ $wR_2 = 0.1020$
R Indices[a,b] (all data)	$R_1 = 0.0310$ $wR_2 = 0.0785$	$R_1 = 0.0368$ $wR_2 = 0.0907$	$R_1 = 0.0618$ $wR_2 = 0.0969$	$R_1 = 0.0914$ $wR_2 = 0.0862$	$R_1 = 0.0744$ $wR_2 = 0.1176$
GOF[c]	1.020	1.030	1.002	0.996	1.011

[a] $R_1 = \Sigma||F_o|-|F_c||/\Sigma|F_o|$. [b] $wR_2 = [\Sigma w(|F_o| - |F_c|)^2/ SwF_o^2]^{1/2}$. [c] GOF (all data) = $[\Sigma w(|F_o| - |F_c|)^2/ (n\text{-}p)]^{1/2}$ n = number of independent reflections, p=number of parameters

Bond distances over the nacnac backbone (d(N1-C2) = 1.321(2) Å, d(C2-C3) = 1.416(2) Å, d(C3-C4) = 1.367(2) Å, and d(C4-N2) = 1.372(2) Å) are no longer symmetric and the pyridine imine displays redox noninnocent behavior with the

following bond distances; d(N2-C18) = 1.355(2) Å, d(C18-C19) = 1.388(2) Å, and d(C19-N3) = 1.383(2) Å. Again, the N1-Fe-N2 bite angle of the nacnac is standard at 90.73(4)^{o} and the N2-Fe-N3 angle of 80.80(4)^{o} is consistent with other compounds bearing the analogous {R(nn)PM}$^{-}$ ligand. Deviations from square pyramidal are noted in the N1-Fe-N3 angle of 146.53(4)^{o}, N3-Fe-C25 angle of 109.50(5)^{o}, and N1-Fe-C25 angle of 103.48(5)^{o}. The N2-Fe-C24 angle approaches linearity (171.08(5)^{o}) and the rest of the core angles comprising the square pyramid approach 90^{o}.

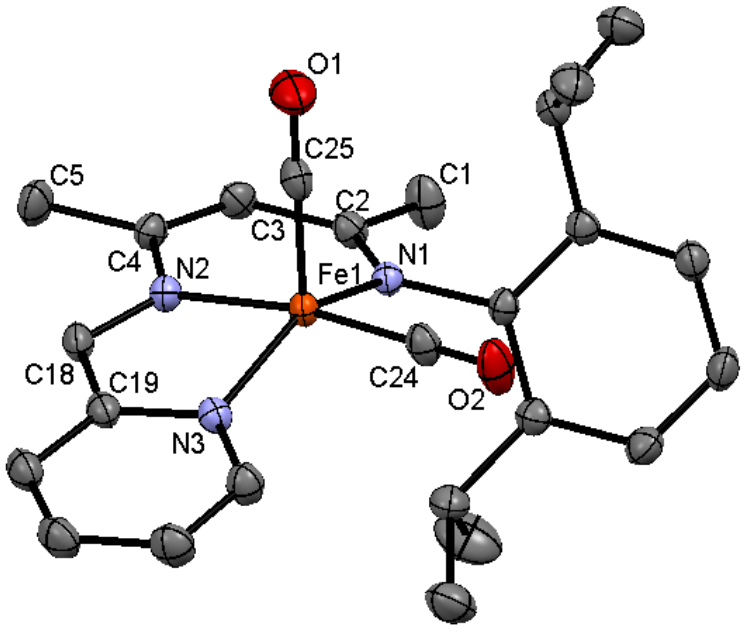

Figure 3.9. Molecular view of {^{i}Pr(nn)PI}Fe(CO)$_2$ (**5-Fe^{iPr}**). Selected interatomic distances (Å) and angels (^{o}): Fe-N1, 1.962(2); Fe-N2, 1.944(2); Fe-N3, 1.952(2); Fe-C24, 1.779(2); Fe-C25, 1.766(2); N1-C2, 1.321(2); C2-C3, 1.416(2); C3-C4, 1.367(2); N2-C4, 1.372(2); N2-C18, 1.355(2); C18-C19, 1.388(2); N3-C19, 1.383(2); C24-O2, 1.149(2); C25-O1, 1.151(2); N1-Fe-N2, 90.73(4); N1-Fe-N3, 146.53(4); N1-Fe-C24, 93.43(5); N1-Fe-C25, 103.48(5); N2-Fe-N3, 80.80(4); N2-Fe-C24, 171.08(5); N2-Fe-C25, 95.33(5); N3-Fe-C24, 91.43(5); N3-Fe-C25, 109.50(5); C24-Fe-C25, 91.37(6); Fe-C24-O2, 174.8(2); Fe-C25-O1, 178.7(2).

4. UV/VIS spectra of {Et(nn)PI}Fe(CO)$_2$ (5-Fe^{Et}) and {^{i}Pr(nn)PM}Fe(CO^{neo}Pe)CO (4-Fe^{iPr})

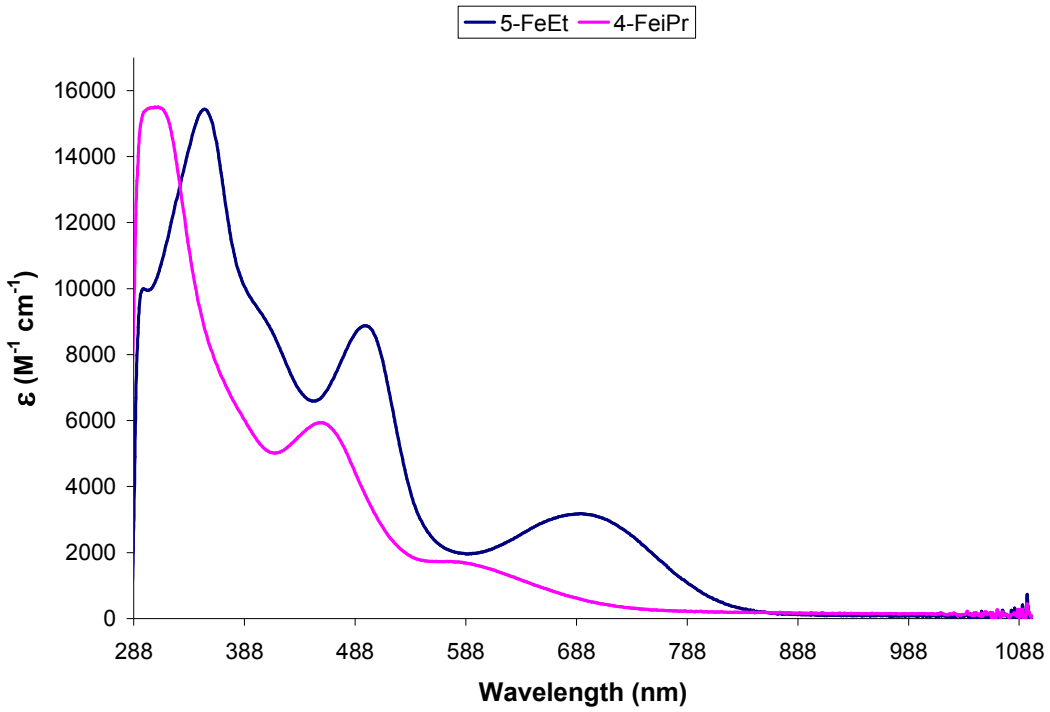

Figure 3.10. UV/VIS spectra of {Et(nn)PI}Fe(CO)$_2$ (**5-Fe^{Et}**) and {^{i}Pr(nn)PM}Fe(CO^{neo}Pe)CO (**4-Fe^{iPr}**)

The intense colors exhibited by **4-Fe^{iPr}** and **5-Fe^{Et}** prompted investigation with UV/VIS spectroscopy, and as expected, both compounds exhibited intense charge transfer bands that obscure the forbidden d-d transitions (Figure 3.10). The spectrum of **4-Fe^{iPr}** displayed 3 bands at 304 nm ($\varepsilon \sim 15000\ M^{-1}\ cm^{-1}$), 453 nm ($\varepsilon \sim 6000\ M^{-1}\ cm^{-1}$), and 577 nm ($\varepsilon \sim 2000\ M^{-1}\ cm^{-1}$). Red shifted slightly, **5-Fe^{Et}** showed comparable absorptions at 349 nm ($\varepsilon \sim 15000\ M^{-1}\ cm^{-1}$), 394 nm ($\varepsilon \sim 10000\ M^{-1}\ cm^{-1}$), 496 nm ($\varepsilon \sim 9000\ M^{-1}\ cm^{-1}$), and 688 nm ($\varepsilon \sim 3000\ M^{-1}\ cm^{-1}$). Interestingly, both

compounds exhibit related spectra despite an unsaturated pyridine-imine ligand on **5-Fe^{Et}** and a saturated ligand on **4-Fe^{iPr}**.

5. Electronic structure of {^{i}Pr(nn)PI}Fe(CO)$_2$ (5-Fe^{iPr})

Comparison of the pyridine-imine bond distances in **5-Fe^{iPr}** to both the bidendate pyridine-imine (PI) ligand and the tetradentate, nacnac derived, {nn(PM)(PI)}^{n} (n = 0, -1, -2) ligand should give insight into the extent of reduction of {^{i}Pr(nn)PI}^{n}.[20] Figure 3.11 shows the crystallographically and computationally determined bond distances for different redox states of various PI frameworks.

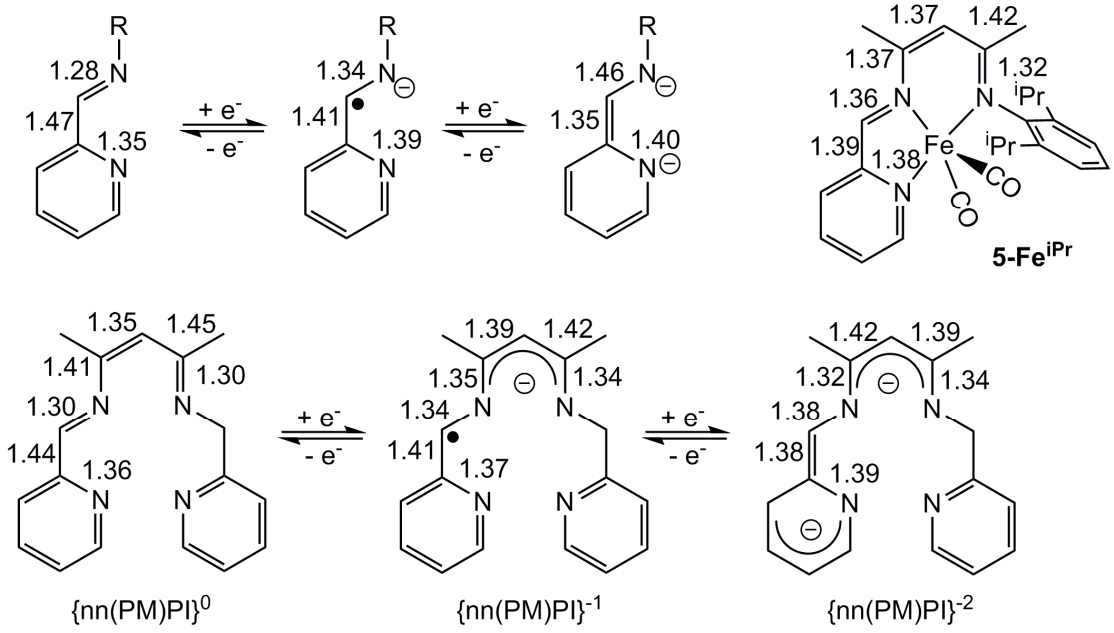

Figure 3.11. Crystallographically and computationally determined bond lengths of neutral and reduced bidentate pyridine-imine (PI), and tetradentate {nn(PM)(PI)} systems. Bond distances of {^{i}Pr(nn)PI}Fe(CO)$_2$ (**5-Fe^{iPr}**) are given as well.

Comparing the metrics of the PI arm of the tridentate ligand to those of {nn(PM)PI}$^{-2}$ suggest that the ligand in **5-Fe^{iPr}** is a bis-reduced, dianionic, chelate, but traversing the nacnac fragment, the bond distances suggest monoanionic character of the ligand.[8]

The distances observed over the pyridine-imine of **5-Fe^{iPr}** show good agreement with those in the bidentate PI^{-1} systems implying monoanionic ligand character. This leads to an electronic structure exhibiting a monoanionic {^{i}Pr(nn)PI}$^{-1}$ ligand antiferromagnetically to low spin Fe(I), but does not eliminate the possibility of low spin Fe(II) bound to a dianionic {^{i}Pr(nn)PI}$^{-2}$ ligand. A more accurate description resembles a strongly covalent system with 2 electrons from the metal distributed over the pyridine imine and carbonyl ligands.

In pursuance of more evidence towards the electronic structure of {^{i}Pr(nn)PI}Fe(CO)$_2$ (**5-Fe^{iPr}**), the molecule was investigated computationally, and the computed structure and bond metrics are given in Figure 3.12 (a). Of note is the agreement between calculated and experimental bond metrics as all the calculated metrics are within 0.02 Å of experimental values. The calculated structure agrees most closely with the {^{i}Pr(nn)PI}$^{-2}$ description and assignment as Fe(II). Also given in Figure 3.9 (b & c) are the computed structures of {^{i}Pr(nn)PI}Li and {^{i}Pr(nn)PI}Mg which model the prototypical {^{i}Pr(nn)PI}$^{-1}$ anion and {^{i}Pr(nn)PI}$^{-2}$ dianion, respectively. Comparison of the bond metrics of **5-Fe^{iPr}** with the model {^{i}Pr(nn)PI}Li and {^{i}Pr(nn)PI}Mg compounds substantiates the claim of a dianionic ligand and Fe(II) as the bond metrics correlate well with those of {^{i}Pr(nn)PI}Mg, especially over the redox-active PI arm.

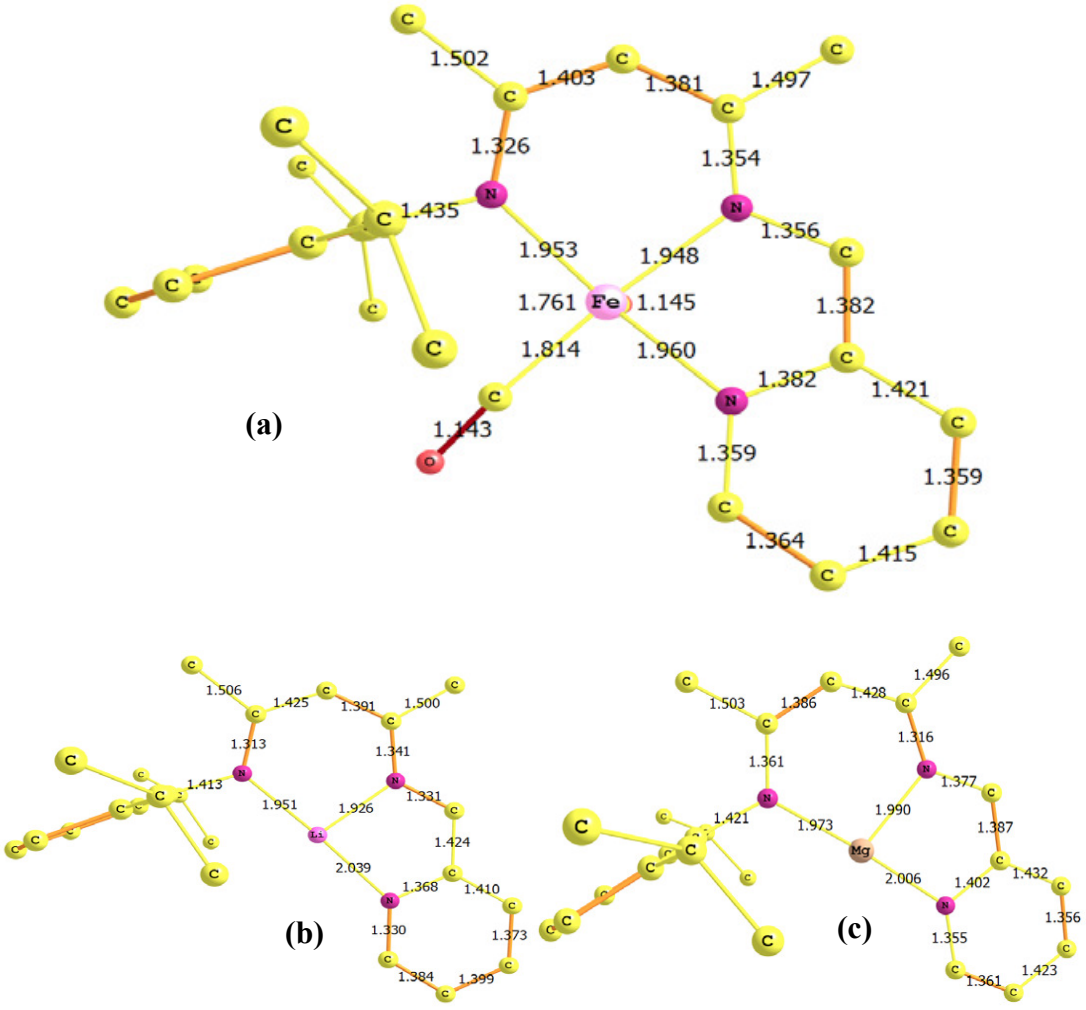

Figure 3.12. Computed geometry and interatomic distances for {iPr(nn)PI}Fe(CO)$_2$ (**5-Fe^{iPr}**) (a), {^{i}Pr(nn)PI}Li (b), and {^{i}Pr(nn)PI}Mg (c).

Molecular orbitals for {^{i}Pr(nn)PI}Fe(CO)$_2$ (**5-Fe^{iPr}**) were calculated and a partial molecular orbital diagram is shown in Figure 3.13. The low symmetry of the molecule (C_1) results in significant mixing of individual d-orbitals over several molecular orbitals and the similar energies of many ligand and metal based orbitals makes assignment of a ligand field very difficult.

The "t_{2g}" set of d-orbitals, all π^b with respect to the CO ligands, can be assigned in the figure as d_{xy} (-7.22 eV), d_{xz} (-7.42 eV), and d_{yz} (-6.18 eV). The

remaining three low lying orbitals show significant π-bonding in the aryl group of the ligand but still contain a noticeable amount of d-character. Supporting the assertion of a ligand dianion ($\{^{i}Pr(nn)PI\}^{-2}$), the HOMO is almost entirely (~80%) ligand pyridine-imine (PI) π^* with the other ~20% metal d_{z2} in character. The unoccupied molecular orbitals (LUMO, LUMO+1, LUMO+2) in Figure 3.10 take on σ^* character with components of the d_{x2-y2} and d_{z2} orbitals.

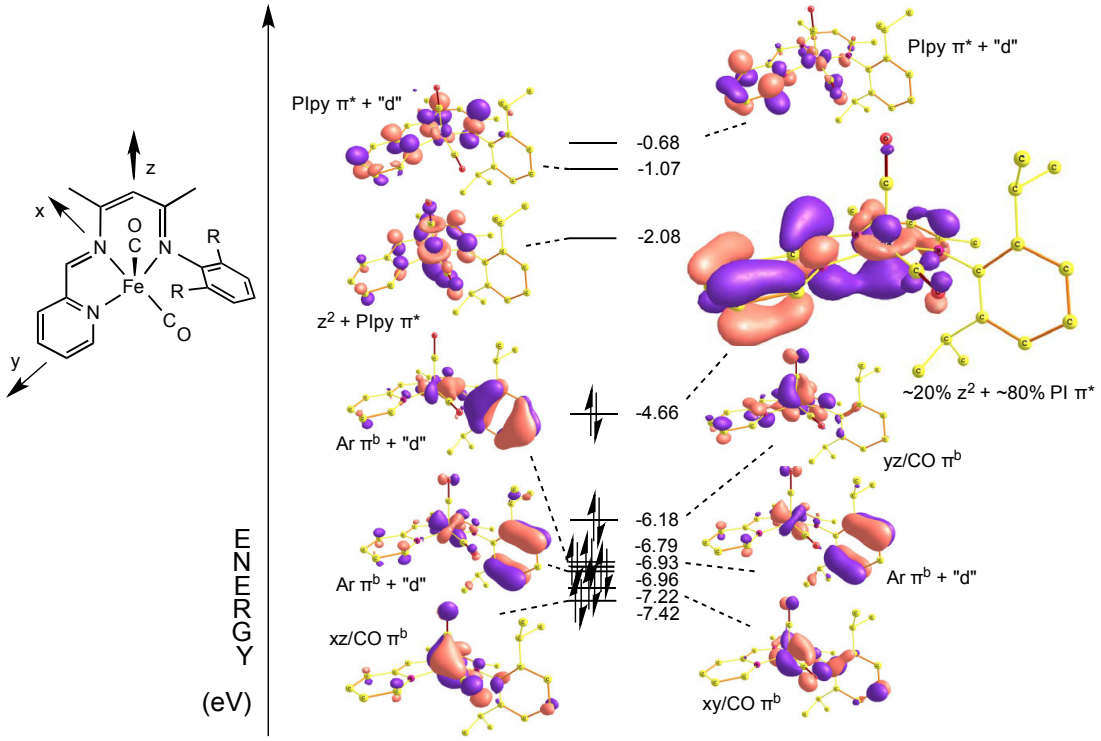

Figure 3.13. Partial molecular orbital diagram for $\{^{i}Pr(nn)PI\}Fe(CO)_2$ showing the HOMO as primarily (~80%) ligand π* character supporting assignment as dianionic $\{^{i}Pr(nn)PI\}^{-2}$. The remaining 6 filled orbitals illustrate the mixing of the d-orbitals over numerous molecular orbitals, making assignment of the ligand field difficult.

E. Carbonylation of $\{^{i}Pr(nn)PM\}CrN(TMS)_2$ (1-Cr^{iPr})

1. Synthesis of $\{\kappa^2$-N,N-pyrim-pyr$\}Cr(CO)_4$ (6-Cr^{iPr})

Carbonylation of **1-Cr^{iPr}** proceeded at room temperature over 24 h with a color change from maroon to yellow-orange and formation of a diamagnetic yellow-orange

solid. The ^{1}H NMR spectrum of the product showed loss of HMDS and a new singlet (δ 5.36) corresponding to the putative imine C-*H* resonance which differs significantly from that of **5-Fe^{iPr}** (δ 7.81) and **5-Fe^{Et}** (δ 7.83). The di-isopropylphenyl groups exhibited 4 distinct doublet resonances for the methyls despite only 2 expected for a molecule with C_s symmetry, and in contrast to the 2 doublets present in the spectrum of **5-Fe^{iPr}**. Additionally, the infrared spectrum showed four terminal CO stretches at 1820, 1851, 1881, and 2001 cm^{-1}, which was not consistent with the expected {^{i}Pr(nn)PI}Cr(CO)$_3$ product, prompting further investigation.

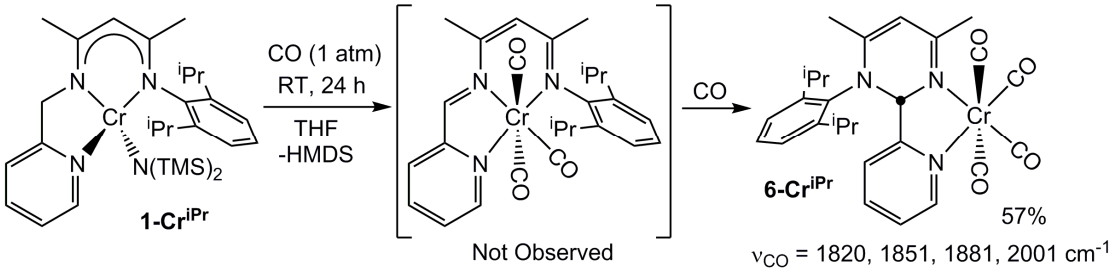

Scheme 3.4. Carbonylation of {^{i}Pr(nn)PM}CrN(TMS)$_2$ (**1-Cr^{iPr}**); synthesis of {κ^2-N,N-pyrim-pyr}Cr(CO)$_4$ (**6-Cr^{iPr}**).

Isolation of a single crystal and subjecting it to an X-ray crystallographic structure determination revealed formation of a new bidentate ligand, 2-H,2-pyridyl,3-DIPP,4,6-dimethyl-pyrimidine, and the compound {κ^2-N,N-2-H,2-pyridyl,3-DIPP,4,6-dimethyl-pyrimidine}Cr(CO)$_4$ ({κ^2-N,N-2-H-pyrim-pyr}Cr(CO)$_4$, **6-Cr^{iPr}**). Scheme 3.4 offers one possible path towards the formation of **6-Cr^{iPr}** through CO promoted loss of HMDS from **1-Cr^{iPr}** and formation of putative {^{i}Pr(nn)PI}Cr(CO)$_3$, which may be unstable towards cyclization leading to formation of **6-Cr^{iPr}** upon capture of an additional equivalent of CO. Akin to the possible redox states of {^{i}Pr(nn)PI}Fe(CO)$_2$

(**5-Fe^{iPr}**), the ligand on {^{i}Pr(nn)PI}Cr(CO)$_3$ could exist as a neutral, anionic, or dianionic chelate bound to Cr(0), Cr(I), or Cr(II), respectively.

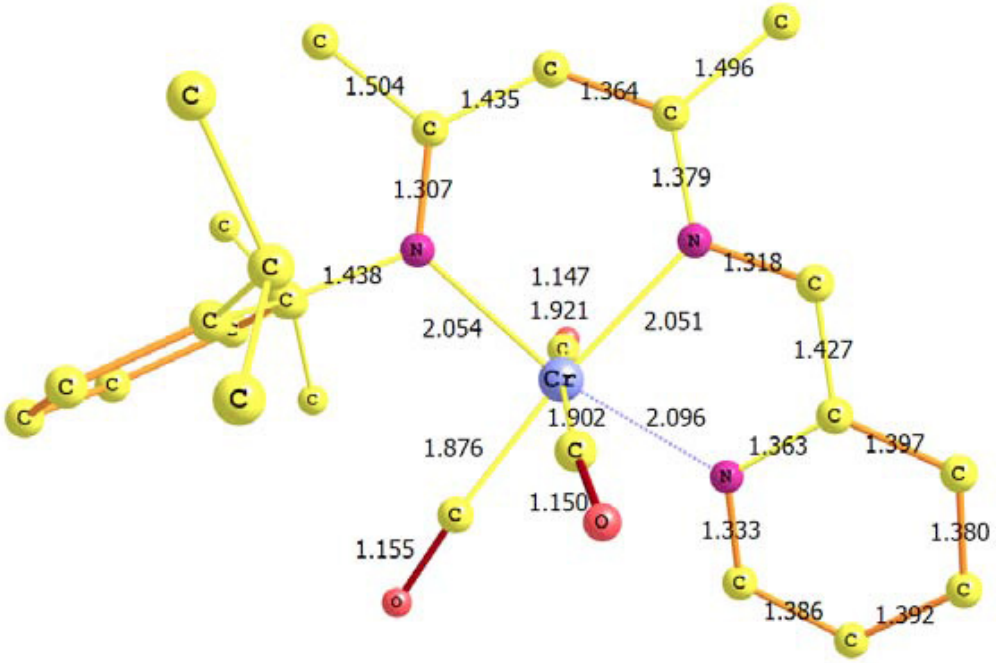

Figure 3.14. Calculated geometry with pertinent interatomic distances of {iPr(nn)PI)Cr(CO)3, the putative intermediate in the formation of {κ^2-N,N-pyrim-pyr}Cr(CO)$_4$ (**6-Cr^{iPr}**).

The geometry of the proposed intermediate, {^{i}Pr(nn)PI}Cr(CO)$_3$, was calculated to gain insight on the electronic factors leading towards formation of {κ^2-N,N-pyrim-pyr}Cr(CO)$_4$ (**6-Cr^{iPr}**) and the structure, with bond distances, is shown in Figure 3.14. Comparing the calculated bond metrics with those in Figure X.7 exposes the ligand as a neutral {^{i}Pr(nn)PI}^{0} ligand. This assertion seems logical as the reduced ligand would be less receptive to nucleophilic attack at the imine, and because the reduced ligand has been shown to be stable in {^{i}Pr(nn)PI}Fe(CO)$_2$ (**5-Fe^{iPr}**). Furthermore, calculations show that the HOMO, HOMO-1, and HOMO-2 are filled d-

orbitals that are π-bonding with respect to the carbonyl ligands and pyridine-imine π^* orbitals are not present at similar energies.

2. Crystal Structure of {κ²-N,N-pyrim-pyr}Cr(CO)₄ (6-Cr^{iPr})

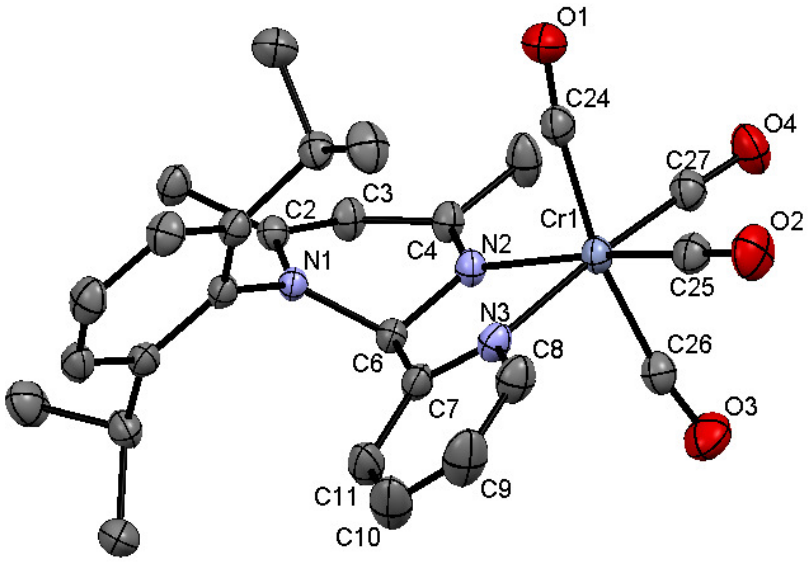

Figure 3.15. Molecular view of {κ²-N,N-pyrim-pyr}Cr(CO)₄ (**6-Cr^{iPr}**) with selected interatomic distances (Å) and angles (°). Hydrogen atoms and 2 molecules of benzene have been omitted for clarity: Cr-N2, 2.139(2); Cr-N3, 2.132(2); Cr-C24, 1.895(2); Cr2-C25, 1.840(2); Cr-C26, 1.910(2); Cr-C27, 1.826(2); N1-C6, 1.498(2); N1-C2, 1.353(2); C2-C3, 1.374(2); C3-C4, 1.425(2); N2-C4, 1.307(2); N2-C6, 1.463(2); C6-C7, 1.508(2); N3-C7, 1.344(2); N3-C8, 1.350(2); C24-O1, 1.149(2); C25-O2, 1.157(2); C26-O3, 1.141(2); C27-O4, 1.169(2); N2-Cr-N3, 75.91(4); N2-Cr-C24, 91.10(5); N2-Cr-C25, 169.96(5); N2-Cr-C26, 94.28(5); N2-Cr-C27, 103.62(5); N3-Cr-C24, 100.59(5); N3-Cr-C25, 94.19(5); N3-Cr-C26, 90.23(5); N3-Cr-C27, 174.97(5); C24-Cr-C25, 89.09(6); C24-Cr-C26, 168.82(6); C24-Cr-C27, 84.14(6); C25-Cr-C26, 87.31(6); C25-Cr-C27, 86.39(6); C26-Cr-C27, 84.80(6); C7-C6-N1, 112.39(9); C7-C6-N2, 110.07(9); C6-N1-C2, 113.16(9); N1-C2-C3, 118.70(10); C2-C3-C4, 117.57(11); C3-C4-N2, 121.43(9); C4-N2-C6, 111.76(10); N1-C6-N2, 111.18(9).

The structure of **6-Cr^{iPr}** (Fig. 3.15) exhibits a pseudo octahedral geometry with the newly formed pyrimidine-pyridine chelate bound to *cis*-coordination sites. The pyridine and pyrimidine are bound at standard distances of 2.132(2) Å and 2.139(2) Å, respectively. The carbonyls *trans* to the κ²–N,N-chelate are bound tighter (d(Cr-C25)

= 1.840(2) Å, d(Cr-C27) = 1.826(2) Å) than those bound *trans* to each other (d(Cr-24) = 1.895(2) Å, d(Cr-C26) = 1.910(2) Å) owing to the greater *trans*-influence of the carbonyl ligand over the nitrogen donors, with parallel C-O distances exhibiting the same correlation. Bond lengths in agreement with alternating double and single bonds are noted in the pyrimidine ring as N2-C4 (1.307(2) Å) and C2-C3 (1.374(2) Å) are consistent with double bonds and C3-C4 (1.425(2) Å) and N1-C2 (1.353(2) Å) are consistent with single bonds. C6 sp^3 is revealed by N2-C6 (1.463(2) Å) and N1-C6 (1.498(2) Å) distances that resemble single bonds.

3. Independent synthesis of 2-H,2-pyridyl,3-DIPP,4,6-dimethyl-pyrimidine

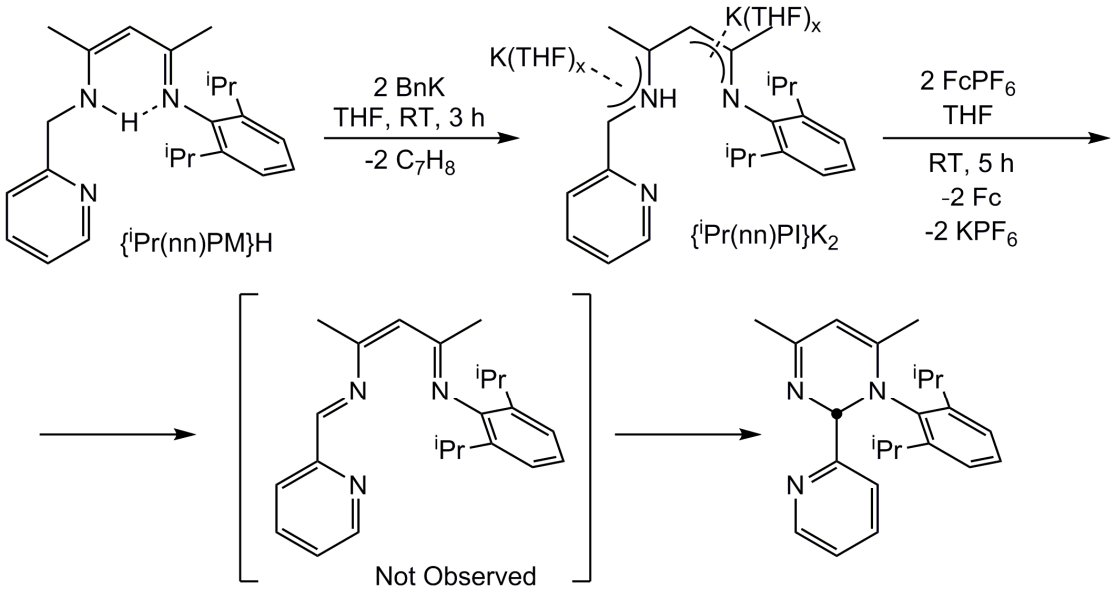

Scheme 3.5. Oxidation of {^{i}Pr(nn)PM}H to 2-H,2-pyridyl,3-DIPP,4,6-dimethyl-pyrimidine.

Having indicted {^{i}Pr(nn)PI}^{0} as the ligand redox state responsible for rearrangement to the pyrimidine-pyridine ligand, a synthesis was sought to independently synthesize {^{i}Pr(nn)PM}^{0}. Deprotonation of {^{i}Pr(nn)PM}H with 2 equivalents of potassium benzyl produced the stable {^{i}Pr(nn)PI}K_2, affirming the

stability of the $\{^{i}Pr(nn)PI\}^{-2}$ fragment observed in $\{^{i}Pr(nn)PI\}Fe(CO)_2$ (**5-Fe^{iPr}**) (Scheme 3.5). Oxidation of $\{^{i}Pr(nn)PI\}K_2$ with two equivalents of ferricinium hexafluorophosphate produced the cyclized product, 2-H,2-pyridyl,3-DIPP,4,6-dimethyl-pyrimidine in 67% yield. It remains unclear whether rearrangement proceeds through the monoanion or neutral $\{^{i}Pr(nn)PI\}^{n}$ (n = -1, 0) species, but reactions with other oxidizing agents including $AgPF_6$ and O_2 produced similar results.

F. Carbon-carbon bond forming reactions of {R(nn)PM}FeN(TMS)$_2$ (R = Et, ^{i}Pr).

1. Reaction of $\{^{i}Pr(nn)PI\}K_2$ with Ferric Chloride

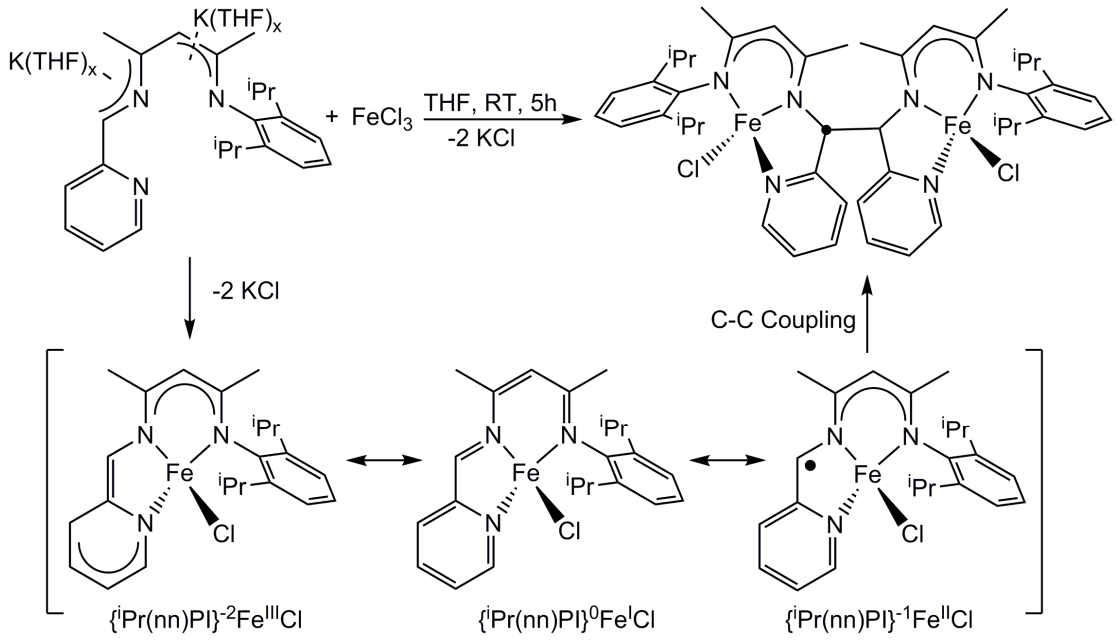

Scheme 3.6. Synthesis of $\{^{i}Pr(nn)CHpy\}_2Fe_2Cl_2$ (**7-Fe^{iPr}**).

The doubly deprotonated ligand, $\{^{i}Pr(nn)PI\}K_2$, was seen as a versatile starting material for establishing the pyridine-imine functionality via salt metathesis routes. Reaction between $\{^{i}Pr(nn)PI\}K_2$ and $FeCl_3$ in THF afforded a yellow product, characterized as $\{^{i}Pr(nn)CHpy\}_2Fe_2Cl_2$ (**7-Fe^{iPr}**) by single crystal X-ray structure determination, in 60% yield. Scheme 3.6 details a plausible route towards production

of **7-Fe^{iPr}** with formation of the new carbon-carbon bond occurring through {^{i}Pr(nn)PI}$^{-1}$Fe^{II}Cl, which can be envisioned as having radical character at the imine carbon.[21,22] The X-ray determined structure showed a C_2 symmetric product, but the crude ^{1}H NMR spectrum (Figure 3.17) showed additional resonances that may correspond to the C_i structure as well.

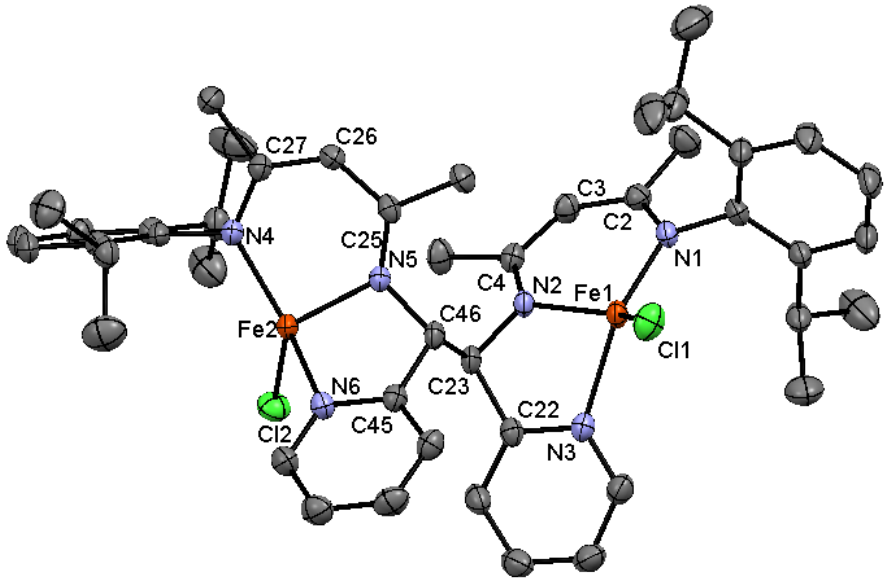

Figure 3.16. Molecular view of {^{i}Pr(nn)CHpy}$_2$Fe$_2$Cl$_2$ (**7-Fe^{iPr}**). Selected interatomic distances (Å) and angles (^{o}): Fe1-N1, (1.999(2); Fe1-N2, 2.026(2); Fe1-N3, 2.156(2); Fe1-Cl1, 2.248(2); Fe2-N4, 1.984(2); Fe2-N5, 2.025(2); Fe2-N6, 2.133(2); Fe2-Cl2, 2.263(2); N1-C2, 1.342(2); C2-C3, 1.397(3); C3-C4, 1.403(2); N2-C4, 1.328(2); N2-C23, 1.454(2); C22-C23, 1.517(2); N3-C22, 1.353(2); N4-C27, 1.346(2); C26-C27, 1.400(2); C25-C26, 1.410(2); N5-C25, 1.319(2); N5-C46, 1.461(2); C45-C46, 1.521(2); N6-C45, 1.353(3); C23-C46, 1.581(2); N1-Fe1-N2, 91.93(6); N1-Fe1-N3, 141.40(6); N1-Fe1-Cl1, 114.76(5); N2-Fe1-N3, 78.46(6); N2-Fe1-Cl1, 138.04(4); N3-Fe1-Cl1, 95.94(5); N4-Fe2-N5, 92.71(6); N4-Fe2-N6, 136.99(6); N4-Fe-Cl2, 120.07(5); N5-Fe2-Cl2, 120.07(5); N5-Fe2-N6, 78.39(6); N5-Fe2-Cl2, 129.92(4); N6-Fe2, Cl2, 96.32(4).

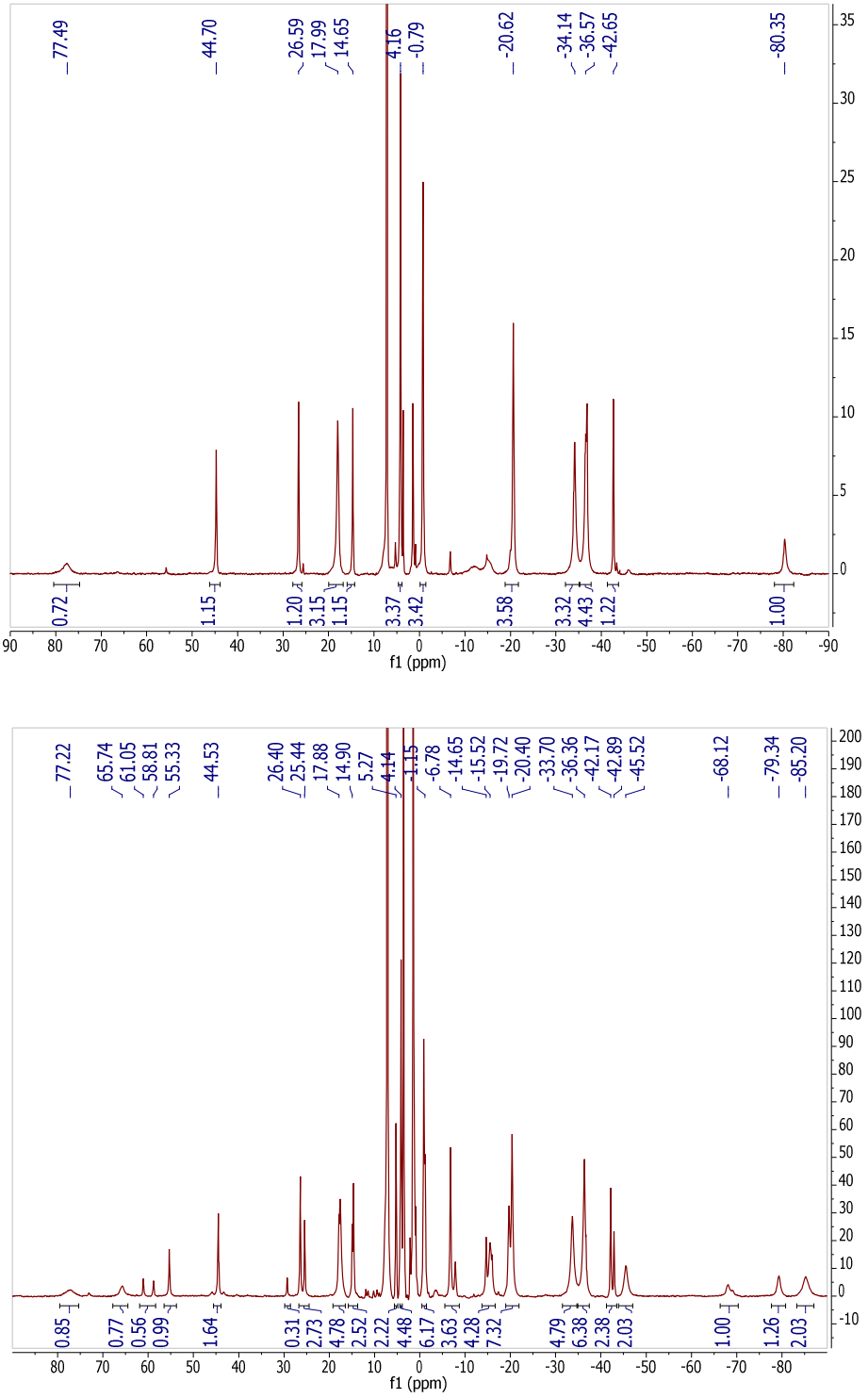

Figure 3.17. ^{1}H NMR spectra of crystallographically characterized C_2 symmetric isomer of **7-Fe^{iPr}** (top), and crude reaction mixture showing resonances that plausibly correspond to C_i isomer as well (bottom).

The crystallographically determined structure of **7-Fe^{iPr}** is shown in Figure 3.16 with pertinent interatomic distances and angles provided within the caption. Of note in the structure is the newly formed carbon-carbon bond (d(C23-C46) = 1.581(2) Å), which is long for a C-C single bond between two sp^3 centers.[23] The geometry about each iron center is reminiscent of the bonds and angles around {^{i}Pr(nn)PM}FeBr (**2-Fe^{iPr}**). Enforced by the molecular structure of the ligand, the nacnac (91.93(6)^{o}, 92.71(6)^{o}) and N_{py}-Fe-N_{nn} (95.94(5)^{o}, 96.32(4)^{o}) bite angles are similar over both halves of **7-Fe^{iPr}** but the N_{py}-Fe-N_{nn} angles are all larger than the comparable angles in **2-Fe^{iPr}**. Variation in the angles about the two iron centers of **7-Fe^{iPr}** is observed in the N_{nn}-Fe-Cl angles (114.76(5)^{o}, 120.07(5)^{o}, 138.04(4)^{o}, and 129.92(4)^{o}) and N_{nn}-Fe-N_{py} angles (141.40(6)^{o} and 136.99(6)^{o}). Other systems exhibiting long C-C bonds showed reversible carbon-carbon coupling,[21] so **7-Fe^{iPr}**, was treated with various hydrogen atom sources in attempts to form {^{i}Pr(nn)PM}FeCl, but no reaction was observed.

2. Reaction of {Et(nn)PM}FeN(TMS)$_2$ (1-Fe^{Et}) with TMS-N$_3$

It was envisioned that trimethylsilyl azide would induce HMDS loss from {Et(nn)PM}FeN(TMS)$_2$ (**1-Fe^{Et}**) en route, with loss of dinitrogen, to an imido compound. As Scheme 3.7 attests, elevated temperatures were required for any reaction to proceed between **1-Fe^{Et}** and TMS-N_3. The major product of the reaction was isolated in 33% yield as a green crystalline solid and shown by X-ray crystallography to be {[Et(nn)CHpy]$_2$}Fe (**8-Fe^{Et}**). Interestingly, a new carbon-carbon bond formed at the imine carbon, and the two coupled ligands have wrapped around one iron center leaving the two pyridine arms unbound to the metal. This required the

loss of one equivalent of iron whose outcome, along with that of any remaining azide, remain unknown. Scheme 3.7 illustrates one tenable pathway in this transformation. Deprotonation induced by incoming trimethylsilyl azide would introduce the unsaturated ligand with loss of HMDS and successive coupling and disproportionation would lead to product. Alternatively, if the trimethylsilyl nitrene were delivered, coupling and disproportionation could occur via the Fe(III) species shown in Scheme 3.7. The latter possibility seems quite plausible as Chirik has observed ligand reduction in pyridine-diimine imido iron species.[24]

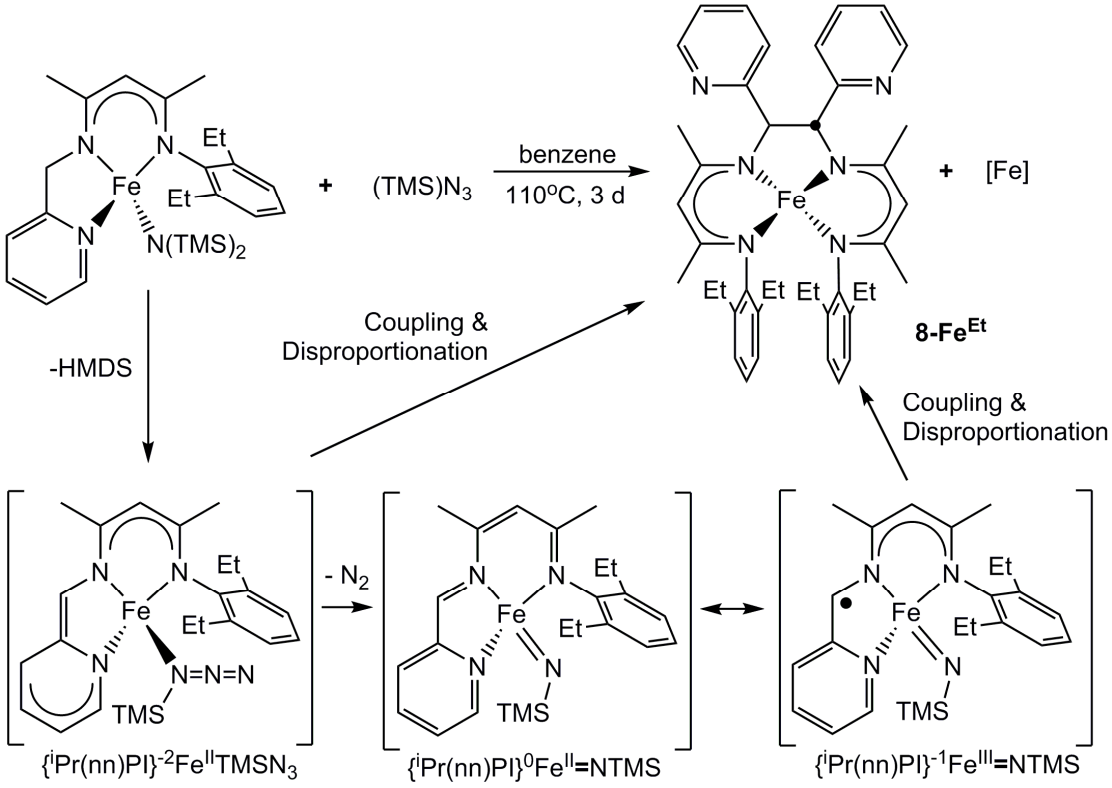

Scheme 3.7. Reaction of {Et(nn)PM}FeN(TMS)$_2$ with trimethylsilyl azide.

The X-ray determined crystal structure of C_2 symmetric {[Et(nn)CHpy]$_2$}Fe (**8-Fe^{Et}**) is shown in Figure 3.18 along with relevant interatomic distances and angles.

The newly formed carbon-carbon bond in **8-Fe^{Et}** (d(C31-C37) = 1.533(7) Å) is notably shorter than that formed in **7-Fe^{iPr}** and is within the standard distance of a sp^3-sp^3 C-C bond. The nacnac fragments are bound at an average distance of 2.045(12) Å which is standard for high spin Fe(II). Locked into this geometry by the new C-C bond, the N3-Fe-N4 (81.2(2)^o) angle is significantly more narrow than the opposite N1-Fe-N2 angle (118.4(2)^o). The average nacnac bite angle is standard and in line with other compounds in this study at 89.9(4)^o, and the angles across opposing nacnac fragments are also nearly identical at 141.2(4)^o.

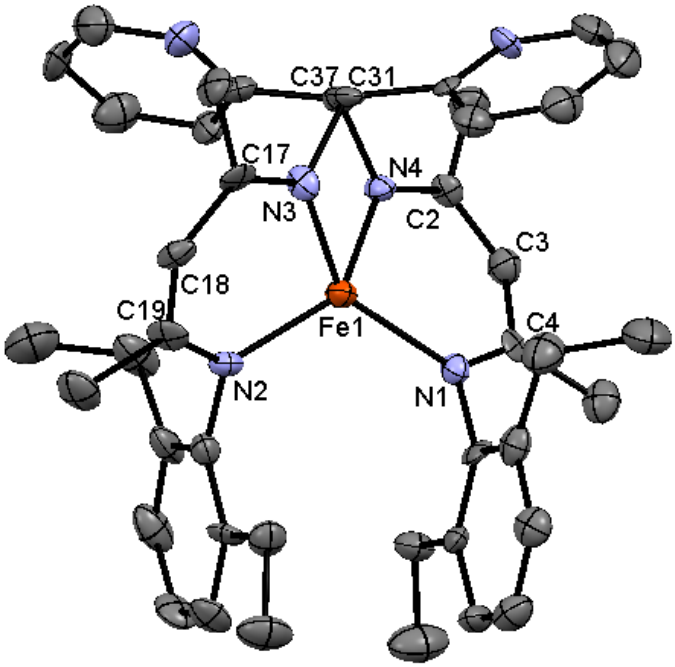

Figure 3.18. Molecular view of {[Et(nn)CHpy]$_2$}Fe (**8-Fe^{Et}**). Selected interatomic distances (Å) and angles (^{o}): Fe-N1, 2.038(7); Fe-N2, 2.037(7); Fe-N3, 2.042(8); Fe-N4, 2.063(7); N1-C4, 1.339(11); C3-C4, 1.408(13); C2-C3, 1.379(10); N4-C2, 1.316(9); N4-C37, 1.482(11); C31-C37, 1.533(7); N3-C31, 1.466(11); N3-C17, 1.303(10); C17-C18, 1.429(11); C18-C19, 1.381(11); N2-C19, 1.348(10); N1-Fe-N2, 118.4(2); N1-Fe-N3, 141.5(3); N1-Fe-N4, 90.2(3); N2-fe-N3, 89.6(3); N2-Fe-N4, 140.9(3); N3-Fe-N4, 81.2(2).

3. Reaction of {^{i}Pr(nn)PM}FeN(TMS)$_2$ (1-Fe^{iPr}) with diphenyldiazomethane

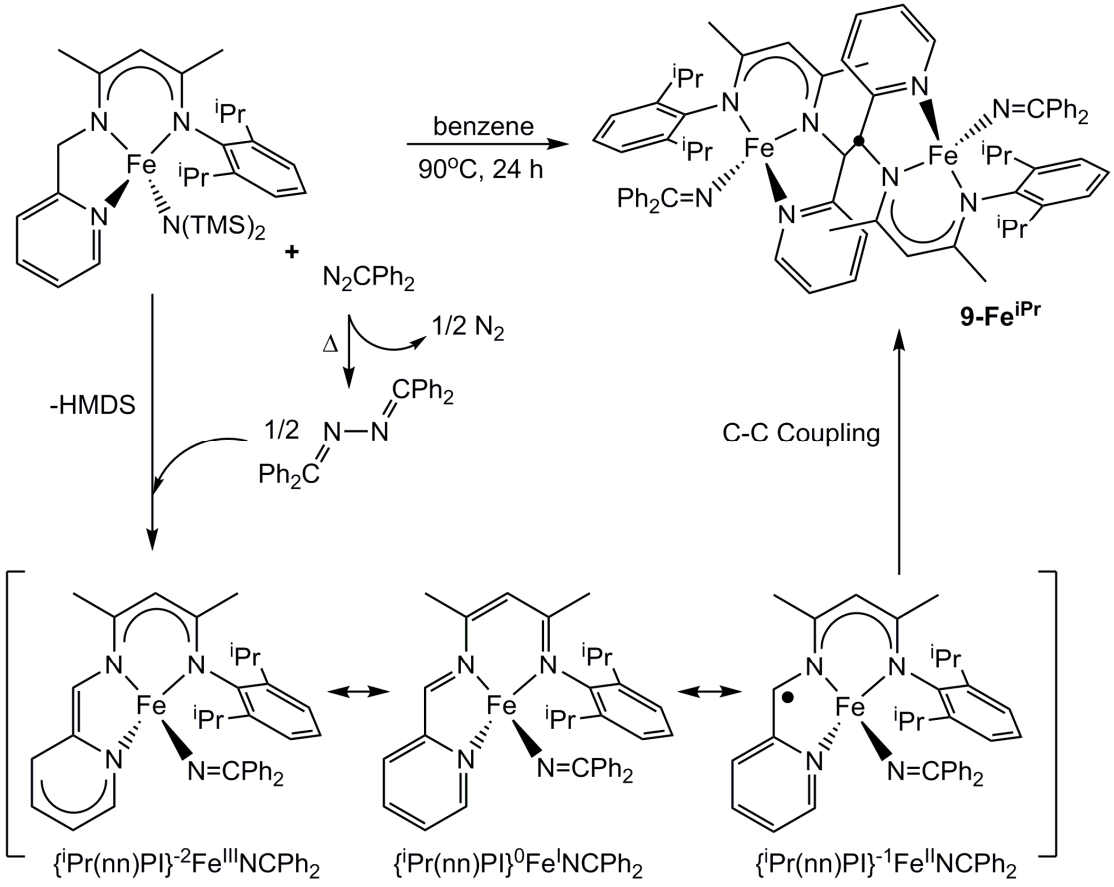

Scheme 3.8. Synthesis of {^{i}Pr(nn)CHpy}$_2$(FeN=CPh$_2$)$_2$ (**9-Fe^{iPr}**).

Diphenyldiazomethane was seen as a viable precursor towards formation of a stable carbene, but again C-C coupling was observed in the formation of {^{i}Pr(nn)CHpy}$_2$(FeN=CPh$_2$)$_2$ (**9-Fe^{iPr}**). The new diphenylimino ligand was evidence that the reaction conditions provoked thermal decomposition of diphenyldiazomethane to benzophenone azine (Ph$_2$C=N-N=CPh$_2$) and dinitrogen.[25,26] Oxidation of **1-Fe^{iPr}** with the diimine and ensuing deprotonation leaves the three resonance structures shown in Scheme X.6 with carbon-carbon bond formation resulting from the radical at the imine position of the ferrous species. Benzophenone azine was synthesized

independently via known methods[27] and treated with **1-Fe^{iPr}** at 90 ^{o}C and **9-Fe^{iPr}** was the only product observed by ^{1}H NMR in good yield, offering support for the mechanism in Scheme 3.8.

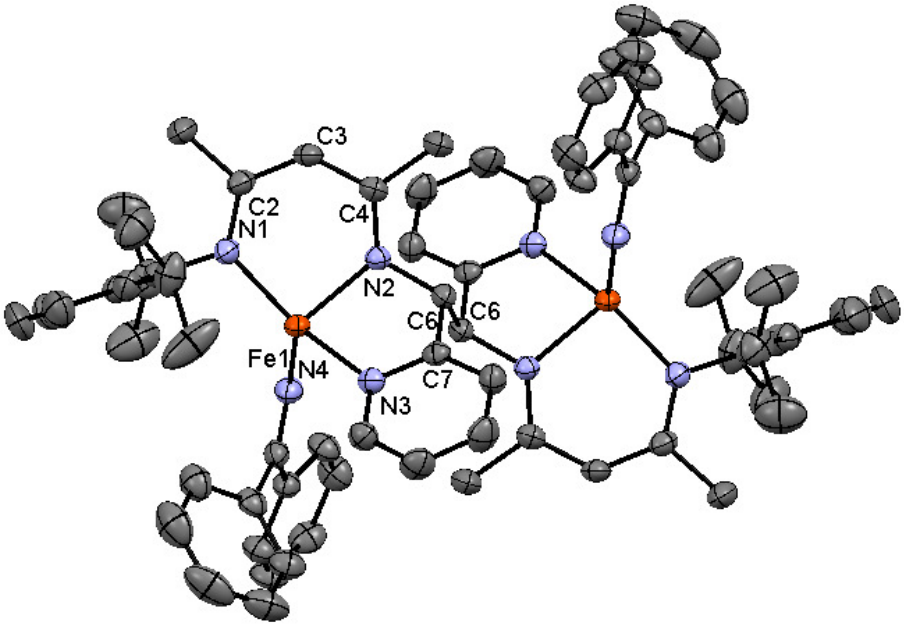

Figure 3.19. Molecular view of {^{i}Pr(nn)CHpy}$_2$(FeN=CPh$_2$)$_2$ (**9-Fe^{iPr}**). Selected interatomic distances (Å) and angles (^{o}): Fe-N1, 1.938(2); Fe-N2, 2.011(2); Fe-N3, 2.200(2); Fe-N4, 1.905(2); N1-C2, 1.341(3); C2-C3, 1.391(3); C3-C4, 1.405(3); N2-C4, 1.323(3); N2-C6, 1.454(3); C6-C7, 1.509(3); N3-C7, 1.352(3); N4-C24, 1.260(3); C6-C6', 1.581(4); N1-Fe-N2, 92.81(7); N1-Fe-N3, 133.26(7); N1-Fe-N4, 122.08(7); N2-Fe-N3, 77.95(7); N2-Fe-N4, 120.84(7); N3-Fe-N4, 101.09(7); Fe-N4-C24, 140.44(17).

The molecular structure of **9-Fe^{iPr}**, as shown in Figure 3.19, displays a molecular and crystallographic center of inversion at the newly formed C-C bond. The core distances are comparable with the other nacnac systems presented here but the Fe-N$_{nn}$ distances are notably shorter at 1.983(2) and 2.011(2) Å. Bonding within the nacnac fragments is symmetric, and at 1.581(4) Å the new C-C bond is notably long and is reminiscent of the carbon-carbon bond present in {^{i}Pr(nn)CHpy}$_2$Fe$_2$Cl$_2$ (**7-**

Fe^{iPr}). The bite angles of the ligand are standard, as the N2-Fe-N4 (120.84(7)^{o}) and N1-Fe-N3 (133.26(7)^{o}) angles are in close agreement to those in {^{i}Pr(nn)PM}FeN(TMS)$_2$ (**1-Fe^{iPr}**) suggesting little perturbation resulting from C-C bond formation or the diphenylimine ligand.

G. Reactions of {^{i}Pr(nn)PM}Fe(CO^{neo}Pe)CO (4-Fe^{iPr}); efforts towards a stable Fischer carbene

Removal of the acyl ligand from {^{i}Pr(nn)PM}Fe(CO^{neo}Pe)CO (**4-Fe^{iPr}**) was not possible with H_2 or phenylacetylene so the synthesis of a Fischer carbene was envisioned. Treatment of **4-Fe^{iPr}** with trimethylsilyl chloride did not show any reaction at temperatures below 100 ^{o}C, and then decomposition was observed concomitant with formation of a grey solid. It was thought that deprotonation of the neopentyl group adjacent to the ketone would allow for a more facile alkylation en route to a carbene complex, but when **4-Fe^{iPr}** was treated with potassium benzyl, deprotonation was observed beside the pyridine with formation of diamagnetic [{^{i}Pr(nn)PI}Fe(CO^{neo}Pe)CO]K (**10-Fe^{iPr}**) in 85% yield (Scheme 3.9). IR spectroscopy showed a new CO stretch at 1872 cm^{-1} and the acyl stretch shifted to 1595 cm^{-1} both of which are consistent with more electron density on iron in the newly formed anion. The ^{1}H NMR spectrum of **10-Fe^{iPr}** exhibited a singlet at 7.41 ppm consistent with formation of an imine. The methylene on the neopentyl group appeared as a set of doublets at 1.49 ppm and 1.63 ppm, indicating deprotonation adjacent to the pyridine. The stability of **10-Fe^{iPr}** is attributed to the dianionic resonance form of the ligand that

allows iron to remain in the +2 oxidation which has been shown to be the preferred oxidation state of iron (vide supra).

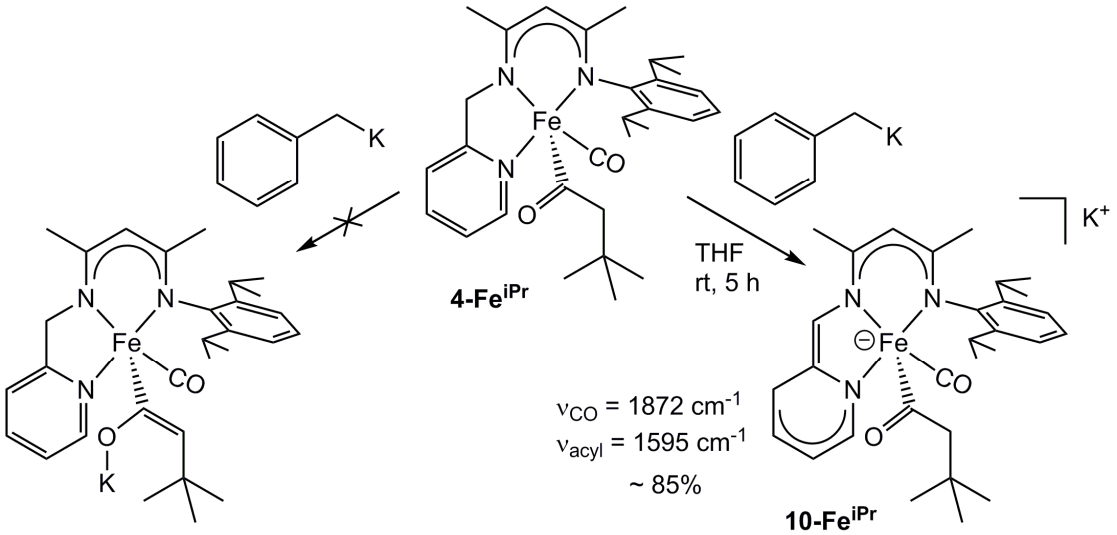

Scheme 3.9. Deprotonation of **4-Fe^{iPr}** with potassium benzyl, formation of [{^{i}Pr(nn)PI}Fe(CO^{Neo}Pe)CO]K (**10-Fe^{iPr}**).

Alkylation of **10-Fe^{iPr}** was realized using triethyloxonium tetrafluroborate as the alkylating agent in 1,2-dichloroethane. Unfortunately, a carbene was not formed, instead favoring alkylation at the imine carbon with formation of a red diamagnetic solid, {^{i}Pr(nn)^{Et}PM}Fe(CO^{neo}Pe)CO (**11-Fe^{iPr}**) (Scheme 3.10). **11-Fe^{iPr}** exhibited a terminal CO stretch in the IR spectrum at 1917 cm^{-1} along with an acyl stretch at 1619 cm^{-1} which are both in good agreement with those observed for **4-Fe^{iPr}** (1906 cm^{-1} and 1638 cm^{-1}). The ^{1}H NMR spectrum exhibited a complex multiplet for the methylene of the new ethyl group while the new methine proton displayed a pseudo triplet at 5.11 ppm. NMR only showed formation of one enantiomer, presumably because the acyl blocks alkylation on one side of the ligand. Repeating the same deprotonation/alkylation procedure did not show any reaction as sterics of the ethyl

and neopentyl acyl prevent deprotonation by benzyl potassium. Methyl iodide also exhibited alkylation at the imine but alkylation occurred on both sides of the ligand.

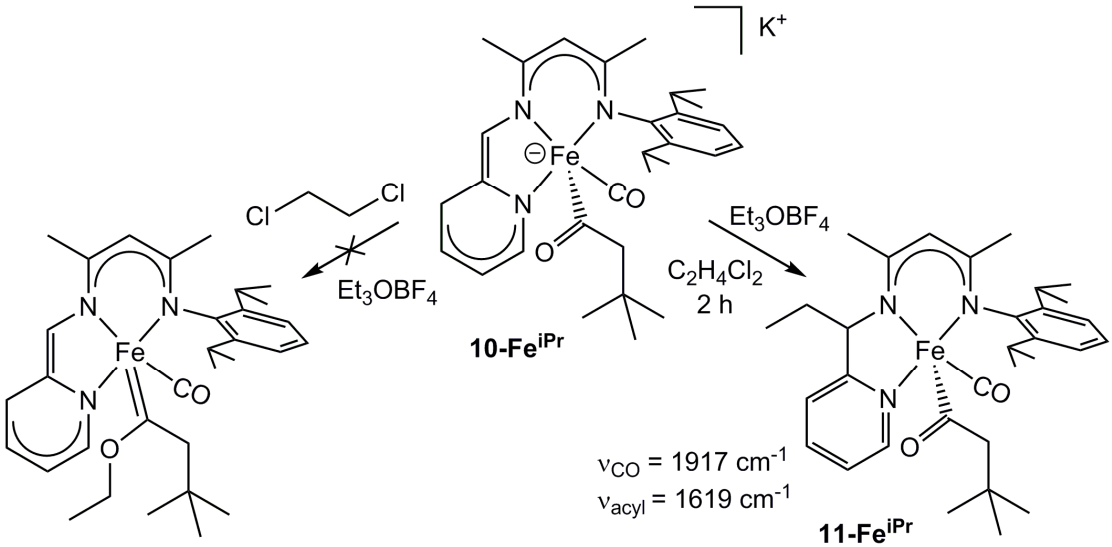

Scheme 3.10. Alkylation of **10-Fe^{iPr}** with Et_3OBF_4 and formation of {^{i}Pr(nn)^{Et}PM}Fe(CO^{neo}Pe)CO (**11-Fe^{iPr}**).

III. Conclusions

Substitution of one pyridine arm of {nacnac$(CH_2py)_2$}$^-$ with a 2,6-disubstituted aryl group afforded the trisubstituted ligand {R(nn)PM}H (R = ^{i}Pr, Et), which upon metallation and deprotonation at the methylene position resulted in the redox-noninnocent pyridine-imine ligand {R(nn)PI}^{n} (n = 0, -1, -2). Differing degrees of ligand stability were observed based on the assigned ligand oxidation state. A neutral ligand resulted in the evolution of a new pyrimidine-pyridine ligand via C-N bond formation, but the dianionic ligand adopted a diamide form that was stable while chelated to Fe(II). Intermolecular carbon-carbon bond formation arose from persistent radical character at the imine carbon when the ligand could be considered in its mono reduced form. The nacnac fragment of the ligand, behaving as a typical closed shell

anion, does not offer significant delocalization of the imine centered radical and in cases where another X-type ligand is bound to a Fe(II) center, C-C coupling ensues.

IV. Experimental

A. General Considerations

All manipulations were performed using either glovebox or high-vacuum techniques unless otherwise indicated. Hydrocarbon and ethereal solvents were dried over sodium and vacuum transferred from sodium benzophenone ketyl (3-4 mL tetraglyme/L were added to hydrocarbons). Benzene-d_6 was sequentially dried over sodium and stored over sodium metal. All glassware was oven dried at 165 ^{o}C before use.

$Cr[N(TMS)_2]_2(THF)_2$,[28] $Fe[N(TMS)_2]_2(THF)$,[29] $Co[N(TMS)_2]_2(THF)$,[30] $NiCl_2(DME)$,[31] were prepared by literature procedures. ^{1}H and ^{13}C NMR spectra were obtained on Varian 300 MHz (Mercury), 400 MHz, and 500 MHz (INOVA) spectrometers. ^{1}H NMR and ^{13}C NMR shifts are referenced to benzene-d_6 (^{1}H, δ 7.16 ppm; ^{13}C 128.39 ppm), tetrahydrofuran-d_8 (^{1}H, δ 3.58 ppm; ^{13}C 67.21 ppm), and chloroform-d (^{1}H, δ 7.26 ppm; ^{13}C 77.16 ppm).

B. Synthesis

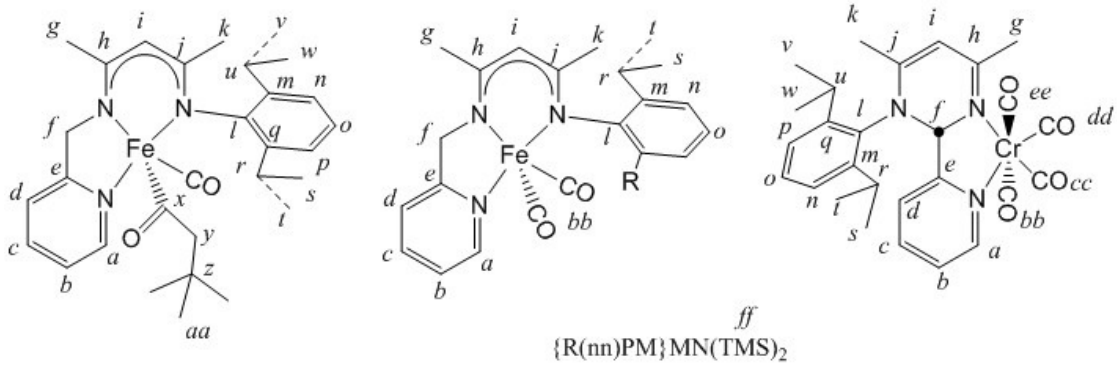

{^{i}Pr(nn)PM}H. This is a modified literature procedure. To a solution of 2,4-pentanedione (8.47 g, 85 mmol) in toluene (40 mL) was added 2,6-diisopropyllaniline (10 g, 67 mmol) and a catalytic amount of p-toluenesulfonic acid. The mixture was refluxed and water was collected in a Dean-Stark trap. After 7 h, the volatiles were removed under vacuum, affording an orange oil. Toluene (40 mL), 2-picolylamine (7.32 g, 68 mmol), and a catalytic amount of p-toluenesulfonic acid were added and the reaction was refluxed for 30 h. Water produced during the reaction was collected in a Dean-Stark trap. The reaction was cooled and volatiles were removed under vacuum. The red oily residue was dissolved in Et_2O (60 mL), and washed with saturated Na_2CO_3 (3 x 15 mL). The organic layer was dried with Na_2SO_4, filtered and the solvent was removed under vacuum. The viscous red oil was dissolved in hot hexanes and was left at 23°C for several days, affording orange crystalline {^{i}Pr(nn)PM}H that was collected by filtration and washed with cold hexanes (8.10 g, 23 mmol, 41%). ^{1}H NMR ($CDCl_3$, 500 MHz, 295K): δ 11.33 (s, 1H, N*H*), 8.52 (d, J=5 Hz, 1H, a), 7.64 (m, 1H, c), 7.31 (m, 1H, d), 7.14 (m, 1H, b), 7.11 (m, 2H, n), 7.03 (m, 1H, o), 4.79 (s, 1H, i), 4.60 (s, 2H, f), 2.93 (sp, J=7 Hz, 2H, r), 1.99 (s, 3H, g), 1.69 (s, 3H, k), 1.18 (d, J=7 Hz, 6H, p), 1.09 (d, J=7 Hz, 6H, o). ^{13}C{^{1}H} NMR ($CDCl_3$, 125 MHz, 295K): δ 166.64 (j), 160.18 (e), 155.68 (h), 149.36 (a), 146.67 (l), 138.06 (m), 136.97 (c), 122.84 (n), 122.79 (o), 122.01 (b), 120.48 (d), 94.51 (i), 48.99 (f), 28.17 (r), 23.91 (t), 23.02 (s), 21.83 (k), 19.42 (g).

{Et(nn)PM}H. To a solution of 2,4-pentanedione (9.39 g, 94 mmol) in toluene (40 mL) was added 2,6-diethylaniline (10 g, 67 mmol) and a catalytic amount of p-toluenesulfonic acid. The mixture was refluxed and water was collected in a Dean-

Stark trap. After 7 h the volatiles were removed under vacuum, leaving an orange oil. Toluene (40 mL), 2-picolylamine (7.25 g, 67 mmol), and a catalytic amount of p-toluenesulfonic acid were added, and the reaction was refluxed for 48 h. Water produced during the reaction was collected in a Dean-Stark trap. The reaction was cooled and volatiles were removed under vacuum. The red oily residue was dissolved in Et_2O (60 mL), and washed with saturated Na_2CO_3 (3 x 15 mL). The organic layer was dried with Na_2SO_4, filtered and solvent was removed under vacuum. The product was collected by vacuum distillation (160-175°C, 0.1 mTorr). The product {Et(nn)PM}H is a viscous orange oil (11.6 g, 35 mmol, 54%). ^{1}H NMR ($CDCl_3$, 400 MHz, 295K): δ 11.54 (s, 1H, N*H*), 8.52 (d, J=5 Hz, a), 7.64 (m, 1H, c) 7.30 (d, J=8 Hz, 1H, d), 7.13 (m, 1H, b), 7.05 (m, 2H, o), 6.95 (m, 2H, n), 4.76 (s, 1H, i), 4.58(d, J=5 Hz, 2H, f), 2.42 (m, 4H, r), 1.96 (s, 3H, g), 1.66 (s, 3H, k), 1.12 (t, J=8 Hz, 6H, s). ^{13}C{^{1}H} NMR ($CDCl_3$, 100 MHz, 295K): δ 166.37 (j), 160.19 (e), 155.76 (h), 149.28 (a), 148.21(l), 136.84 (c), 133.44 (m), 125.70 (n), 122.44 (o), 121.19 (b), 120.44 (d), 94.53 (i), 48.88 (f), 24.73 (r), 21.50 (k), 19.13 (g), 14.14 (s). Anal for $C_{21}H_{27}N_3$ (calc), C 78.46, H 8.47, N 13.07; (found), C 78.41, H 8.37, N 13.19.

*{^{i}Pr(nn)PM}CrN(TMS)$_2$ (**1-Cr^{iPr}**).* To a 50 mL flask charged with $Cr[N(TMS)_2]_2(THF)_2$ (0.600g, 1.16 mmol) and {^{i}Pr(nn)PM}H (0.406 g, 1.16 mmol) at -78°C was vacuum transferred 20 mL benzene. The reaction mixture was allowed to warm to 23°C, and the deep red solution was stirred for 10 h. The solvent was removed under vacuum and the resulting solid was triturated with 3 x 10 mL hexanes to ensure removal of residual amine. 20 mL Et_2O was added, and the solution was filtered, concentrated and cooled to -78°C, resulting in 270 mg (0.481 mmol, 41%) of

red, crystalline **1**-Cr^{iPr}. ^{1}H NMR (C_6D_6, 400MHz, 295K): δ 122.41 ($\nu_{1/2} \approx 2400$ Hz, 2H), 107.11 ($\nu_{1/2} \approx 2200$ Hz, 2H), 40.31 ($\nu_{1/2} \approx 2600$ Hz, 28H), 22.48 ($\nu_{1/2} \approx 880$ Hz, 2H), 11.74 ($\nu_{1/2} \approx 321$ Hz, 3H), 9.03 ($\nu_{1/2} \approx 480$ Hz, 9H), -12.41 ($\nu_{1/2} \approx 1200$ Hz, 1H), -67.96 ($\nu_{1/2} \approx 1400$ Hz, 1H). μ_{eff} (Evans): 4.9 μ_B. Anal. for $C_{29}H_{48}CrN_4Si_2$ (calc), C 62.10, H 8.63, N 9.99; (found)

*{^{i}Pr(nn)PM}FeN(TMS)$_2$ (**1-Fe^{iPr}**).* To a 50 mL flask charged with {^{i}Pr(nn)PM}H (545 mg, 1.6 mmol) and Fe[N(TMS)$_2$]$_2$(THF) (700 mg, 1.6 mmol) at -78°C was vacuum transferred 15 mL benzene. The reaction mixture was allowed to warm to 23°C, and the yellow solution was stirred for 10 h. The benzene was removed under vacuum and 15 mL toluene was added. The solution was filtered and concentrated. Pentane was added at -78 ^{o}C to precipitate **1**-Fe^{iPr} as a yellow solid (660 mg, 1.2 mmol, 75%). ^{1}H NMR (C_6D_6, 400 MHz, 295K): δ 49.96 ($\nu_{1/2} \approx 100$ Hz, 1H), 39.57 ($\nu_{1/2} \approx 36$ Hz, 2H), 38.06 ($\nu_{1/2} \approx 500$ Hz, 7H), 31.83 ($\nu_{1/2} \approx 350$ Hz, 3H), 20.98 ($\nu_{1/2} \approx 130$ Hz, 2H), 5.25 ($\nu_{1/2} \approx 150$ Hz, 3H), 2.74 ($\nu_{1/2} \approx 100$ Hz, 1H), -6.34 ($\nu_{1/2} \approx$ 100 Hz, 4H), -14.94 ($\nu_{1/2} \approx 36$ Hz, 1H), -19.02 ($\nu_{1/2} \approx 170$ Hz, 4H), -26.62 ($\nu_{1/2} \approx 133$ Hz, 5H), -27.63 ($\nu_{1/2} \approx 300$ Hz, 9H), -38.57 ($\nu_{1/2} \approx 60$ Hz, 5H), -77.87 ($\nu_{1/2} \approx 310$ Hz, 1H). μ_{eff} (Evans): 5.3 μ_B. Anal. for $C_{29}H_{48}FeN_4Si_2$ (calc), C 61.68, H 8.57, N 9.92; (found) C 61.83, H 8.58, N 9.33.

*{Et(nn)PM}FeN(TMS)$_2$ (**1-Fe^{Et}**).* To a 50 mL flask charged with Fe[N(TMS)$_2$]$_2$(THF) (2.31 g, 5.1 mmol) and {Et(nn)PM}H (1.65 g, 5.1 mmol) at -78°C was added 25 mL benzene. The flask was allowed to warm to 23°C, and the resulting yellow solution was stirred for 8 h. Solvent was removed under vacuum and

25 mL fresh toluene was added. The solution was filtered and concentrated. Pentane was added to precipitate **1**-Fe^{Et} as a yellow solid at -78°C that was collected by filtration (1.72 g, 3.2 mmol, 63%). ^{1}H NMR (C_6D_6, 400 MHz, 295K): δ 50.86 ($\nu_{1/2}$ ≈ 88 Hz, 1H), 43.46 ($\nu_{1/2}$ ≈ 38 Hz, 1H), 30.76 ($\nu_{1/2}$ ≈ 430 Hz), 8.30 ($\nu_{1/2}$ ≈ 800 Hz, 1H), -17.06 ($\nu_{1/2}$ ≈ 110 Hz, 5H), -26.67 ($\nu_{1/2}$ ≈ 120 Hz, 5H), -38.63 ($\nu_{1/2}$ ≈ 48 Hz, 1H), -78.09 ($\nu_{1/2}$ ≈ 360 Hz, 1H). μ_{eff} (Evans): 5.3 μ_B. Anal for $C_{27}H_{44}FeN_4Si_2$ (calc), C 60.42, H 8.26, N 10.44; (found), 61.32, H 8.37, N 10.42.

*{Et(nn)PM}CoN(TMS)$_2$ (**1-Co^{Et}**).* A 25 mL round bottom flask was charged with $Co[N(TMS)_2]_2(THF)$ (350 mg, 0.78 mmol) and 10 mL benzene. In a scintillation vial {Et(nn)PM}H (249 mg, 0.78 mmol) was dissolved in 2 mL benzene. The solution of ligand in benzene was added dropwise to the round bottom flask. This round bottom flask containing a red solution was attached to a 180^o needle valve adapter and degassed on the vacuum line. After stirring at room temperature for 12 h, a bright green solution was obtained. The solvent was removed under vacuum and 15 mL pentane was added. The reaction was filtered, concentrated, cooled to -78 ^{o}C, and filtered to yield 220 mg (0.41 mmol, 53%) of bright green crystalline **1**-Co^{Et}. ^{1}H NMR (C_6D_6, 400MHz, 295K): δ 202.52 ($\varpi_{1/2}$ ≈ 350 Hz, 1H), 101.37 ($\varpi_{1/2}$ ≈ 740 Hz, 1H), 50.98 ($\varpi_{1/2}$ ≈ 55 Hz, 1H), 47.29 ($\varpi_{1/2}$ ≈ 60 Hz, 2H), 35.39 ($\nu_{1/2}$ ≈ 520 Hz, 1H), 25.02 ($\nu_{1/2}$ ≈ 430 Hz, 1H), 19.98 ($\nu_{1/2}$ ≈ 230 Hz, 3H), 14.08 ($\nu_{1/2}$ ≈ 360 Hz, 9H), -0.47 ($\nu_{1/2}$ ≈ 160 Hz, 3H), -1.14 ($\nu_{1/2}$ ≈ 110 Hz, 3H), -2.56 ($\nu_{1/2}$ ≈ 30 Hz, 1H), -6.34 ($\nu_{1/2}$ ≈ 130 Hz, 4H), -6.72 ($\nu_{1/2}$ ≈ 220 Hz, 9H), -33.15 ($\nu_{1/2}$ ≈ 37 Hz, 1H), -58.15 ($\nu_{1/2}$ ≈ 110 Hz, 3H), -

103.10 ($\nu_{1/2} \approx 260$ Hz, 1H). μ_{eff} (Evans): 4.5 μ_B. Anal. for $C_{27}H_{44}CoN_4Si_2$ (calc), C 60.08, H 8.22, N 10.38; (found) C 59.36, H 8.04, N 10.21.

*{^{i}Pr(nn)PM}FeBr (**2-Fe^{iPr}**).* To a 50 mL 2 neck flask charged with {^{i}Pr(nn)PM}H (1.0 g, 2.9 mmol) and $LiN(TMS)_2$ (0.48 g, 2.9 mmol), and having an attached addition finger charged with $FeBr_2$ (0.62 g, 2.9 mmol), was added 25 mL THF at -78°C. The reaction was allowed to warm to 23°C and turned red. After 3 h, the $FeBr_2$ was added, and the became dark yellow/brown. After 12 h at 23°C, the reaction mixture was filtered to remove LiBr. Concentration and cooling of the filtrate to -78°C gave a bright green solid (**2**-Fe^{iPr}, 1.08 g, 2.2 mmol, 76%). ^{1}H NMR (C_6D_6, 400 MHz, 295K): δ 100.91 ($\nu_{1/2} \approx 800$ Hz, 1H), 62.40 ($\nu_{1/2} \approx 73$ Hz, 2H), 61.85 ($\nu_{1/2} \approx 70$ Hz, 2H), 20.02 ($\nu_{1/2} \approx 50$ Hz, 2H), 0.54 ($\nu_{1/2} \approx 50$ Hz, 7H), -9.68 ($\nu_{1/2} \approx 100$ Hz, 3H), -15.19 ($\nu_{1/2} \approx 140$ Hz, 7H), -23.02 ($\nu_{1/2} \approx 113$ Hz, 3H), -37.24 ($\nu_{1/2} \approx 44$ Hz, 1H), -77.50 ($\nu_{1/2} \approx 220$ Hz, 1H). μ_{eff} (Evans): 5.0 μ_B. Anal. for $C_{23}H_{30}BrFeN_3$ (calc), C 57.05, H 6.24, N 8.68; (found) C 57.33, H 6.28, N 8.55.

*{Et(nn)PM}FeBr (**2-Fe^{Et}**).* Procedure *5.2.7.* was followed with {Et(nn)PM}H (350 mg, 1.1 mmol), $LiN(TMS)_2$ (182 mg, 1.1 mmol), and $FeBr_2$ (235 mg, 1.1 mmol) in 12 mL THF. Product **2**-Fe^{Et} was a bright green solid (420 mg, 85%). ^{1}H NMR (C_6D_6, 400MHz, 295K): δ 103.92 ($\nu_{1/2} \approx 800$ Hz, 1H), 63.70 ($\nu_{1/2} \approx 116$ Hz, 2H), 62.86 ($\nu_{1/2} \approx 116$ Hz, 2H), 21.55 ($\nu_{1/2} \approx 105$ Hz, 2H), 14.45 ($\nu_{1/2} \approx 511$ Hz, 2H), -10.63 ($\nu_{1/2} \approx 164$ Hz, 5H), -11.01 ($\nu_{1/2} \approx 120$ Hz, 3H), -15.49 ($\nu_{1/2} \approx 104$ Hz, 1H), -25.13 ($\nu_{1/2} \approx 168$ Hz, 3H), -39.45 ($\nu_{1/2} \approx 102$ Hz, 1H), -83.53 ($\nu_{1/2} \approx 264$ Hz, 1H). μ_{eff} (Evans): 5.4

μ_B. Anal. for $C_{21}H_{26}BrFeN_3$ (calc), C 55.29, H 5.74, N 9.21; (found) C 55.22, H 5.85, N 9.13.

*{^{i}Pr(nn)PM}Fe^{neo}Pe (**3-Fe^{iPr}**).* To a 25 mL flask charged with **2**-Fe^{iPr} (600 mg, 1.2 mmol) and neopentyllithium (97 mg, 1.2 mmol) at -78°C was distilled 12 mL THF (12 mL), and the reaction was allowed to warm to 23°C. After stirring for 12 h, a dark red solution was obtained, and solvent was removed under vacuum. The solid was triturated with benzene (3 x 5 mL) to remove residual THF. The solution was filtered, concentrated and cooled to -78^{o}C to give **3**-Fe^{iPr} as an orange solid (320 mg, 0.67 mmol, 55%). ^{1}H NMR (C_6D_6, 400MHz, 295K): δ 64.42 ($\nu_{1/2} \approx 64$ Hz, 1H), 56.57 ($\nu_{1/2} \approx 35$ Hz, 1H), 15.81 ($\nu_{1/2} \approx 441$ Hz, 9H), 1.65 ($\nu_{1/2} \approx 93$ Hz, 6H), -19.81 ($\nu_{1/2} \approx 95$ Hz, 3H), -25.38 ($\nu_{1/2} \approx 135$ Hz, 3H), -29.90 ($\nu_{1/2} \approx 43$ Hz, 1H), -38.34 ($\nu_{1/2} \approx 35$ Hz, 1H), -73.65 ($\nu_{1/2} \approx 325$ Hz, 1H). μ_{eff} (Evans, 295K) = 5.2 μ_B. Anal. for $C_{28}H_{41}FeN_3$ (calc), C 70.73, H 8.69, N 8.84; (found) C 70.81, H 8.68, N 8.48.

*{Et(nn)PM}Fe^{neo}Pe (**3-Fe^{Et}**).* Procedure for **3-Fe^{iPr}** was followed with {Et(nn)PM}FeBr (825 mg, 1.8 mmol) and neopentyllithium (141 mg, 1.8 mmol) in 15 mL THF. The orange product precipitated from a 1:1 mixture of pentane/toluene (321 mg, 0.72 mmol, 40%). ^{1}H NMR (C_6D_6, 400 MHz, 295K): δ 66.82 ($\nu_{1/2} \approx 86$ Hz, 1H), 58.52 ($\nu_{1/2} \approx 47$ Hz, 1H), 20.98 ($\nu_{1/2} \approx 450$ Hz, 7H), -24.50 ($\nu_{1/2} \approx 130$ Hz, 3H), -29.21 ($\nu_{1/2} \approx 150$ Hz, 2H), -30.61 ($\nu_{1/2} \approx 48$ Hz, 1H, -42.88 ($\nu_{1/2} \approx 58$ Hz, 1H), -73.88 ($\nu_{1/2} \approx 320$ Hz, 1H). μ_{eff} (Evans, 295K) = 5.1 μ_B. Anal. for $C_{26}H_{37}FeN_3$ (calc) C 69.79, H, 8.34, N 9.39; (found) C 67.09, H 7.20, N 10.57.

*{^{i}Pr(nn)PM}Fe(CO^{neo}Pe)CO (**4-Fe^{iPr}**).* To a 100 mL flask charged with **3**-Fe^{iPr} (200 mg, 1.2 mmol) at -78°C was distilled 10 mL benzene, and 1 atm of CO was admitted over the solution. The reaction immediately turned purple and after stirring for 2 d at 23°C all volatiles were removed under vacuum resulting in **4**-Fe^{iPr} as a red solid (185 mg, 0.37 mmol, 87%). ^{1}H NMR (400 MHz, 295K): δ 8.97 (d, J=5 Hz, 1H, a), 7.26 (m, 1H, p), 7.22 (m, 1H, o), 7.11 (m, 1H, n), 6.65 (m, 1H, c), 6.37 (d, J=7 Hz, 1H, d), 6.20 (m, 1H, b), 5.79 (s, 1H, i), 4.77 (d, J=21 Hz, 1H, f), 4.57 (d, J=21 Hz, 1H, f), 3.27 (sept, J=7 Hz, 1H, r), 2.96 (d, J=16 Hz, 1H, y), 2.45 (d, J=16 Hz, 1H, y), 2.26 (s, 3H, g), 2.15 (sept, J=7 Hz, 1H, u), 1.86 (s, 3H, k), 1.68 (d, J=7 Hz, 3H, s), 1.26 (d, J=7 Hz, 3H, t), 1.18 (d, J=7 Hz, 3H, v), 0.92 (d, J=7 Hz, 3H, w), 0.83 (s, 9H, z). ^{13}C{^{1}H} NMR (C_6D_6, 100 MHz, 295 K): δ 218.88 (bb), 181.32 (x), 165.08 (e), 161.98 (j), 158.93 (h), 155.69 (l), 155.33 (a), 141.72 (m), 139.36 (q), 132.98 (c), 125.94 (o), 124.25 (p), 123.56 (n), 122.65 (b), 117.41 (d), 101.60 (i), 62.28 (f), 61.33 (y), 31.86 (z), 29.59 (aa), 28.41 (u), 27.80 (r), 25.27 (s), 24.46 (t), 24.43 (v), 24.23 (w), 23.95 (k), 22.99 (g). IR (C_6D_6): ν(CO) 1906 cm^{-1}, ν(acyl) 1638 cm^{-1}. Anal. for $C_{29}H_{41}FeN_3O$ (calc), C 69.18, H 8.21, N 8.35; (found), C 67.81, H 7.75, N 7.14.

*{^{i}Pr(nn)PI}Fe(CO)$_2$ (**5-Fe^{iPr}**).* A 100 mL gas bomb was charged with **1**-Fe^{iPr} (300 mg, 0.53 mmol), and 10 mL THF was added at -78°C. 1 atm CO was admitted to the bomb, and the solution was heated at 60°C for 2 d. After cooling, the red-brown solution was removed from the bomb, and the THF was removed. Dark blue **5**-Fe^{iPr} was crystallized from a dark red/brown THF/pentane solution at -78 ^{o}C (185 mg, 0.40 mmol, 76%). ^{1}H NMR (C_6D_6, 500 MHz, 295K): δ 8.85 (d, J = 6 Hz, 1H, a), 7.81 (s, 1H, f), 7.15 (m, 1H, d), 7.11 (m, 3H, n, o), 6.67 (m, 1H, c), 6.24 (m, 1H, b), 6.11 (s,

1H, i), 2.63 (sp, 2H, n), 2.34 (s, 3H, g), 1.80 (s, 3H, k), 1.31 (d, J = 7 Hz, 6H, t), 0.97 (d, J = 7 Hz, 6H, s). $^{13}C\{^{1}H\}$ NMR (C_6D_6, 125 MHz, 295 K): δ 218.36 (bb), 160.09 (j), 155.77 (l), 152.90 (a), 152.71 (e), 146.99 (h), 138.64 (m), 127.39 (c), 126.64 (o), 124.26 (f), 124.12 (n), 121.51 (d), 113.25 (b), 111.81 (i), 27.94 (n), 24.59 (t), 24.10 (s), 23.34 (k), 22.28 (g). IR (C_6D_6): ν(CO) 1960, 1909 cm^{-1}. Anal. for $C_{25}H_{31}FeN_3O_2$ (calc), C 65.37, H 6.36, N 9.15; (found) C 66.09, H 6.81, N 9.28.

*{Et(nn)PI}Fe(CO)$_2$ (**5**-Fe^{Et}).* Procedure for **5-Fe^{iPr}** was followed with 1-Fe^{Et} (1.0 g, 1.9 mmol) in 20 mL THF. Dark blue **5**-Fe^{Et} was crystallized from a dark red/brown THF/pentane solution at -78 ^{o}C (550 mg, 1.27 mmol, 69 %). ^{1}H NMR (C_6D_6, 500 MHz, 295K): δ 8.82 (d, J = 6 Hz, 1H, a), 7.83 (s, 1H, f), 7.14 (m, 1H, d), 7.09 (m, 3H, n, o), 6.66 (m, 1H, c), 6.19 (m, 1H, b), 6.09 (m, 1H, i), 2.41 (m, 2H, r), 2.35 (s, 3H, g), 2.14 (m, 2H, r), 1.69 (s, 3H, k), 1.07 (t, J = 7 Hz, 6H, s). $^{13}C\{^{1}H\}$ NMR (C_6D_6, 125 MHz, 295 K): δ 218.16 (bb), 160.02 (j), 157.29 (l), 153.06 (a), 152.86 (e), 147.12 (h), 133.81 (m), 127.47 (c), 126.20 (n), 125.94 (o), 124.22 (f), 121.45 (d), 113.24 (b), 111.88 (i), 24.01 (r), 22.94 (k), 22.30 (g), 14.04 (s). IR (C_6D_6): ν(CO) 1971, 1910 cm^{-1} Anal. for $C_{23}H_{27}FeN_3O_2$ (calc), C 63.75, H 6.28, N 9.70; (found) C 64.53, H 5.86, N 9.70.

*{κ^2-N,N-pyrim-pyr}Cr(CO)$_4$ (**6-Cr^{iPr}**).* To a 100 mL flask charged with **1**-Cr^{iPr} at -78°C was distilled 10 mL THF, and 1 atm CO was admitted over the solution. The reaction was stirred at 23°C for 24 h, and the solvent was removed under vacuum. The resulting yellow solid was triturated with benzene (2 x 10 mL) to remove residual THF. Yellow-orange **6**-Cr^{iPr} was crystallized from THF/pentane (138 mg, 0.26 mmol, 57%). ^{1}H NMR (C_6D_6, 500 MHz, 295K): δ 9.02 (d, J = 5 Hz, 1H, a), 6.94 (m, 1H, o),

6.86 (d, J = 7 Hz, n), 6.59 (d, J=7 Hz, p), 6.28 (m, 1H, c), 6.17 (m, 1H, d), 6.03 (m, 1H, b), 5.36 (s, 1H, f), 5.04 (s, 1H, i), 2.83 (sept, J = 7 Hz, 1H, r), 2.61 (sept, J = 7 Hz, 1H, u), 2.46 (s, 3H, g), 1.24 (s, 3H, k), 1.09 (d, J = 7 Hz, 3H, v), 1.01 (J= 7 Hz, 3H, w), 0.84 (d, J = 7 Hz, 3H, s), 0.47 (d, J = 7 Hz, 3H, t). $^{13}C\{^{1}H\}$ NMR (C_6D_6, 125 MHz, 295 K): δ 228.64 (bb), 228.16 (cc), 217.22 (dd), 216.43 (ee), 173.31 (h), 157.25 (e), 154.10 (j), 152.87 (a), 148.69 (m), 147.66 (q), 135.77 (l), 134.16 (c), 129.72 (o), 125.06 (n), 124.62 (p), 123.78 (d), 123.10 (b), 102.85 (i), 81.58 (f), 28.86 (u), 28.80 (r), 27.85 (g), 25.19 (v), 24.94 (w), 24.38 (s), 22.38 (t), 19.09 (k). IR (C_6D_6): ν(CO) 2001, 1880, 1851, 1818 cm^{-1}. Anal. for $C_{27}H_{29}CrN_3O_4 \cdot 2(C_6H_6)$ (calc), C 70.15, H 6.19, N 6.29; (found) C 69.98, H 5.95, N 6.32.

2-H,2-pyridyl,3-DIPP,4,6-dimethyl-pyrimidine (pyrim-pyr). To a 25 mL flask charged with $[\{^{i}Pr(nn)PI\}^{2-}](K^{+}(THF)_x)_2$ (378 mg, 0.78 mmol) and $[Cp_2Fe]PF_6$ (520 mg, 1.6 mmol) at -78°C was vacuum transferred 15 mL THF. The reaction was allowed to slowly warm to 23°C, and was stirred for 3 h. Solvents were removed under vacuum and resulting red/orange oil was triturated with benzene (3 x 5 mL). The oil was dissolved in 15 mL methylene chloride, filtered through a plug of celite, and the solvent was removed. The product was purified on an alumina column, which was loading with ethyl acetate with a gradient of 1:1 Hex:EtOAc, EtOAc, and 5% MeOH in EtOAc. After removal of solvent from the later fractions, a red solid was obtained (183 mg, 0.55 mmol, 67%). ^{1}H NMR (C_6D_6, 500 MHz, 295K): δ 8.44 (d, J = 5 Hz, 1H, a), 7.55 (m, 2H, c, d), 7.16 (m, 1H, o), 7.10 (m, 2H, b, p), 6.93 (m, 1H, n), 5.89 (s, 1H, f), 5.05 (s, 1H, i), 3.17 (sp, J = 7 Hz, 1H, u), 2.98 (sp, J = 7 Hz, 1H, r), 1.96 (s, 3H, g), 1.60 (s, 3H, k), 1.23 (d, J = 7 Hz, 3H, v), 1.09 (d, J = 7 Hz, 3H, w),

0.98 (d, J = 7 Hz, 3H, s), 0.29 (d, J = 7 Hz, 3H, t). $^{13}C\{^{1}H\}$ NMR (C_6D_6, 125 MHz, 295 K): δ 161.78 (h), 159.74 (e), 151.24 (j), 148.16 (m), 147.88 (a), 146.58 (q), 137.74 (l), 135.61 (c), 127.45 (o), 123.88 (p), 123.18 (n), 122.01 (b), 121.34 (d), 95.02 (f), 82.75 (i), 26.95 (r), 26.87 (u), 23.82 (w), 23.39 (v), 23.16 (s), 23.07 (g), 22.97 (t), 19.15 (k).

$[\{^{i}Pr(nn)PI\}^{2-}](K^{+}(THF)_x)_2$. To a 50 mL flask was charged with $\{^{i}Pr(nacnac)PM\}H$ (1.34 g, 3.8 mmol) and potassium benzyl (1.0 g, 7.7 mmol) at -78°C was transferred 25 mL THF. The intensely colored pink solution was allowed to slowly warm to 23°C over 0.5 h, and stirred for 3 h. Volatiles were removed under vacuum and the dark red solid was triturated with benzene (2 x 10 mL) to remove residual THF. The product was isolated and used without further purification (1.68 g, 3.5 mmol, 91%). ^{1}H NMR (THF-d_8, 500MHz, 295K): δ 6.88 (m, 1H, a, n), 6.63 (m, 1H, o), 5.81 (m, 1H, c), 5.51 (m, 1H, d), 5.42 (s, 1H, f), 4.57 (m, 1H, b), 3.97 (s, 1H, i), 3.25 (sp, J=7 Hz, 2H, r), 1.68 (s, 3H, g), 1.50 (s, 3H, k), 1.16 (d, J=7 Hz, 6H, t), 1.05 (d, J=7 Hz, 6H, s). $^{13}C\{^{1}H\}$ NMR (THF-d_8, 500MHz, 295K): δ 154.94 (l), 153.36 (j), 151.21 (a), 150.52 (e), 141.55 (m), 140.61 (h), 129.93 (c), 123.25 (n), 119.52 (o), 117.00 (d), 100.11 (f), 96.47 (b), 93.53 (i), 27.79 (r), 25.44 (k), 25.28 (s), 24.60 (t), 20.67 (g).

*$\{^{i}Pr(nn)CHpy\}_2Fe_2Cl_2$ (**7-Fe^{iPr}**).* To a 50 mL flask charged with $[\{^{i}Pr(nn)PI\}^{2-}](K^{+}(THF)_x)_2$ (550 mg, 1.1 mmol) and $FeCl_3$ (179 mg, 1.1 mmol) at -78°C was transferred 15 mL of THF. The reaction was warmed to 23°C and after stirring for 14 h, the deep red solution became yellow-brown in color. The reaction was filtered and solids were washed with THF. The combined filtrate was

concentrated, and cooled to -78°C to precipitate **7**-Fe^{iPr} as a yellow solid (291 mg, 0.33 mmol, 60%). ^{1}H NMR (C_6D_6, 400MHz, 295K): δ 77.63 ($\nu_{1/2}$ ≈ 750 Hz, 1H), 44.70 ($\nu_{1/2}$ ≈ 77 Hz, 1H), 26.59 ($\nu_{1/2}$ ≈ 50 Hz, 1H), 17.99 ($\nu_{1/2}$ ≈ 170 Hz, 3H), 14.65 ($\nu_{1/2}$ ≈ 80 Hz, 1H), 4.16 ($\nu_{1/2}$ ≈ 50 Hz, 4H), -0.79 ($\nu_{1/2}$ ≈ 63 Hz, 4H), -20.62 ($\nu_{1/2}$ ≈ 140 Hz, 3H), -34.13 ($\nu_{1/2}$ ≈ 230 Hz, 3H), -36.85 ($\nu_{1/2}$ ≈ 300 Hz, 5H), -42.65 ($\nu_{1/2}$ ≈ 60 Hz, 1H), -80.35 ($\nu_{1/2}$ ≈ 300 Hz, 1H). μ_{eff} (Evans): 6.4 μ_B. Anal. for $C_{46}H_{58}Fe_2N_{46}$ (calc), C 62.96, H 6.66, N 9.58; (found) 63.26, H 6.79, N 9.15.

*{[Et(nn)CHpy]$_2$}Fe (**8-Fe^{Et}**).* To a 25 mL glass bomb charged with **1**-Fe^{Et} (129 mg, 0.24 mmol) and $TMSN_3$ (28 mg, 0.24 mmol) at -78°C was transferred 4 mL benzene. The bomb was allowed to warm to 23°C, degassed and placed in a 110 °C oil bath for 3 d. The reaction mixture turned dark red, and was cooled, degassed, and the solvent was removed under vacuum. The red solid was taken up in Et_2O and filtered. The Et_2O was removed under vacuum and the product was crystallized by heating the residual solid in hexanes and slowly cooling the solution to afford **8**-Fe^{Et} as a green crystalline solid (55mg, 0.08 mmol, 33%). ^{1}H NMR (C_6D_6, 400MHz, 295K): δ 82.28 ($\nu_{1/2}$ ≈ 241 Hz, 2H), 47.87 ($\nu_{1/2}$ ≈ 490 Hz, 2H), 33.93 ($\nu_{1/2}$ ≈ 170 Hz, 6H), 19.87 ($\nu_{1/2}$ ≈ 43 Hz, 2H), 5.27 ($\nu_{1/2}$ ≈ 55 Hz, 2H), 3.89 ($\nu_{1/2}$ ≈ 160 Hz, 8H), 1.43 ($\nu_{1/2}$ ≈ 90 Hz, 10H), 0.88 ($\nu_{1/2}$ ≈ 33 Hz, 2H), -1.54 ($\nu_{1/2}$ ≈ 30 Hz, 2H), -17.85 ($\nu_{1/2}$ ≈ 60 Hz, 2H), -29.24 ($\nu_{1/2}$ ≈ 230 Hz, 6H), -31.87 ($\nu_{1/2}$ ≈ 49 Hz, 2H), -80.87 ($\nu_{1/2}$ ≈ 890 Hz, 2H), -85.52 ($\nu_{1/2}$ ≈ 950 Hz, 2H). μ_{eff} (Evans): 5.6 μ_B. Anal. for $C_{42}H_{50}FeN_6$ (calc), C 72.61, H 7.25, N 12.10; (found) C 72.73, H 7.34, N 12.07.

*{^{i}Pr(nn)CHpy}$_2$(FeN=CPh$_2$)$_2$ (**9-Fe^{iPr}**).* A 25 mL glass bomb was charged with **1**-Fe^{iPr} (200 mg, 0.35 mmol), diphenyldiazomethane (137 mg, 0.71 mmol), and 10 mL benzene. The reaction vessel was degassed on the vacuum line and placed in a 90 ^{o}C oil bath. Over the course of 3 d, the reaction turns dark red. After this time the bomb was degassed. The solution was transferred to a round bottom flask and the solvent removed under vacuum. Remaining organics were removed by washing the solid with small amounts of chilled benzene leaving an orange solid (83 mg, 0.071 mmol, 40%). ^{1}H NMR (C_6D_6, 400MHz, 295K): δ 40.63 ($\nu_{1/2} \approx 77$ Hz, 1H), 28.58 ($\nu_{1/2} \approx 100$ Hz, 5H), 14.67 ($\nu_{1/2} \approx 70$ Hz, 1H), 10.84 ($\nu_{1/2} \approx 52$ Hz, 1H), 3.59 ($\nu_{1/2} \approx 110$ Hz, 3H), -5.56 ($\nu_{1/2} \approx 72$ Hz, 3H), -9.39 ($\nu_{1/2} \approx 48$ Hz, 2H), -28.48 ($\nu_{1/2} \approx 210$ Hz, 4H), -40.30 ($\nu_{1/2} \approx 190$ Hz, 2H), -41.19 ($\nu_{1/2} \approx 380$ Hz, 3H), -46.43 ($\nu_{1/2} \approx 120$ Hz, 1H), -53.59 ($\nu_{1/2} \approx 70$ Hz, 1H). μ_{eff} (Evans): 6.5 μ_B.

*[{^{i}Pr(nn)PI}Fe(CO^{neo}Pe)CO]K (**10-Fe^{iPr}**).* A 25 mL flask was charged with **4-Fe^{iPr}** (350 mg, 0.659 mmol) and potassium benzyl (86 mg, 0.659 mmol). 12 mL THF was added at -78 ^{o}C and the solution was allowed to warm to room temperature. After stirring for 3 h the red solution was filtered and concentrated in vacuo. Benzene and pentane were added and the red solid was collected by filtration (319 mg, 0.56 mmol, 85%). ^{1}H NMR (C_6D_6, 400 MHz, 295 K): δ 8.31 (m, 1H), 7.41 (s, 1H), 7.20 (m, 2H), 7.00 (m, 3H), 6.43 (m, 1H), 6.39 (s, 1H), 6.17 (m, 1H), 5.67 (m, 1H), 3.25 (sept, J = 7 Hz, 1H), 2.88 (s, 3H), 2.15 (s, 3H), 2.15 (s, 3H), 1.62 (d, J = 17 Hz, 1H), 1.49 (d, J = 17 Hz, 1H), 1.45 (sept, J = 7 Hz, 1H), 1.36 (d, J = 7 Hz, 3H), 1.30 (d, J = 7 Hz, 3H), 0.72 (d, J = 7 Hz, 3H), 0.66 (d, J = 7 Hz, 3H), 0.62 (s, 9H). IR; ν_{CO} = 1872 cm^{-1}, ν_{acyl} = 1595 cm^{-1}.

*Small scale synthesis of {^{i}Pr(nn)^{Et}PM}Fe(CO^{neo}Pe)CO (**11-Fe^{iPr}**).* A flask was charged with **10-Fe^{iPr}** (50 mg, 0.078 mmol) and triethyloxonium tetrafluoroborate (15 mg, 0.078 mmol). 5 mL 1,2-dichloroethane was added at -78 ^{o}C and the reaction was warmed to room temperature giving a green solution. After 2 h, solvent was removed under vacuum and the reaction was triturated with pentane to leave a red solid. ^{1}H NMR of the crude reaction mixture showed formation of a prominent diamagnetic product in ~90 % yield. ^{1}H NMR (C_6D_6, 400 MHz, 295 K): δ 8.85 (m, 1H), 7.28 (m, 1H), 7.22 (m, 1H), 7.11 (m, 1H), 6.63 (m, 1H), 6.40 (m, 1H), 6.18 (m, 1H), 5.64 (s, 1H), 5.10 (t, J = 6 Hz, 1H), 3.32 (sept, J = 7 Hz, 1H), 3.25 (d, J = 15 Hz, 1H), 2.36 (d, J = 15 Hz, 1H), 2.33 (s, 3H), 2.25 (sept, J = 7 Hz, 1H), 1.84 (s, 3H), 1.74 (d, J = 7 Hz, 3H), 1.58 (m, 2H), 1.28 (d, J = 7 Hz, 3H), 1.22 (d, J = 7 Hz, 3H), 0.99 (d, J = 7 Hz, 3H), 0.79 (s, 9H), 0.42 (t, J = 7 Hz, 3H). IR; ν_{CO} = 1917 cm^{-1}, ν_{acyl} = 1619 cm^{-1}.

C. Single Crystal X-Ray Diffraction Studies.

Upon isolation, the crystals were covered in polyisobutenes and placed under a 173 K N_2 stream on the goniometer head of a Siemens P4 SMART CCD area detector (graphite-monochromated MoK_α radiation, λ = 0.71073 Å). The structures were solved by direct methods (SHELXS). All non-hydrogen atoms were refined anisotropically unless stated, and hydrogen atoms were treated as idealized contributions (Riding model). Any deviation from this protocol will be noted for the individual descriptions below.

*{^{i}Pr(nn)PM}CrN(TMS)$_2$ (**1-Cr^{iPr}**).* A red block (0.20 x 0.15 x 0.10 mm^3) of **1**-Cr^{iPr} was obtained from pentane diffusion into a concentrated benzene solution. A total of 30077 reflections were collected with 7709 determined to be symmetry independent

(R_{int} = 0.0405), and 5842 were greater than 2σ(I). A semi-empirical absorption correction from equivalents was applied, and the refinement utilized $w^{-1} = \sigma^2(F_o^2) + (0.0370p)^2 + 0.5529p$, where $p = ((F_o^2 + 2F_c^2)/3)$.

*{^{i}Pr(nn)PM}FeN(TMS)$_2$ (**1-Fe^{iPr}**).* A yellow block (0.15 x 0.10 x 0.05 mm^3) of **1**-Fe^{iPr} was obtained from pentane diffusion into a concentrated benzene solution. A total of 30373 reflections were collected with 7733 determined to be symmetry independent (R_{int} = 0.0401), and 5630 were greater than 2σ(I). A semi-empirical absorption correction from equivalents was applied, and the refinement utilized $w^{-1} = \sigma^2(F_o^2) + (0.0706p)^2 + 0.7411p$, where $p = ((F_o^2 + 2F_c^2)/3)$.

*{Et(nn)PM}CoN(TMS)$_2$ (**1-Co^{Et}**).* A green plate (0.40 x 0.20 x 0.05 mm^3) of **1**-Co^{Et} was obtained from pentane diffusion into a concentrated benzene solution. A total of 20872 reflections were collected with 5120 determined to be symmetry independent (R_{int} = 0.0399), and 3860 were greater than 2σ(I). A semi-empirical absorption correction from equivalents was applied, and the refinement utilized $w^{-1} = \sigma^2(F_o^2) + (0.0427p)^2 + 1.4064p$, where $p = ((F_o^2 + 2F_c^2)/3)$.

*{^{i}Pr(nn)PM}Fe(CO^{neo}Pe)CO (**4-Fe^{iPr}**).* A black needle (0.60 x 0.20 x 0.10 mm^3) of **4**-Fe^{iPr} was obtained from pentane diffusion into a concentrated THF solution. A total of 30125 reflections were collected with 9102 determined to be symmetry independent (R_{int} = 0.0223), and 7530 were greater than 2σ(I). A semi-empirical absorption correction from equivalents was applied, and the refinement utilized $w^{-1} = \sigma^2(F_o^2) + (0.0455p)^2 + 0.4216p$, where $p = ((F_o^2 + 2F_c^2)/3)$.

*{^{i}Pr(nn)PI}Fe(CO)$_2$ (**5-Fe^{iPr}**).* A black block (0.30 x 0.10 x 0.05 mm^3) of **5**-Fe^{iPr} was obtained from pentane diffusion into a concentrated THF solution. A total of 28882 reflections were collected with 8479 determined to be symmetry independent (R_{int} = 0.0173), and 7564 were greater than 2σ(I). A semi-empirical absorption correction from equivalents was applied, and the refinement utilized $w^{-1} = \sigma^2(F_o^2) + (0.0469p)^2 + 0.3653p$, where $p = ((F_o^2 + 2F_c^2)/3)$.

*{κ^2-N,N-pyrim-pyr}Cr(CO)$_4$ (**6-Cr^{iPr}**).* An orange block (0.50 x 0.40 x 0.35 mm^3) of **6**-Cr^{iPr} was obtained from pentane diffusion into a concentrated benzene solution. A total of 21706 reflections were collected with 5527 determined to be symmetry independent (R_{int} = 0.0204), and 5047 were greater than 2σ(I). A semi-empirical absorption correction from equivalents was applied, and the refinement utilized $w^{-1} = \sigma^2(F_o^2) + (0.0426p)^2 + 0.6802p$, where $p = ((F_o^2 + 2F_c^2)/3)$.

*{^{i}Pr(nn)CHpy}$_2$Fe$_2$Cl$_2$ (**7-Fe^{iPr}**).* A green plate (0.50 x 0.25 x 0.08 mm^3) of **7**-Fe^{iPr} was obtained from slow evaporation of a concentrated benzene solution. A total of 49724 reflections were collected with 13618 determined to be symmetry independent (R_{int} = 0.0459), and 9572 were greater than 2σ(I). A semi-empirical absorption correction from equivalents was applied, and the refinement utilized $w^{-1} = \sigma^2(F_o^2) + (0.0462p)^2 + 0.0000p$, where $p = ((F_o^2 + 2F_c^2)/3)$. SQEEZE was applied to one disordered benzene solvent molecule.

*{[Et(nn)CHpy]$_2$}Fe (**8-Fe^{Et}**).* A green plate (0.25 x 0.20 x 0.02 mm^3) of **8**-Fe^{Et} was obtained from slow evaporation of a concentrated Et_2O solution. A total of 78074 reflections were collected with 3248 determined to be symmetry independent (R_{int} =

0.0840), and 2181 were greater than 2σ(I). A semi-empirical absorption correction from equivalents was applied, and the refinement utilized $w^{-1} = \sigma^2(F_o^2) + (0.0213p)^2 + 0.0000p$, where $p = ((F_o^2 + 2F_c^2)/3)$. Data resolution was low due to small sample volume (very thin plate).

*{^{i}Pr(nn)CHpy}$_2$(FeN=CPh$_2$)$_2$ (**9-Fe^{iPr}**).* A red block (0.40 x 0.35 x 0.20 mm^3) of **9**-Fe^{iPr} was obtained from slow cooling of a hot benzene solution. A total of 29395 reflections were collected with 7201 determined to be symmetry independent (R_{int} = 0.0428), and 4936 were greater than 2σ(I). A semi-empirical absorption correction from equivalents was applied, and the refinement utilized $w^{-1} = \sigma^2(F_o^2) + (0.0588p)^2 + 1.6150p$, where $p = ((F_o^2 + 2F_c^2)/3)$.

D. Mössbauer Spectroscopy.

^{57}Fe Mössbauer spectra were recorded on a WissEl Mössbauer spectrometer (MRG-500) at 77 K in constant acceleration mode. ^{57}Co/Rh was used as the radiation source. WinNormos for Igor Pro software has been used for the quantitative evaluation of the spectral parameters (least-squares fitting to Lorentzian peaks). The minimum experimental line widths were 0.20 mms^{-1}. The temperature of the samples was controlled by an MBBC-HE0106 MÖSSBAUER He/N$_2$ cryostat within an accuracy of ±0.3 K. Isomer shifts were determined relative to α-iron at 298 K.

REFERENCES

(1) Frazier, B. A.; Bartholomew, E. R.; Wolczanski, P. T.; DeBeer, S.; Santiago-Berrios, M.; Abruña, H. D.; Lobkovsky, E. B.; Bart, S. C.; Mossin, S.; Meyer, K.; Cundari, T. R. *Inorg. Chem.* **2011**, *50*, 12414–12436.

(2) Frazier, B. A.; Wolczanski, P. T.; Keresztes, I.; DeBeer, S.; Lobkovsky, E. B.; Pierpont, A. W.; Cundari, T. R. *Inorg. Chem.* **2012**, *51*, 8177–8186.

(3) Frazier, B. A.; Williams, V. A.; Wolczanski, P. T.; Bart, S. C.; Meyer, K.; Cundari, T. R.; Lobkovsky, E. B. *Inorg. Chem.* **2013**, *52*, 3295–3312.

(4) Hulley, E. B.; Wolczanski, P. T.; Lobkovsky, E. B. *J. Am. Chem. Soc.* **2011**, *133*, 18058–18061.

(5) Tejel, C.; del Río, M. P.; Asensio, L.; van den Bruele, F. J.; Ciriano, M. A.; Tsichlis i Spithas, N.; Hetterscheid, D. G. H.; de Bruin, B. *Inorg. Chem.* **2011**, *50*, 7524–7534.

(6) Tejel, C.; Ciriano, M. A.; del Río, M. P.; van den Bruele, F. J.; Hetterscheid, D. G. H.; Tsichlis i Spithas, N.; de Bruin, B. *J. Am. Chem. Soc.* **2008**, *130*, 5844–5845.

(7) Tejel, C.; Ciriano, M. A.; del Río, M. P.; Hetterscheid, D. G. H.; Tsichlis i Spithas, N.; Smits, J. M. M.; de Bruin, B. *Chem. – Eur. J.* **2008**, *14*, 10932–10936.

(8) Williams, V. A.; Wolczanski, P. T.; Sutter, J.; Meyer, K.; Lobkovsky, E. B.; Cundari, T. R. *Inorg. Chem.* **2014**, *53*, 4459–4474.

(9) Xu, X.; Chen, Y.; Zou, G.; Sun, J. *Dalton Trans.* **2010**, *39*, 3952–3958.

(10) Gutlich, P.; Bill, E. *Mossbauer Spectroscopy and Transition Metal Chemistry*; Springer: New York, 2011.

(11) Figgis, B. N.; Hitchman, M. A. *Ligand Field Theory and Its Applications*; Wiley-VCH, 2000.

(12) Schäffer, C. E.; Jørgensen, C. K. *Mol. Phys.* **1965**, *9*, 401–412.

(13) Gunanathan, C.; Milstein, D. *Acc. Chem. Res.* **2011**, *44*, 588–602.

(14) Langer, R.; Leitus, G.; Ben-David, Y.; Milstein, D. *Angew. Chem. Int. Ed.* **2011**, *50*, 2120–2124.

(15) Collins, R. L.; Pettit, R. *J. Chem. Phys.* **1963**, *39*, 3433–3436.

(16) Dias, G. H. M.; Morigaki, M. K. *Polyhedron* **1992**, *11*, 1629–1636.

(17) Vasudev, P.; Jones, C. H. W. *Can. J. Chem.* **1973**, *51*, 405–410.

(18) Lee, Y.; Mankad, N. P.; Peters, J. C. *Nat. Chem.* **2010**, *2*, 558–565.

(19) Tondreau, A. M.; Milsmann, C.; Lobkovsky, E.; Chirik, P. J. *Inorg. Chem.* **2011**, *50*, 9888–9895.

(20) Lu, C. C.; Bill, E.; Weyhermüller, T.; Bothe, E.; Wieghardt, K. *J. Am. Chem. Soc.* **2008**, *130*, 3181–3197.

(21) Franceschi, F.; Solari, E.; Scopelliti, R.; Floriani, C. *Angew. Chem. Int. Ed.* **2000**, *39*, 1685–1687.

(22) De Angelis, S.; Solari, E.; Gallo, E.; Floriani, C.; Chiesi-Villa, A.; Rizzoli, C. *Inorg. Chem.* **1996**, *35*, 5995–6003.

(23) Allen, F. H.; Kennard, O.; Watson, D. G.; Brammer, L.; Orpen, A. G.; Taylor, R. *J. Chem. Soc. Perkin Trans. 2* **1987**, S1–S19.

(24) Bowman, A. C.; Milsmann, C.; Bill, E.; Turner, Z. R.; Lobkovsky, E.; DeBeer, S.; Wieghardt, K.; Chirik, P. J. *J. Am. Chem. Soc.* **2011**, *133*, 17353–17369.

(25) Parham, W. E.; Hasek, W. R. *J. Am. Chem. Soc.* **1954**, *76*, 935–936.

(26) Miller, R. J.; Shechter, H. *J. Am. Chem. Soc.* **1978**, *100*, 7920–7927.

(27) Laouiti, A.; Rammah, M. M.; Rammah, M. B.; Marrot, J.; Couty, F.; Evano, G. *Org. Lett.* **2012**, *14*, 6–9.

(28) Horvath, B.; Strutz, J.; Horvath, E. G. *Z. Für Anorg. Allg. Chem.* **1979**, *457*, 38–50.

(29) Olmstead, M. M.; Power, P. P.; Shoner, S. C. *Inorg. Chem.* **1991**, *30*, 2547–2551.

(30) Bryan, A. M.; Long, G. J.; Grandjean, F.; Power, P. P. *Inorg. Chem.* **2013**, *52*, 12152–12160.

(31) Ward, L. G. L.; Pipal, J. R. In *Inorganic Syntheses*; Cotton, F. A., Ed.; John Wiley & Sons, Inc.: Hoboken, NJ, USA, 1972; Vol. 13, pp. 154–164.

(32) Gaussian 09, Revision **D.01**, Frisch, M. J.; Trucks, G. W.; Schlegel, H. B.; Scuseria, G. E.; Robb, M. A.; Cheeseman, J. R.; Scalmani, G.; Barone, V.; Mennucci, B.; Petersson, G. A.; Nakatsuji, H.; Caricato, M.; Li, X.; Hratchian, H. P.; Izmaylov, A. F.; Bloino, J.; Zheng, G.; Sonnenberg, J. L.; Hada, M.; Ehara, M.; Toyota, K.; Fukuda, R.; Hasegawa, J.; Ishida, M.; Nakajima, T.; Honda, Y.; Kitao, O.; Nakai, H.; Vreven, T.; Montgomery, J. A., Jr.; Peralta, J. E.; Ogliaro, F.; Bearpark, M.; Heyd, J. J.; Brothers, E.; Kudin, K. N.; Staroverov, V. N.; Kobayashi, R.; Normand, J.; Raghavachari, K.; Rendell, A.; Burant, J. C.; Iyengar, S. S.; Tomasi, J.; Cossi, M.; Rega, N.; Millam, N. J.;

Klene, M.; Knox, J. E.; Cross, J. B.; Bakken, V.; Adamo, C.; Jaramillo, J.; Gomperts, R.; Stratmann, R. E.; Yazyev, O.; Austin, A. J.; Cammi, R.; Pomelli, C.; Ochterski, J. W.; Martin, R. L.; Morokuma, K.; Zakrzewski, V. G.; Voth, G. A.; Salvador, P.; Dannenberg, J. J.; Dapprich, S.; Daniels, A. D.; Farkas, Ö.; Foresman, J. B.; Ortiz, J. V.; Cioslowski, J.; Fox, D. J. Gaussian, Inc., Wallingford CT, 2009.

CHAPTER 4

THE ELECTRONIC PROPERTIES OF A TETRADENTATE REDOX NON-INNOCENT DIIMINE LIGAND ON FIRST ROW TRANSITION METALS

I. Introduction

The limited reactivity observed in three coordinate systems bearing redox non-innocent ligands prompted investigation into the use of four coordinate ligands that would force the metal into a pseudo square planar coordination geometry. Square planar and square pyramidal compounds have shown utility in catalyzing useful reactions through group transfer chemistry.

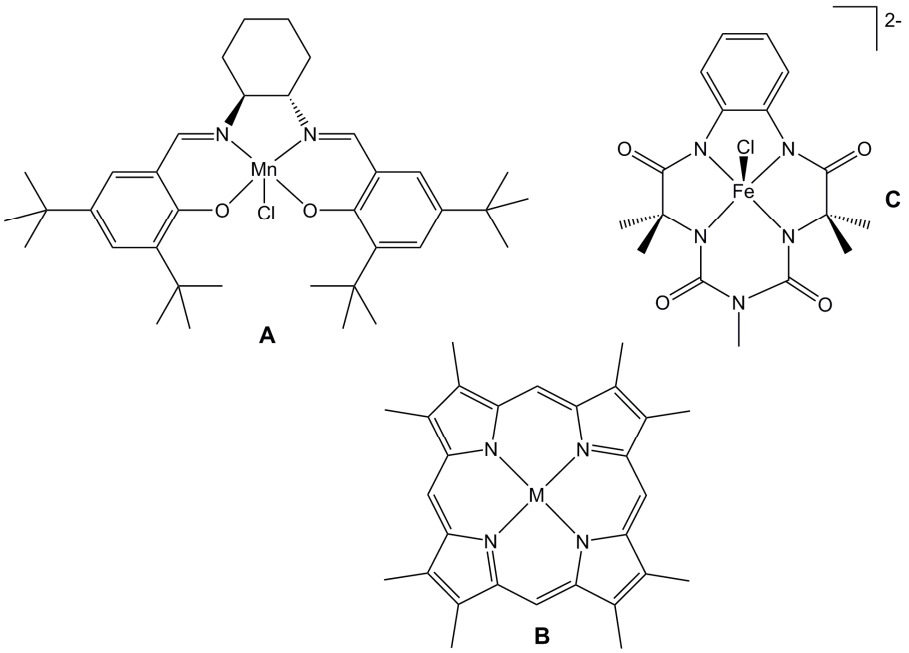

Figure 4.1. Pseudo square planar ligands used in catalysis.

Jacobsen has used acyclic Mn(III) salen complexes (Figure 4.1 A) for the asymmetric epoxidation of alkenes in high yield and with good turnover numbers.[1–3] The reaction is believed to proceed through a cycle where a transient Mn(V) oxo, derived from O-atom transfer to Mn(III), delivers the oxygen atom to the olefin.[4]

Metal porphyrin compounds (Figure 4.1 B) have also been used to promote group transfer reactions through the use of metal-heteroatom multiple bonds.[5–8] The TAML class of ligands developed by Collins (Figure 4.1 C) can stabilize a high valent Fe(V) oxo,[9] which has been used to oxidize unactivated C-H bonds.[10,11]

Incorporation of redox non-innocence into 4-coordinate ligands bearing nitrogen donors may offer improved reactivity or mechanistic insights into the aforementioned systems. Both di- and tri-anionic, pseudo square planar ligands were envisioned as scaffolds for supporting compounds containing metal-ligand multiple bonds.

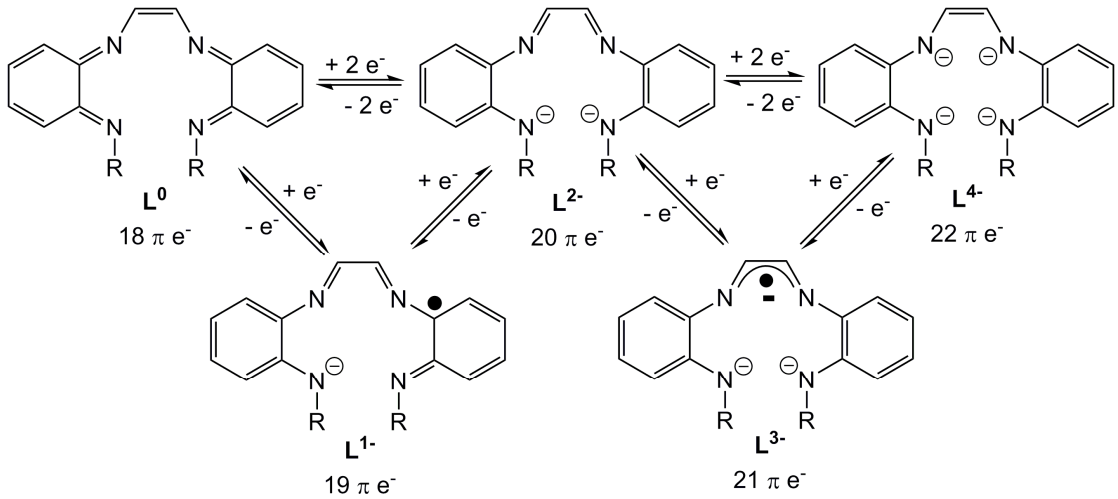

Figure 4.2. Ligand oxidation states available to a 4-coordinate ligand bearing alpha-diimine and ortho-phenylenediamine components.

Figure 4.2 shows a ligand containing alpha diimine and o-phenylenediamine components whose redox non-innocent functional groups may allow for the ligand to adopt five different oxidation states from neutral to tetraanionic. The ability to shuttle electrons to and from the ligand in pseudo square planar complexes may offer support for new and interesting types of reactivity with metal-ligand multiple bonds.

II. Results and Discussion

A. Ligand Synthesis

1. Synthesis of tetradentate ligands

Bulky, N-(2-aminophenyl)-2,6-diisopropylaniline (**1**) proved useful in initial reaction screenings. The first condensation with acetylacetone showed no reaction in refluxing toluene but when ethanol was used halfnac **2** was isolated as a red solid in 60% yield.

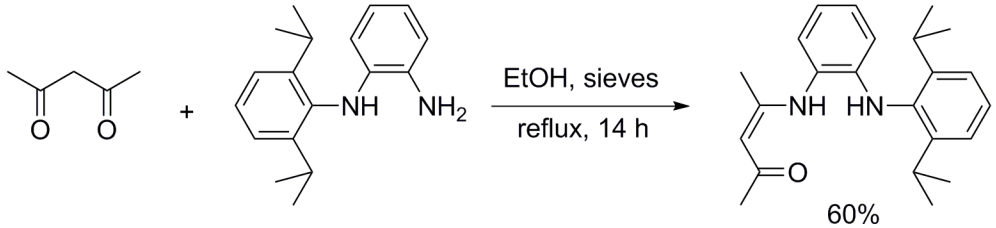

1 **2**

Equation 4.1.

As expected, condensation of a second equivalent of aniline proved difficult as simple condensation routes with catalytic acid failed to give any product in both toluene and ethanol. Alkylation of the ketone with triethyloxonium tetrafluoroborate in CH_2Cl_2 increased the electrophilicity enough to allow substitution with **1** to proceed. The reaction required elevated temperatures, and the resulting iminium salt was deprotonated in-situ with aqueous KOH to give the free amine. The product was identified in the crude reaction mixture in >80% yield by ^{1}H NMR spectroscopy but was never isolated, and preliminary ^{1}H NMR assignments in $CDCl_3$ are shown in Figure 1.1.

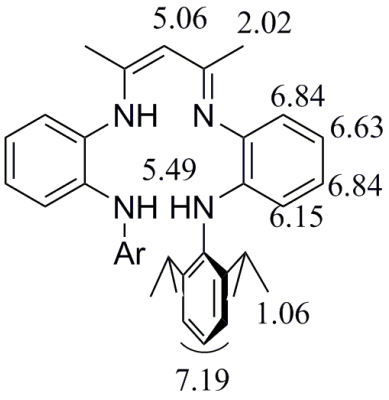

Figure 4.3. NMR assignments for **3**.

Attempts to isolate **3** by column chromatography on silica gel resulted in hydrolysis of the imine and attempts at crystallization resulted in products oiling out. The lower solubility of the iminium salt in organic solvents may ease crystallization, although this was not attempted.

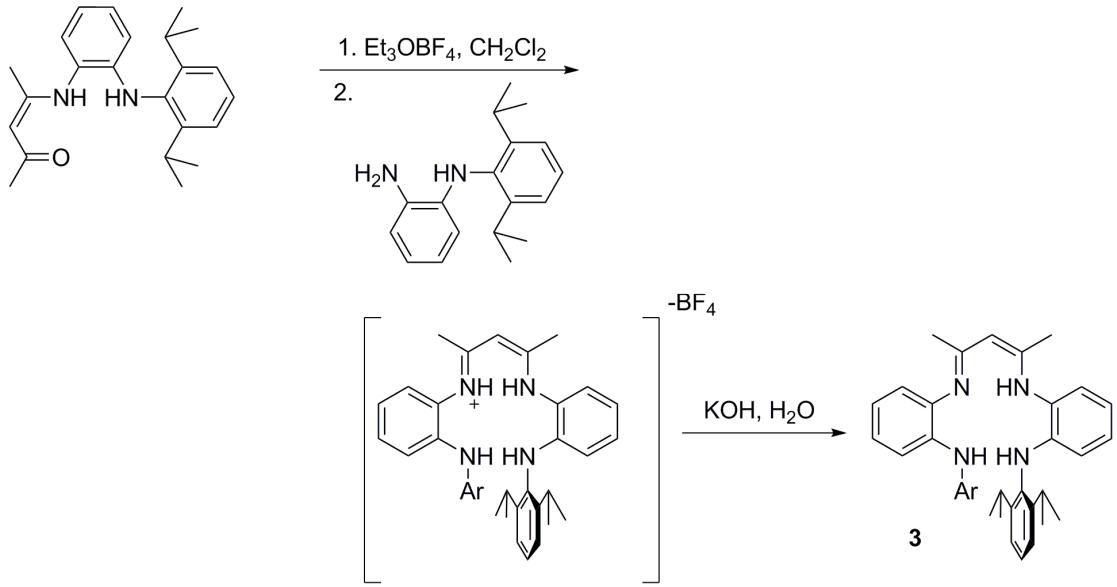

Scheme 4.1. Synthesis of nacnac tetradentate ligand.

The limited success achieved with beta-diketones as starting materials prompted investigation into condensations with alpha-diimines. Condensation of 2

equivalents of **1** with glyoxal (solution in H_2O) resulted in formation of a dark red solution and precipitation of a bright orange, flocculent, solid. Isolation of the orange solid by filtration and washing with methanol gave the pure 4-coordinate alpha-diimine ligand (**4**, Equation 4.2) in 24% yield. ^{1}H NMR reveals a symmetric product with only one signal shown for the iso-propyl C-H and a broad singlet for the isopropyl methyl groups. The spectrum showed a singlet resonance at 8.65 ppm, consistent with the assignment as a C-H imine proton. Concentration of the filtrate and analysis of the red residue by ^{1}H NMR spectroscopy did not show any additional **4**, and the other products made in this reaction could not be identified but may result from cyclization reactions (vide infra).

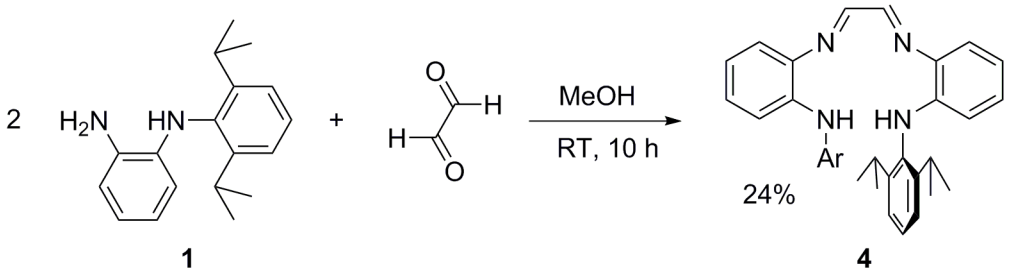

Equation 4.2. Synthesis of 4-coordinate diimine ligand

2. Attempts to synthesize ligands with other substituents

Treatment of a methanolic solution of glyoxal with less bulky anilines resulted in a deep red solution with no solid precipitation. Removal of the solvent and analysis by ^{1}H NMR showed clean conversion to the N-substituted benzimidazoles (Equation 4.3). This was confirmed with GC/MS, which showed one major product with a mass corresponding to the cyclized product. Condensations with acetylacetone showed a similar cyclization with acetone as the byproduct.

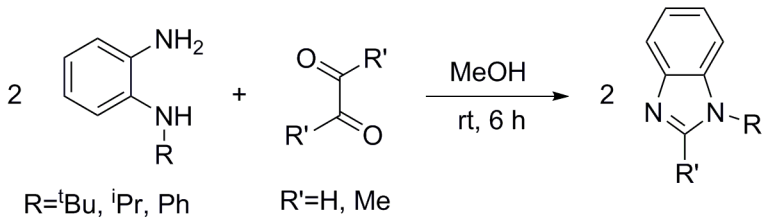

Equation 4.3.

The 2,6-diisopropyphenyl substituted aniline (**1**) is the only aniline that gave the desired product but the modest yield (24%) indicates that some cyclization is likely present in this case as well. Condensations with more bulky diketones showed no reaction as greater steric bulk at the ketone inhibits cyclization while also hindering condensation.

B. Metallation with $M[N(TMS)_2]_2(THF)$

1. Synthesis of 5-Fe.

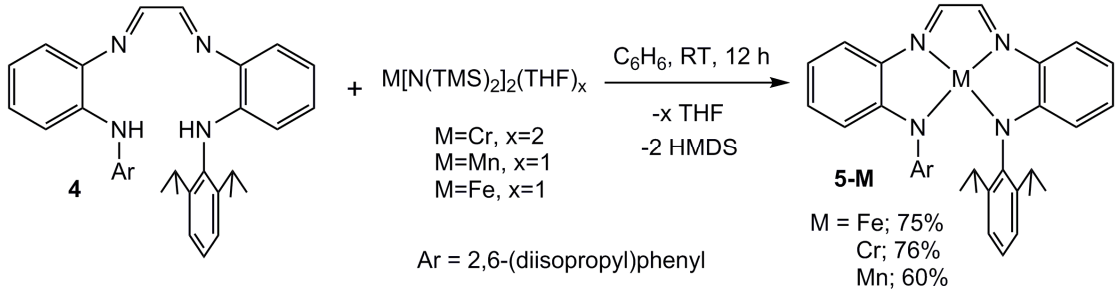

Equation 4.4.

Metallation of tetradentate ligand **4** proved easy using metal bis-amide precursors. Addition of benzene to a flask containing **4** and $Fe[N(TMS)_2]_2(THF)$ instantly resulted in a dark green color, and a dark green paramagnetic solid was isolated in 75% yield. The complex exhibited a ^1H NMR spectrum that showed diagnostic resonances for a symmetric product, but when compared to the corresponding reaction performed in a J. Young tube, the same set of resonances were

shifted. It is plausible that HMDS remaining in the NMR tube reaction interacts with the metal center and causes the resonances to shift slightly. The magnetic moment of **5-Fe** was determined by solution Evans[12] measurement to be $\mu_{eff} = 4.7\ \mu_B$, which is low for an S=2 system expected for high spin Fe(II). Temperature dependent magnetic measurements are underway to determine the cause of the low magnetic moment.

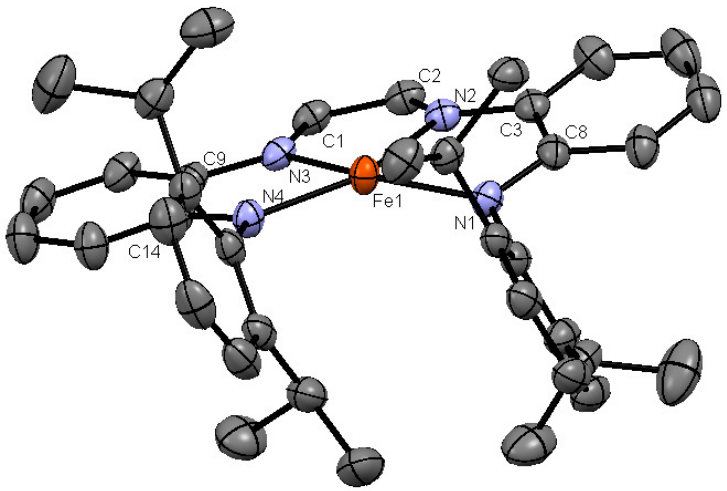

Figure 4.4. Molecular view of **5-Fe**. Hydrogen atoms have been omitted for clarity.

A single crystal suitable for X-Ray analysis was obtained by slow evaporation of a concentrated pentane solution. The crystal structure **5-Fe** shows a pseudo square planar geometry about Fe (sum of angles 359.32°), and the 2,6-diisopropylphenyl groups are rotated to minimize steric interaction of the adjacent aryl groups. The average metal amide distance of 1.996 Å is shorter than the Fe-N_{imine} distance of 2.131 as expected, and both are within standard ranges. Inspection of the bond distances of the α-diimine ligand backbone indicated no significant ligand reduction, as the N2-C2 distance of 1.293 Å is consistent with a C-N double bond and the C1-C2 bond distance of 1.437 Å is reasonable for the C-C bond in alpha diimines. No ligand oxidation is observed in the bond distances within the *o*-phenylenediamine arms, as these are all in

the expected ranges. Pertinent interatomic distances and bond angles are given in Table 4.2**.**

2. Synthesis of 5-Mn

Synthesis of the manganese 4-coordinate compound was performed in a similar fashion starting with $Mn[N(TMS)_2]_2(THF)$. **5-Mn** was isolated in 60% yield as a dark green solid with a ^1H NMR spectrum that is paramagnetically shifted and broadened, making interpretation difficult. Solution Evans method measurements showed a S=5/2 system with a μ_{eff} of 5.3 μ_B which is low for a high spin (H.S.) Mn(II) as it deviates from the spin-only value (5.92 μ_B). To investigate the extent of ligand reduction by bond distance analysis, a single crystal was obtained by slow evaporation of a concentrated solution of **5-Mn** in diethyl ether.

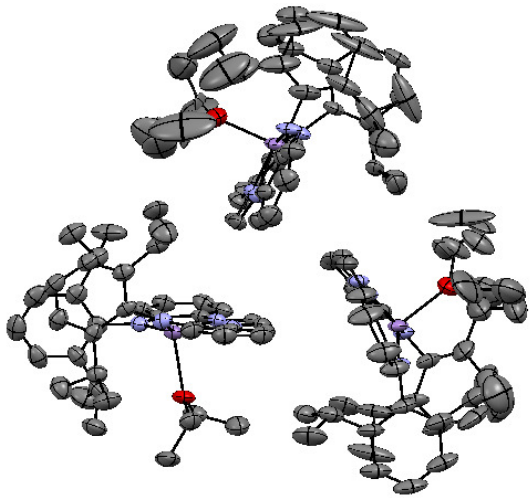

Figure 4.5. Molecular view of asymmetric unit in the solid state crystal structure of **5-Mn**. Hydrogen atoms have been omitted for clarity.

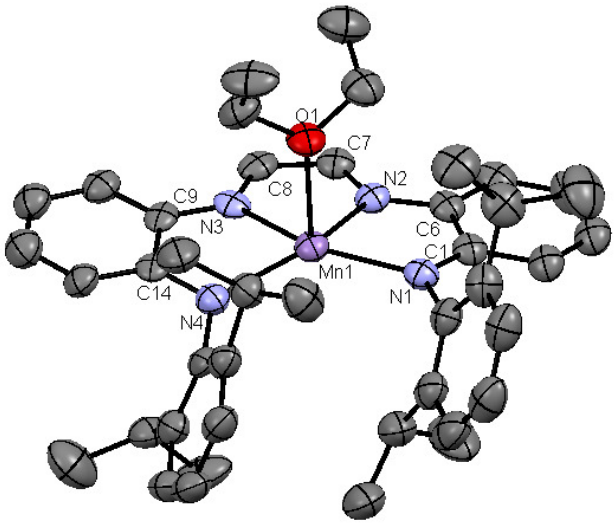

Figure 4.6. Molecular view of one molecule of five coordinate, **5-Mn**, showing bound ether molecule. Hydrogen atoms have been omitted for clarity.

5-Mn crystallized with 3 unique molecules in the asymmetric unit. The differences in the metric parameters between each molecule are not significant and may arise from packing effects. The apical position is disordered between molecules of Et_2O and THF which showed that the isopropyl groups do not block access to the metal center. The planar ligand forces Mn into a square pyramidal geometry (sum of Mn-N angles; 353.85°), with deviations from square pyramidal arising from sterics of the adjacent 2,6-diisopropylphenyl groups. As expected, the average Mn-N_{amide} (2.104 Å) distance is shorter than the average Mn-N_{imine} (2.239 Å) distance and the Mn-O_{ether} bond averages 2.253 Å. The bond distances in the diimine fragment indicate no reduction with a C-N_{imine} distance of 1.300 Å (avg.) and C-C distance of 1.424 Å (avg.).

3. Synthesis of 5-Cr

The ligand was installed on chromium using $Cr[N(TMS)_2]_2(THF)_2$ and a burgundy paramagnetic solid was isolated in 76% yield. The ^1H NMR was very broad,

limiting any insight into structure, but Evans measurements showed an S = 1 system with a room temperature magnetic moment of 2.7 μ_B (spin only 2.8 μ_B). An S = 1 ground state is unusual for Cr(II) and was not expected considering **5-Fe** and **5-Cr** are both high spin M(II).

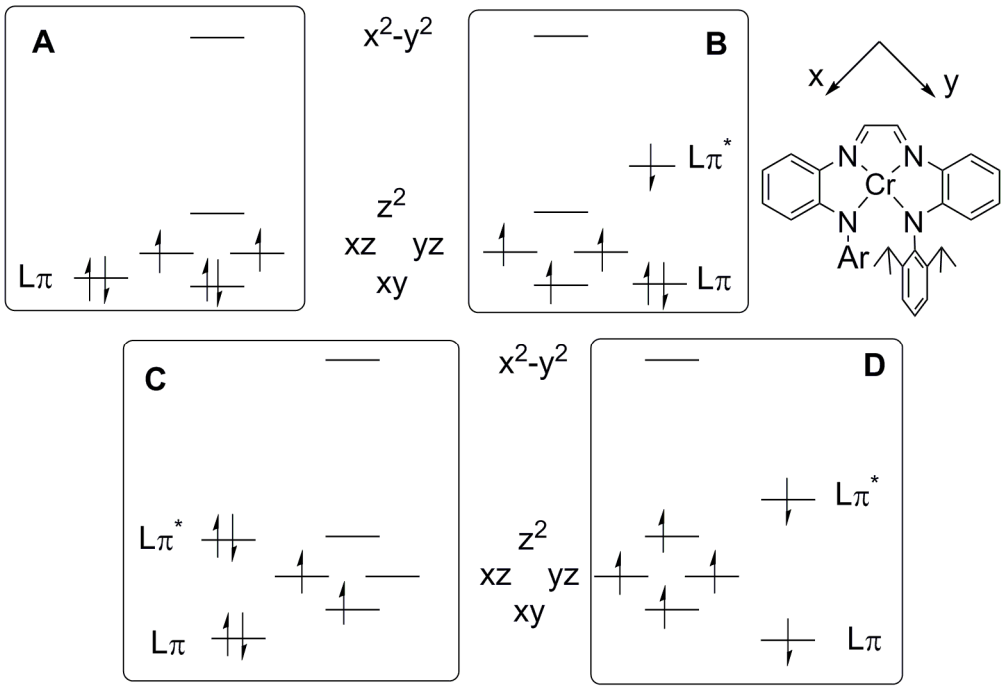

Figure 4.7. Partial MO diagrams showing possible electronic structure of S=1 **5-Cr**.

Figure 4.6 shows the electronic structure possibilities that would result in an S=1 system for pseudo square planar **5-Cr**. A standard ligand field description shows a configuration with two electrons paired in d_{xy} and a pair with parallel spin in the degenerate d_{xz} and d_{yz} orbitals. While this would result in an intermediate spin S=1 Cr(II) system, the field is not strong enough to pay the energetic cost of pairing electrons in d_{xy}.[13] Invoking redox non-innocence allows for 2 more possibilities, both involving the placement of electrons into ligand based π* orbitals that are comparable in energy to the metal d orbitals. Oxidation of the metal (reduction of the ligand) by

one electron (B in Figure 4.7) and antiferromagnetic coupling of the ligand localized electron with a complement on the metal would result in a S=1 ground state. If the ligand was reduced by two electrons and those electrons were paired then a situation like C in Figure 4.7, with a formal HS Cr(IV), would be the cause of the unexpected magnetic moment. This situation is not operable as Cr^{III} is very unlikely to have the necessary potential to reduce the ligand by an additional electron. Lastly, antiferromagentic coupling of HS Cr(II) to the triplet excited state of the alpha diimine fragment on the ligand would also give an S=1 ground state. In order to determine the electronic structure of **5-Cr** a single crystal was isolated by slow diffusion of pentane into a concentrated THF solution at -35 ^{o}C, and subjected to single crystal X-Ray diffraction.

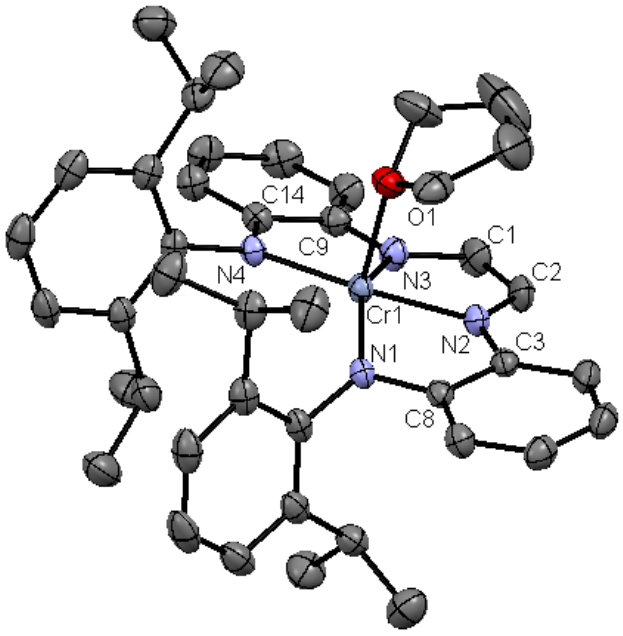

Figure 4.8. Molecular view of **5-Cr** with coordinated molecule of THF. Hydrogen atoms have been removed for clarity.

5-Cr crystallizes as a THF adduct with 2 unique molecules in the asymmetric unit that possess nearly identical bond metrics. The geometry about chromium is square pyramidal with the ligand occupying the equatorial plane and the single molecule of THF in the apical position. Inspection of the metal-ligand and ligand bond distances shows a significant variation from the metric parameters of **5-Fe** and **5-Mn**.

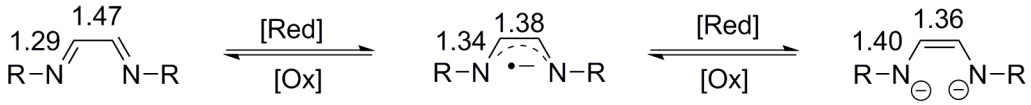

Figure 4.9. Typical bond metrics for reduced alpha-diimine ligands.

Table 4.1. Selected crystallographic and refinement data for **5-M** (M = Fe, Mn, and Cr).

	Fe	Mn	Cr
Formula	$C_{38}H_{44}FeN_4$	$C_{126}H_{160.13}Mn_3N_{12}O_3$	$C_{42}H_{52}CrN_4O$
Formula Weight	612.64	2055.61	680.88
Crystal System	Monoclinic	Monoclinic	Triclinic
Space Group	$P2_1/c$	Cc	P-1
Z	4	4	4
a (Å)	12.7432(6)	17.8551(14)	12.0237(5)
b (Å)	19.2721(9)	30.521(2)	18.1933(9)
c (Å)	14.4594(6)	22.2700(17)	19.6461(9)
α (°)	90	90	65.547(2)
β (°)	98.966(2)	107.543(3)	82.660(2)
γ (°)	90	90	71.705(2)
V (Å^3)	3507.7(3)	11571.1(15)	3714.4(3)
Density (g cm^{-3})	1.160	1.180	1.218
μ (mm^{-1})	0.460	0.378	0.345
Temperature (K)	183(2)	173(2)	173(2)
λ (Å)	0.71703	0.71073	0.71073
Final R indices [I>2σ(I)][a,b]	R_1 = 0.0458, wR_2 = 0.1477	R_1 = 0.0580, wR_2 = 0.1257	R_1 = 0.0487, wR_2 = 0.1240
R indices (all data)[a,b]	R_1 = 0.0673, wR_2 = 0.1610	R_1 = 0.0914, wR_2 = 0.1441	R_1 = 0.0868, wR_2 = 0.1430
Goodness-of-fit[c]	1.043	1.016	1.052

[a] $R_1 = \Sigma||F_o|-|F_c||/ \Sigma|F_o|$. [b] $wR_2 = [\Sigma w(|F_o| - |F_c|)^2/ SwF_o^2]^{1/2}$. [c] GOF (all data) = $[\Sigma w(|F_o| - |F_c|)^2/ (n-p)]^{1/2}$, n = number of independent reflections, p=number of parameters

Table 4.2. Selected interatomic distances and angles for **5-M** (M = Fe, Cr, Mn).

	Fe	Cr		Mn	
M-N_{im}	2.1284(18)	1.9694(15)	1.9474(17)	2.237(3)	2.237(3)	2.243(3)
M-$N_{im'}$	2.1337(16)	1.9465(17)	1.9741(16)	2.236(3)	2.238(3)	2.244(3)
M-N_{amide}	1.9928(17)	1.9849(16)	2.0062(16)	2.105(3)	2.124(3)	2.092(3)
M-$N_{amide'}$	1.9983(17)	2.0110(15)	1.9891(16)	2.091(4)	2.126(3)	2.088(3)
M-O_{ether}	-	2.1865(13)	2.2058(13)	2.255(3)	2.257(3)	2.246(4)
C_{im}-$C_{im'}$	1.437(3)	1.360(3)	1.361(3)	1.413(6)	1.447(6)	1.412(6)
C_{im}-N_{im}	1.293(3)	1.364(3)	1.376(3)	1.306(5)	1.289(5)	1.301(5)
$C_{im'}$-$N_{im'}$	1.294(3)	1.375(3)	1.371(3)	1.317(5)	1.294(5)	1.295(5)
N_{im}-C_{aryl}	1.392(3)	1.374(2)	1.392(3)	1.361(5)	1.392(5)	1.365(5)
$N_{im'}$-$C_{aryl'}$	1.390(3)	1.388(2)	1.375(3)	1.368(6)	1.371(5)	1.366(5)
C_{aryl}-C_{aryl}	1.428(3)	1.420(3)	1.419(3)	1.458(6)	1.422(6)	1.452(6)
$C_{aryl'}$-$C_{aryl'}$	1.420(3)	1.422(3)	1.425(3)	1.475(6)	1.432(6)	1.447(6)
C_{aryl}-N_{amide}	1.377(3)	1.391(2)	1.392(2)	1.361(5)	1.352(5)	1.353(5)
$C_{aryl'}$-$N_{amide'}$	1.370(2)	1.390(2)	1.394(2)	1.359(5)	1.361(5)	1.381(6)
N_{amide}-M-N_{im}	78.11(7)	79.66(6)	79.83(7)	74.84(13)	75.42(12)	74.75(12)
N_{im}-M-$N_{im'}$	73.32(7)	77.85(7)	77.75(7)	71.47(13)	71.21(12)	71.13(13)
$N_{im'}$-M-$N_{amide'}$	78.27(7)	79.82(7)	79.43(7)	74.87(13)	74.68(12)	75.42(13)
N_{amide}-M-$N_{amide'}$	129.61(7)	118.96(6)	119.29(6)	133.35(12)	132.54(13)	133.63(14)
N_{im}-M-$N_{amide'}$	151.53(7)	157.26(7)	146.08(7)	139.04(14)	141.29(12)	146.46(13)
N_{amide}-M-$N_{im'}$	147.53(7)	148.69(6)	157.43(7)	146.17(13)	145.69(13)	138.73(12)

The average C2-N2 distance has lengthened significantly to 1.370 Å, which is more indicative of single bond character, and the C1-C2 distance has shortened to 1.360 Å, which is more consistent with a double bond in reduced alpha diimines. Comparison of these metrics with other diimine metal complexes studied extensively by

Wieghardt[14,15] and others[16,17] shows distances somewhere between a bis-reduced and mono-reduced diimine fragment. Metal-ligand bond distances also confirm ligand reduction, as the Cr-N_2 and Cr-N_3 distances are now shorter (d_{avg} = 1.958 Å) than the Cr-N_1 and Cr-N_4 distances (d_{avg} = 1.998 Å), which are all in the range of typical metal-amide bonds. The average Cr-O_{THF} bond measures 2.187 Å. The bond distances over the *o*-phenylenediamine fragments are similar for **5-Cr**, **5-Fe**, and **5-Mn** and indicate little involvement in redox non-innocence. Calculations offered additional insight into the unusual spin state of **5-Cr.**

4. Calculations of 5-M.

Density functional theory (DFT) calculations were used to probe the relative energies of the 4-coordinate compounds (**5-M**) in different electronic configurations, and the results are given in Table 4.3. The calculations of **5-Mn** show the sextet to be more stable than the quartet and this was observed experimentally with Evans measurements (μ_{eff} = 5.3 μ_B). Calculated bond distances over the diimine (d(N=C) = 1.29 Å, d(C-C) = 1.45 Å) correlate with those observed crystallographically (d(N=C) = 1.300 Å (avg.), d(C-C) = 1.424 Å (avg.)), and confirm the assignment as an overall dianionic ligand with a neutral diimine fragment. A dianionic ligand was calculated for **5-Fe** and matches with the observed d(N=C) of 1.293 Å and d(C-C) of 1.437 Å.

DFT calculations in Table 4.3 present two different electronic structures of **5-Cr**, one with a dianionic ligand bound to high spin (HS) Cr(II), and one with a S = 1

Table 4.3.

Metal	Spin	Sym.	Spin on Metal	$d(M\text{-}N)_{avg}$ (Å)	d(N=C) (Å)	d(C-C) (Å)	G_{rel}	d(C-C)-d(N-C)	Ligand Form	Configuration
Ti	0	C_s	0	2.01	1.37	1.36	0	-0.02	N-C=C-N	$(d^0\text{-}Ti^{IV})(L^{4-})$
Ti	1	C_{2v}	1.3	2.10	1.34	1.39	0.2	0.05	Interm.	$(d^1\text{-}Ti^{III})^{\uparrow}(L^{3-})^{\uparrow}$
V	1/2	C_{2v}	2.2	2.06	1.34	1.38	0	0.03	Interm.	$(d^2\text{-}V^{III})^{\uparrow\uparrow}(L^{3-})^{\downarrow}$
V	3/2	C_1	2.4	2.06	1.34	1.39	5.0	0.05	Interm.	$(d^2\text{-}V^{III})^{\uparrow\uparrow}(L^{3-})^{\uparrow}$
Cr	1	C_{2v}	3.8	1.99	1.36	1.38	0	0.02	N-C=C-N	$(d^4\text{-}Cr^{II})^{\uparrow\uparrow\uparrow\uparrow}(L^{2-})^{\downarrow\downarrow}$
Cr	2	C_{2v}	4.1	2.05	1.30	1.44	1.0	0.14	N=C-C=N	$(d^4\text{-}Cr^{II})^{\uparrow\uparrow\uparrow\uparrow}(L^{2-})$
Mn	3/2	C_{2v}	3.9	1.95	1.34	1.39	3.1	0.06	Interm.	$(d^4\text{-}Mn^{III})^{\uparrow\uparrow\uparrow\uparrow}(L^{3-})^{\downarrow}$
Mn	5/2	C_{2v}	4.9	2.26	1.29	1.45	0	0.16	N=C-C=N	$(d^5\text{-}Mn^{II})^{\uparrow\uparrow\uparrow\uparrow\uparrow}(L^{2-})$
Fe	2	C_{2v}	3.8	2.20	1.29	1.45	0	0.16	N=C-C=N	$(d^6\text{-}Fe^{II})^{\uparrow\downarrow\uparrow\uparrow\uparrow\uparrow}(L^{2-})$
Co	1/2	C_{2v}	1.4	1.86	1.34	1.40	2.7	0.06	Interm.	$(d^6\text{-}Co^{III})^{\uparrow\downarrow\uparrow\downarrow\uparrow\uparrow}(L^{3-})^{\downarrow}$
Co	3/2	C_{2v}	2.7	2.15	1.29	1.44	0	0.15	N=C-C=N	$(d^7\text{-}Co^{II})^{\uparrow\downarrow\uparrow\downarrow\uparrow\uparrow\uparrow}(L^{2-})$
Ni	1	C_2	1.5	2.06	1.29	1.45	0	0.15	N=C-C=N	$(d^8\text{-}Ni^{II})^{\uparrow\downarrow\uparrow\downarrow\uparrow\downarrow\uparrow\uparrow}(L^{2-})$
Cu	1/2	C_{2v}	0.6	2.02	1.29	1.45	0	0.15	N=C-C=N	$(d^9\text{-}Cu^{II})^{\uparrow\downarrow\uparrow\downarrow\uparrow\downarrow\uparrow\downarrow\uparrow}(L^{2-})$
Zn	0	C_{2v}	0	2.23	1.28	1.46	0	0.18	N=C-C=N	$(d^{10}\text{-}Zn^{II})(L^{2-})$

M06/6-311+G(d) optimized M-N, N=C and C-C distances

ligand antiferromagnetically coupled to HS Cr(II) (Figure 4.7, D). Only the latter matches the experimentally determined triplet spin state. The calculated bond distances (d(N=C) = 1.36 Å, d(C-C) = 1.38 Å) are in reasonable agreement with those determined experimentally (d(N=C) = 1.370 Å, d(C-C) = 1.360 Å). Further supporting the assignment of **5-Cr** as d^4 Cr(II) is the calculated Cr spin density of 3.8 which does not support an electronic structure with a reduced diimine fragment.

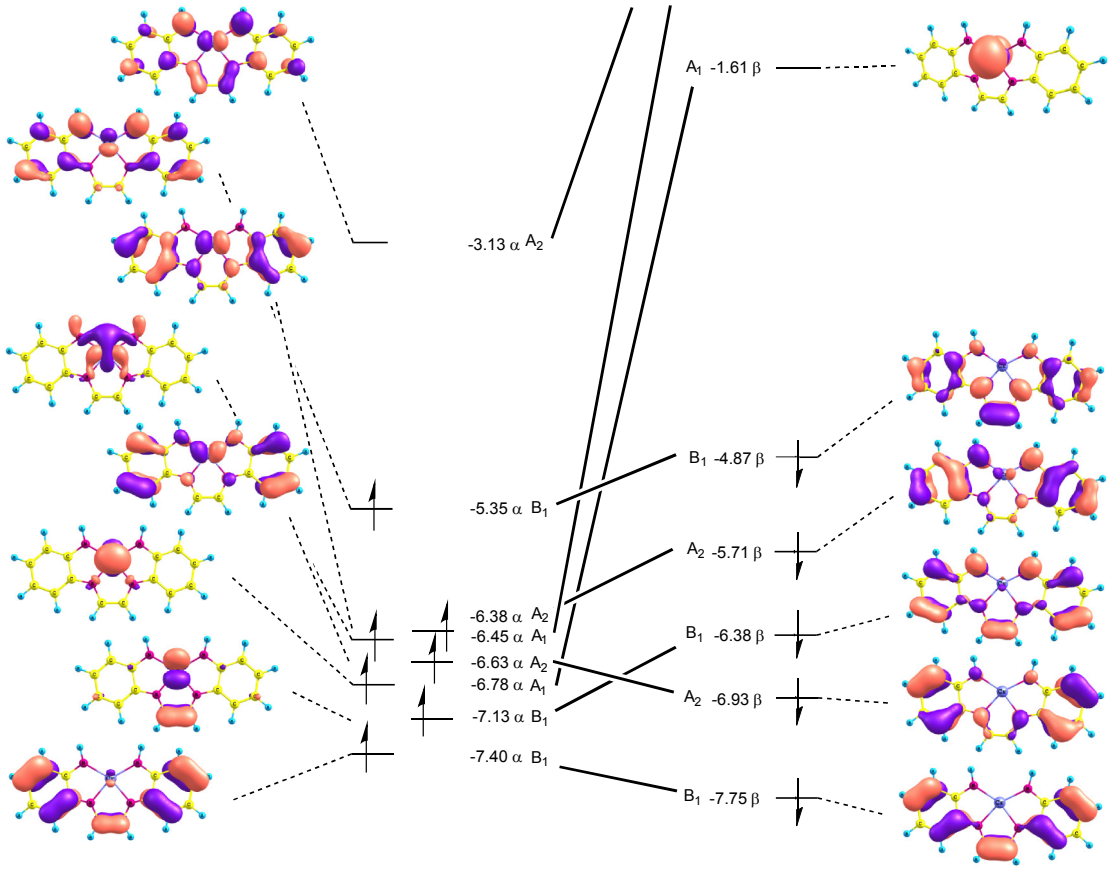

Figure 4.10. Partial molecular orbital diagram derived from multi-configurational self-consistent field (MCSCF) calculations of **5-Cr** showing significant mixing of Cr and ligand orbitals. Alpha spins are shown on left and Beta spins are shown on right.

Shown in Figure 4.10 is a partial molecular orbital diagram of **5-Cr** that was derived from high level multi-configurational self-consistent field (MCSCF) calculations. A traditional d-orbital splitting diagram is hard to extract from this data as the Cr d-orbitals undergo significant mixing with the ligand orbitals and are therefore distributed over several molecular orbitals. The metal center was calculated to have a spin density of 3.6 electrons which was in good agreement with that obtained via DFT, and supports the notion of a high spin Cr(II) metal center. It is still plausible that the calculations are depicting an electronic structure with a reduced diimine ligand trianion antiferromagnetically coupled to high spin Cr(III) (Figure 4.7 B), but the alternative with S = 2 Cr(II) antiferromagnetically coupled to a S = 1 ligand dianion (Figure 4.7 D) is significantly more interesting on a fundamental level.

4. Synthesis with MX_2; M=Fe, Mn

The tetradentate ligand (**4**) is quite stable at elevated temperatures and upon deprotonation with LiHMDS, and allowed for synthesis of metal compounds via salt metathesis routes. Treatment of **4** with 2 equivalents of LiHMDS in THF produced a dark blue-green solution indicating formation of the dianion (**6**), and further addition of MX_2 (M = Fe, Mn) and stirring for 14 hours produced green solutions for both Fe and Mn. Inspection of the ^{1}H NMR spectra confirmed formation of **5-Fe** and **5-Mn**. As these were run as small pot reactions there is no isolated yield, but examination of the ^{1}H NMR spectra of the crude reaction showed >85% conversion to **5-M** (M = Fe, Mn) and validated salt metathesis as a viable synthetic strategy.

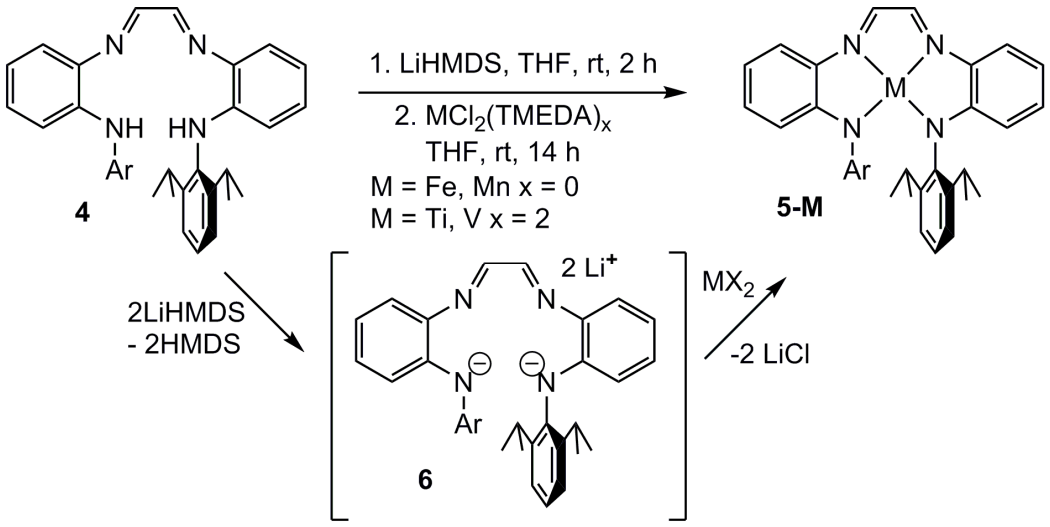

Scheme 4.2. Synthesis of **5-M** (M = Ti, V, Fe, Mn) via salt metathesis (Ar = 2,6-(diisopropyl)phenyl).

In a synthesis analogous to the above, the free ligand was deprotonated twice to generate **6** *in situ*, and allowed to react with $TiCl_2(TMEDA)_2$ in THF. The result was a green solution and analysis of the product by ^{1}H NMR spectroscopy (Figure 4.11) showed formation of one major symmetric, diamagnetic product, **5-Ti**. The upfield chemical shift of the imine C-*H* (6.68 ppm) relative to the free ligand (8.48 ppm) suggests increased electron density on the diimine framework and possibly redox non-innocent behavior. This is shown calculationally in Table 4.3 as the ground state was calculated with Ti(IV) coordinated to a bis reduced (L^{4-}) ligand. Ti(III) antiferromagnetically coupled to a monoreduced ligand would also give rise to a diamagnetic NMR spectrum and cannot be ruled out as a possible electronic structure. Isolation of the pure compound for X-Ray analysis has been hindered by excess TMEDA remaining in the reaction mixture.

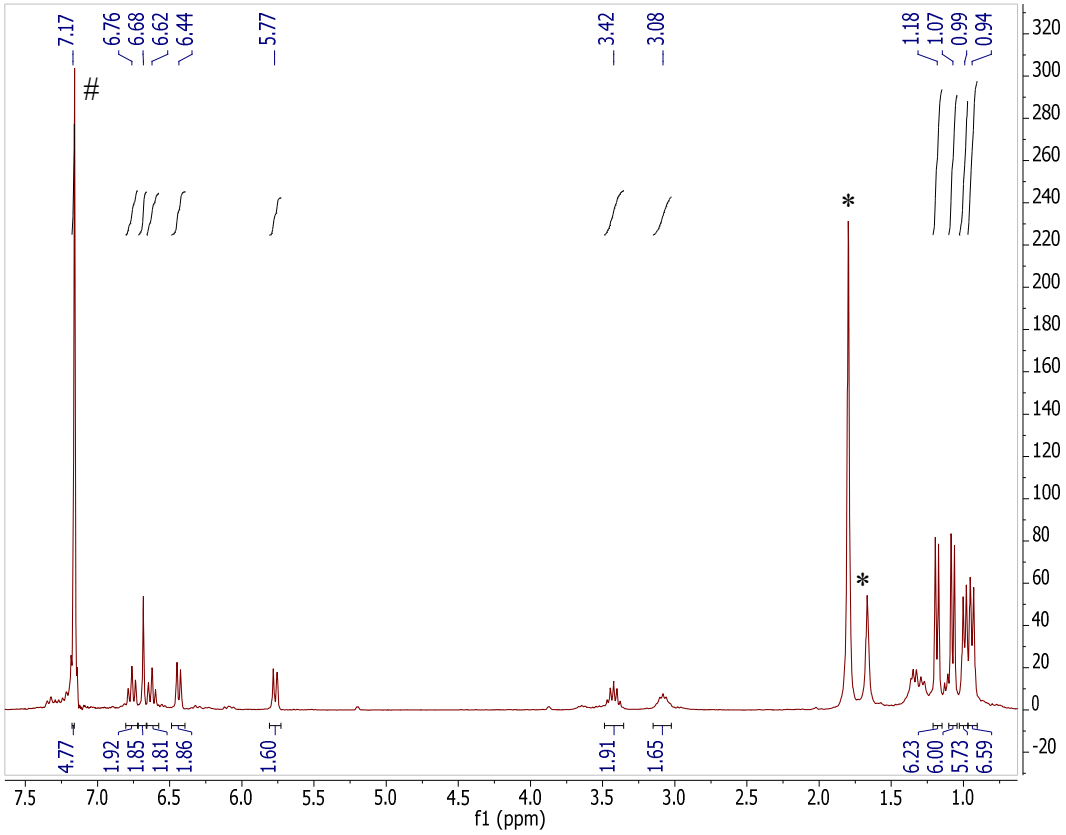

Figure 4.11. ^{1}H NMR spectrum of **5-Ti**. Residual TMEDA (*) and C_6D_5H (#) are indicated.

Treatment of **4** with LiHMDS followed by $VCl_2(TMEDA)_2$ at room temperature resulted in an orange/brown solution after stirring overnight. ^{1}H NMR of the crude reaction mixture showed residual THF and TMEDA that had been broadened by the presence of a paramagnetic species. Isolation and characterization of this species has been hindered by the presence of residual TMEDA.

D. Syntheses with ClM[N(TMS)$_2$]$_2$(THF)

Another attractive class of starting materials were M(III) bis-amide halides (ClM[N(TMS)$_2$]$_2$(THF)**)**. Two deprotonations by the amides would provide a formerly M(III), square pyramidal compound with a halide that could be converted to other reactive functional groups. Treatment of ClTi[N(TMS)$_2$]$_2$(THF) with **4** in C_6D_6 in a

1:1 mole ratio resulted in a diamagnetic ^{1}H NMR spectrum showing a 1:1 mole ratio of unreacted **4** and a new symmetric product. Addition of one more equivalent of $ClTi[N(TMS)_2]_2(THF)$ to the dark orange reaction resulted in complete conversion to the new symmetric product (**7**). The proposed product is shown in Equation 4.5 with NMR assignments in Figure 4.12. Each titanium center contributes 1 electron toward reduction of the diimine resulting in two formally Ti(IV) metal centers. The upfield shift of the imine C-*H* resonance at 6.55 ppm in the ^{1}H NMR spectrum and corresponding ^{13}C resonance at 109.45 ppm indicate increased electron density at these positions and probable diimine reduction. Amine deprotonation has not occurred as a singlet corresponding to the amine N-*H* was observed at 5.52 ppm in the ^{1}H NMR spectrum and there is no free HMDS present in the spectrum.

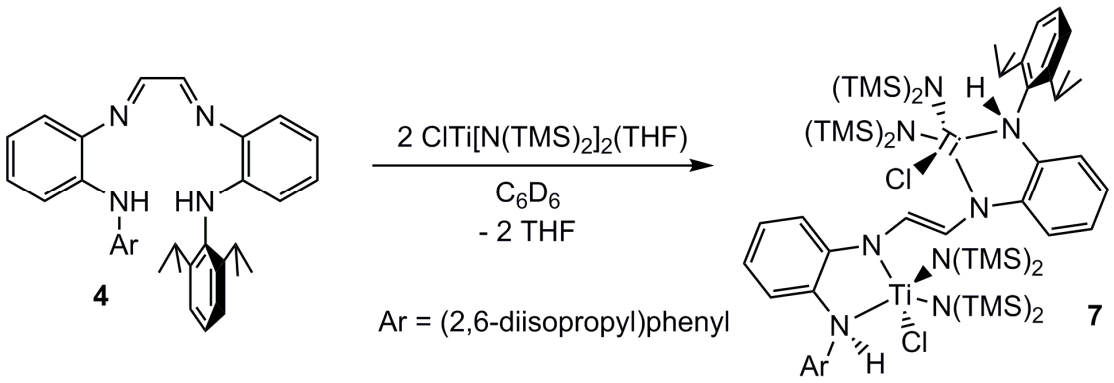

Equation 4.5.

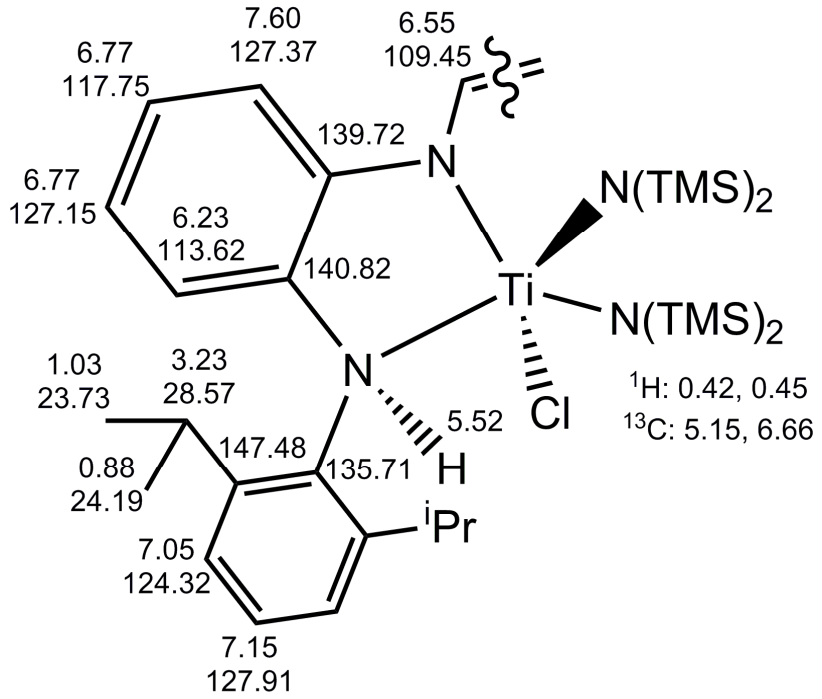

Figure 4.12. ^{1}H and ^{13}C NMR assignments of Ti dimer (**7**).

An analogous reaction between $ClV[N(TMS)_2]_2(THF)$ and **4** produced a deep orange solution, and the ^{1}H NMR spectrum of the reaction mixture showed a mixture of at least 4 prominent diamagnetic products, one of which is free ligand.

E. Metallation attempts with Co & Ni.

Attempts to metallate the four coordinate ligand (**4**) with dibasic metal precursors and the dianion (**6**) with metal dihalides proved fruitless when the metal was cobalt or nickel. When $NiCl_2(DME)$ was added to a solution of **6** in THF a deep red color was observed. Removal of the solvent and analysis of the resulting solid gave a complex NMR spectrum with a mixture of multiple paramagnetic and diamagnetic products. Treatment of **4** with $Ni[N(SiMe_3)(DIPP)]_2$ (Equation 4.6) in C_6D_6 also gave a convoluted ^{1}H NMR spectrum with resonances in the diamagnetic and paramagnetic regions. Free amine ($HN(SiMe_3)(DIPP)$) was observed in the NMR

spectrum indicating that deprotonation had taken place, but resonances corresponding to the desired product, **5-Ni**, were not identified.

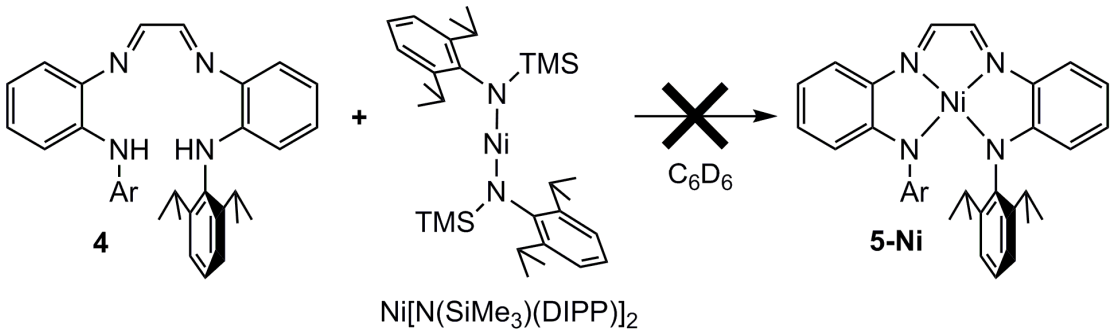

Equation 4.6.

Several cobalt dihalide starting materials were assayed for the synthesis of **5-Co**. Anhydrous $CoCl_2$, $CoCl_2$(THF), and $CoCl_2$(py) were all used in reactions with **6**, and all resulted in olive green solutions with ^{1}H NMR spectra exhibiting multiple products over the full spectral window. When $Co[N(TMS)_2]_2$(THF) was used as a starting material, the solution again turned dark green and the ^{1}H NMR spectrum offered no insight into what was being formed in the reaction. Current efforts are devoted to trying to synthesize a stable Co(I) or Co(III) species through salt metathesis in the presence of either oxidizing or reducing agents.

F. UV/VIS Spectra of 5-Cr and 5-Fe.

The UV/VIS spectra of 4-coordinate compounds **5-M** (M = Cr, Mn, Fe) are shown in Figure 4.14, and the large extinction coefficients suggest the major transitions are due to charge transfer (CT) transitions. The intense green color of the lithium dianion salt (**6**) indicated that similar electronic transitions were present, so it was also investigated by UV/VIS spectroscopy. **6** exhibited 2 absorptions at 773 nm ($\varepsilon \sim 21000\ M^{-1}cm^{-1}$) and 305 nm ($\varepsilon \sim 16000\ M^{-1}cm^{-1}$) and both were assigned as

intraligand charge transfer (ILCT) bands. The low energy band has a shoulder at 720 nm and another absorption at 838 nm, which plausibly correspond to a 1000 cm^{-1} vibronic progression. A vibronic progression is observed when excitations occur from the ground state to different vibrational states within the excited state and this is depicted in Figure 4.13 (A).[18] The energy of the progression corresponds to the energy separation of the vibronic levels in the excited state and is likely to roughly correspond to an absorption at that energy in the infrared spectrum. Figure 4.13 (B) presents a generic description of possible charge transfer transitions within the 4 coordinate compounds. ILCT bands, as the name implies, could correspond to absorptions from ligand π to ligand π^* molecular orbitals. Metal to ligand charge transfers (MLCT) and ligand to metal charge transfers (LMCT) correspond to transitions out of and into the d-orbital manifold, respectively.

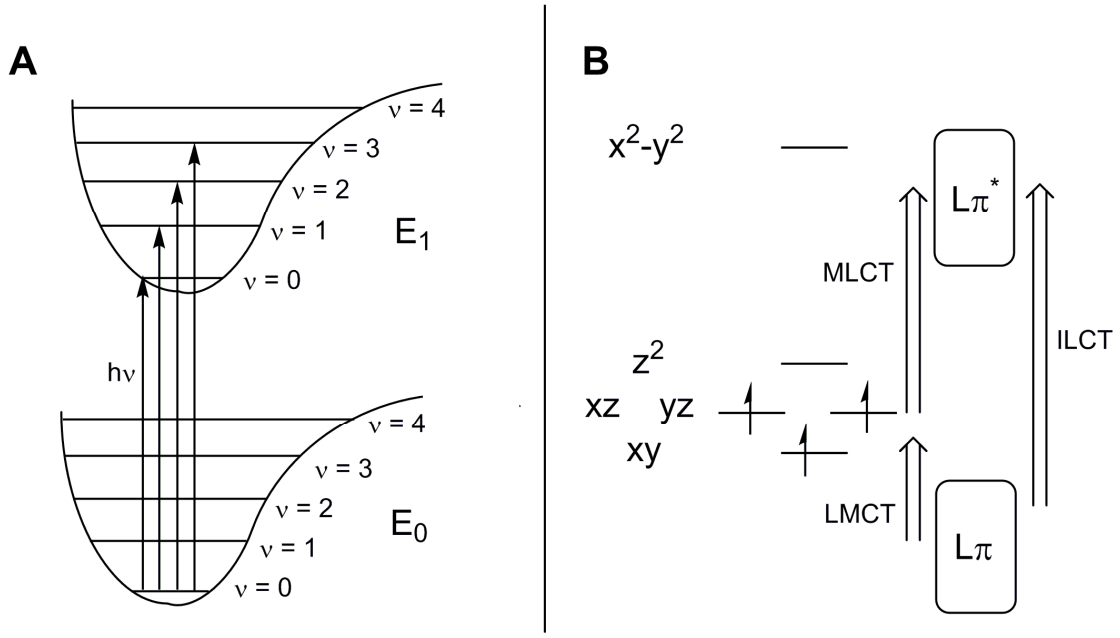

Figure 4.13. (A) Energy diagram showing absorptions responsible for vibronic progression in UV/VIS spectra. (B) Generic molecular orbital diagram showing origins of different charge transfer transitions.

The spectra of **5-Fe** and **5-Mn** displayed similar spectral features to the dilithium salt, **6,** so are also assigned as ILCT bands. The lower energy band of **6** split into two bands for **5-Fe** at 687 nm ($\varepsilon \sim 5000\ M^{-1}cm^{-1}$) and 881 nm ($\varepsilon \sim 6000\ M^{-1}cm^{-1}$) and a higher energy ILCT band was also observed at 380 nm ($\varepsilon \sim 11000\ M^{-1}cm^{-1}$). Additionally, **5-Mn** showed two absorptions in the low energy region of the spectrum at 729 nm ($\varepsilon \sim 8000\ M^{-1}cm^{-1}$) and 931 nm ($\varepsilon \sim 12000\ M^{-1}cm^{-1}$), while the high energy intraligand band appeared at 392 nm ($\varepsilon \sim 7000\ M^{-1}cm^{-1}$).

The UV/VIS spectrum of **5-Cr** was markedly different than the other 4-coordinate compounds **5-Fe** and **5-Mn**. The high energy intraligand (IL) band was blueshifted and revealed a 1300 cm^{-1} vibronic progression within the excited state with absorbances at 494 nm ($\varepsilon \sim 8000\ M^{-1}cm^{-1}$), 537 nm ($\varepsilon \sim 8000\ M^{-1}cm^{-1}$), 573 nm ($\varepsilon \sim 7000\ M^{-1}cm^{-1}$), and 607 nm ($\varepsilon \sim 5000\ M^{-1}cm^{-1}$). The ~1300 cm^{-1} difference was observed as an absorption in the ground state infrared spectrum and was assigned to the diimine fragment. The high energy IL band appeared at a similar energy to the other 4-coordinate compounds (400 nm; $\varepsilon \sim 19000\ M^{-1}cm^{-1}$) and an additional absorption was noted at 330 nm ($\varepsilon \sim 12000\ M^{-1}cm^{-1}$). The low energy region showed several absorptions (>780 nm) over a relatively flat region ($\varepsilon \sim 2500\ M^{-1}cm^{-1}$) and plausibly correspond to spin forbidden absorptions to a low lying excited state. Any d-d transitions were not observed as they are hidden under the much more intense charge transfer bands.

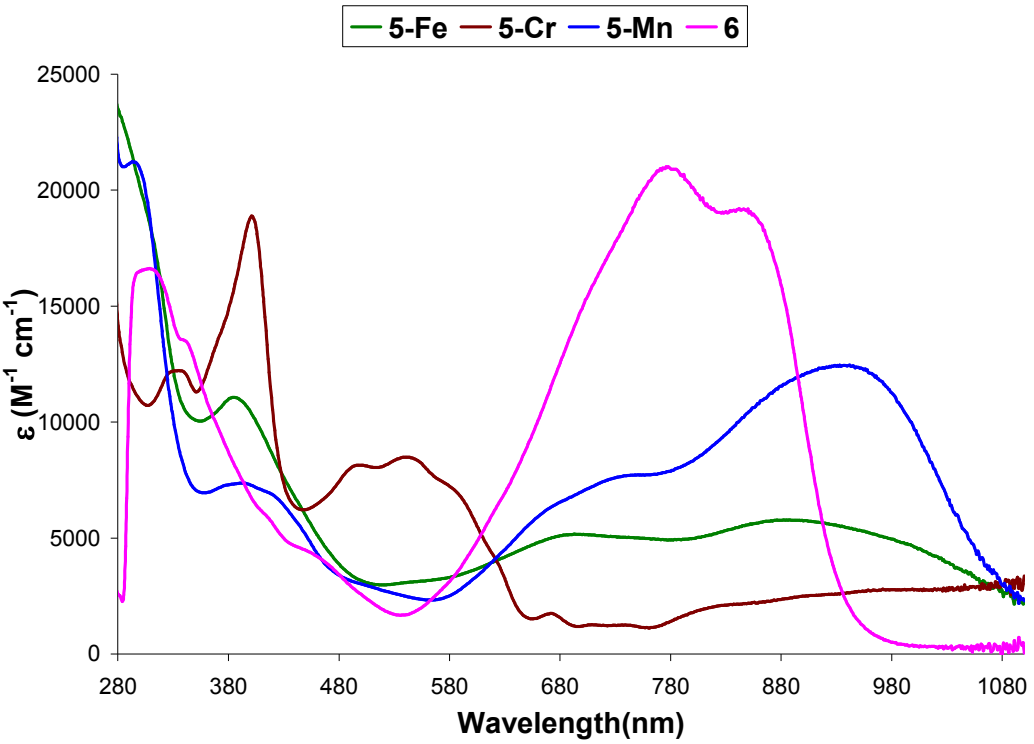

Figure 4.14. UV-VIS spectra of **5-Fe** (green), **5-Cr** (red), **5-Mn** (blue) in C_6H_6. The UV-VIS spectrum of the dianionic lithium salt (**6**, pink) in THF is also shown.

G. Electrochemical studies of 5-Mn and 5-Cr.

Cyclic voltammetry (CV) was used to investigate the accessibility of other redox states in **5-Mn** and **5-Cr**. The CV of **5-Mn** (Figure 4.15) showed 2 reversible one-electron reductions at -1.96 V and -3.00 V vs. Ag/Ag^+ which were assigned as sequential ligand based reductions of the diimine. A reversible reduction was observed at -2.46 V and was assigned to a small amount of impurity in the sample. Cycling to oxidative potentials showed irreversible oxidations at -0.62 V and -0.38 V that led to complex decomposition by ligand loss. Studies on scan rate dependence revealed that at slow scan rates the irreversible oxidations caused an increase in the cathodic feature at -2.50 V which was assigned as an irreversible reduction of free ligand **4**. Concomitant with the increase of the reductive signal at -2.50 V, the intensity of the

reversible reductions of **5-Mn** decreased in agreement with complex decomposition. A summary of the cyclic voltammetry results for **5-Mn** is shown in Figure 4.16.

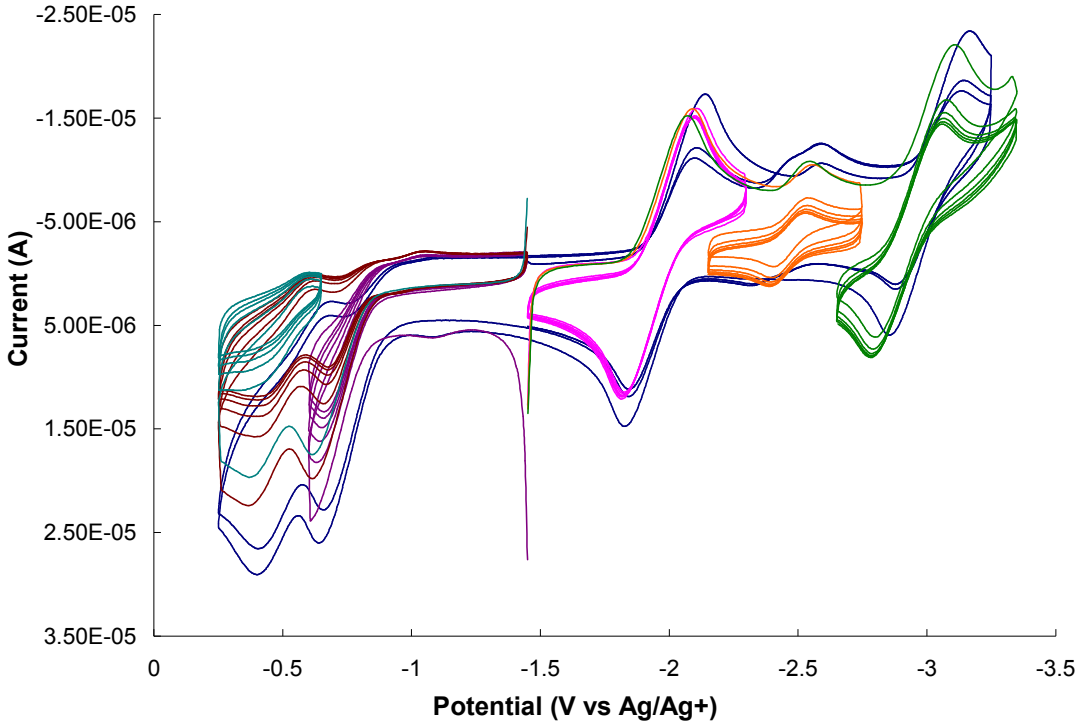

Figure 4.15. CV (200 mV/s) of **5-Mn** (1 mM) in THF with TBAP (0.1 M) as supporting electrolyte, glassy carbon working electrode, Pt wire counter electrode, and Ag wire as pseudoreference electrode.

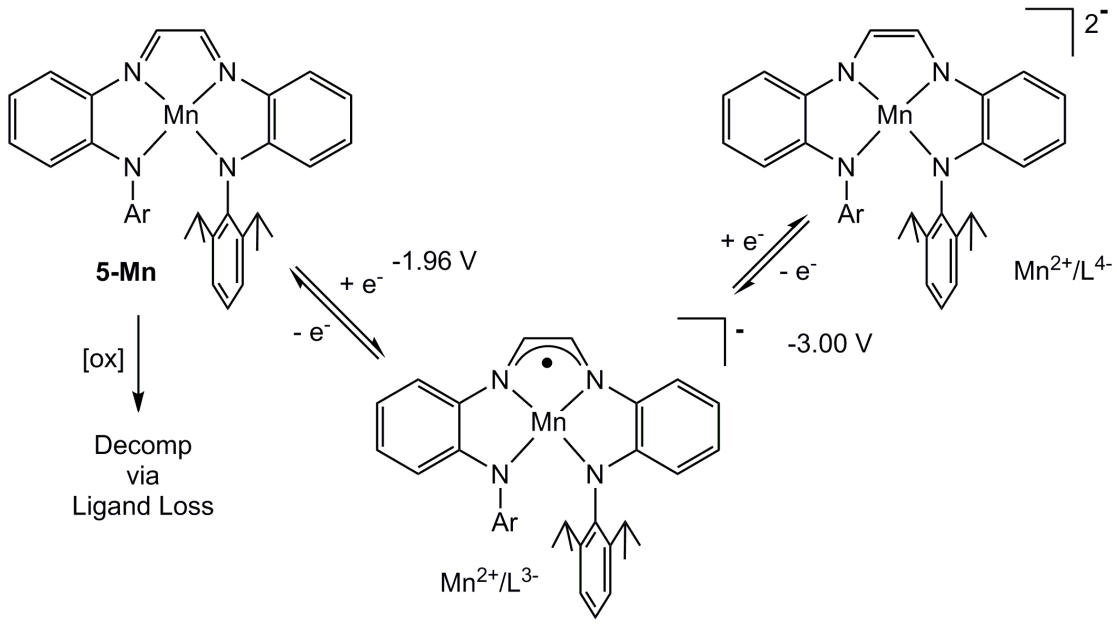

Figure 4.16. Electrochemically generated species formed from reduction of **5-Mn**. Reduction potentials are listed vs. Ag/Ag^{+}.

The cyclic voltammetry of **5-Cr** at a scan rate of 200 mV/s is shown in Figure 4.17. Two reversible reductions were observed (-2.23 V and -2.99 V vs. Ag/Ag^{+}) corresponding to consecutive diimine ligand reductions, while cycling to oxidative potentials afforded three quasi-reversible oxidations at -1.57 V, -1.33 V, and -1.11 V. The cathodic feature at -1.80 V was only observed after scanning to potentials more positive than -1.3 V and a small anodic feature was observed there. The anodic signals at -1.16 V and -0.97 V are coupled to the cathodic features at -1.49 V and -1.25 V, respectively. The first oxidation at -1.57 V was assigned to the $Cr^{2+/3+}$ redox couple and the next two oxidations plausibly arise from ligand based oxidations of the ortho-phenylenediamine. At slower scan rates down to 10 mV/s there was no noticeable change in the CV indicating stability of all the electrochemically generated species.

Figure 4.18 shows the anticipated products derived from the reduction and oxidation of **5-Cr**.

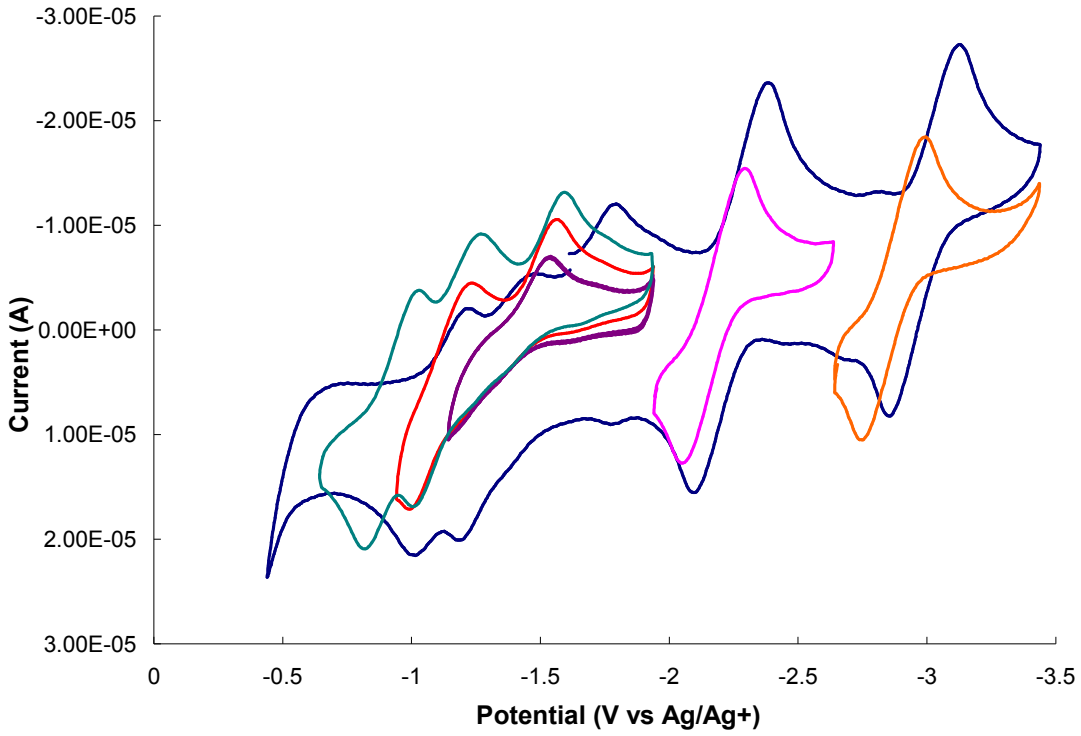

Figure 4.17. CV (200 mV/s) of **5-Cr** (1 mM) in THF with TBAP (0.1 M) as supporting electrolyte, glassy carbon working electrode, Pt wire counter electrode, and Ag wire as pseudoreference electrode.

The $Mn^{2+/0}$ redox couple was not detected for **5-Mn** as only 1-electron ligand based reduction processes were observed. Oxidation of **5-Mn** occurred at the ligand as the $Mn^{3+/2+}$ redox couple is too positive to be detected at these potentials,[19] but the oxidized ligand does not bind strongly enough to prevent dissociation from the labile, high spin, d^5 metal center.[20] The more negative $Cr^{3+/2+}$ redox couple[19] allowed for a metal oxidation of **5-Cr** to be observed and the empty d_{x2-y2} orbital makes the complex less labile so ligand dissociation was not detected even when ligand oxidations were observed.[20]

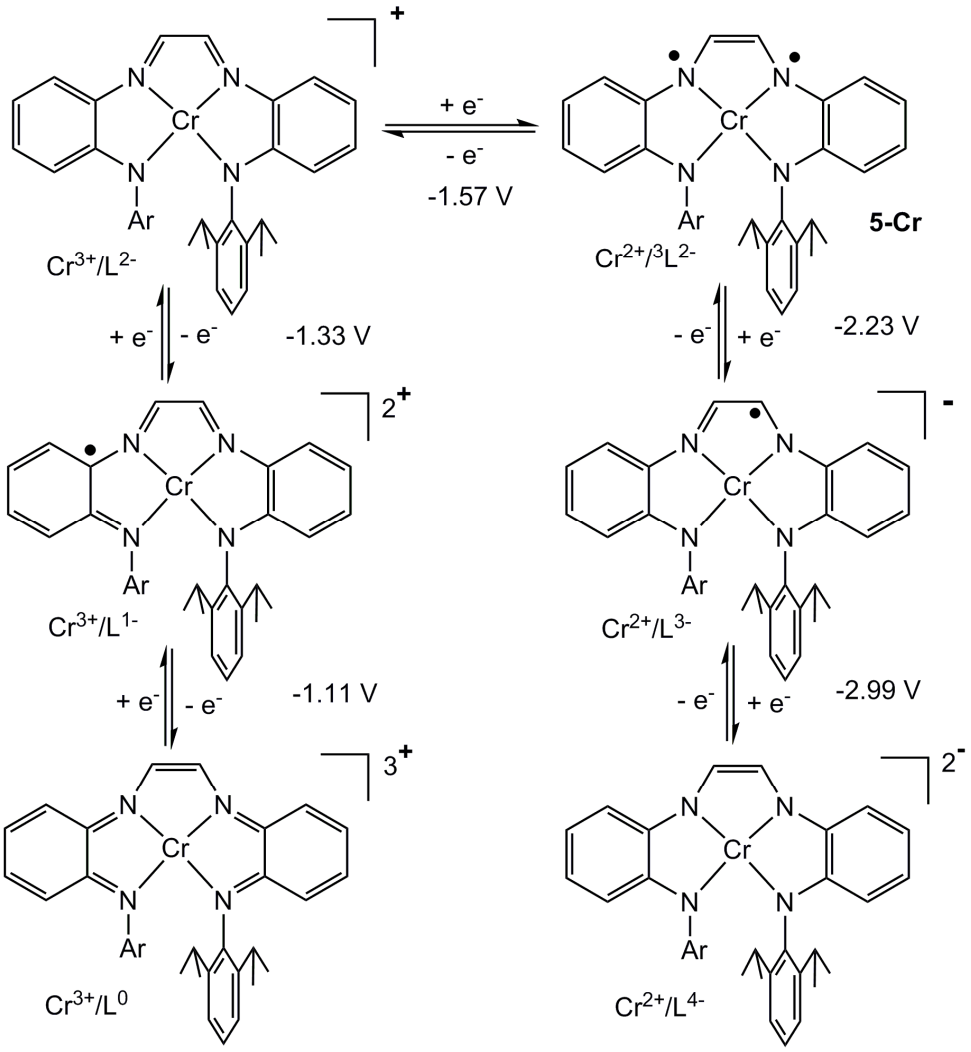

Figure 4.18. Electrochemically produced species derived from **5-Cr**. Redox potentials are listed vs. Ag/Ag^{+}.

H. Reactivity studies of 5-M.

1. Oxidations

Oxidations of **5-M** (M = Fe, Mn) to M(III) halides with sources of halide radical would provide a convenient route towards substitutions on the metal center. Treatment of **5-Fe**, **5-Mn**, and **5-Cr** with chlorine atom sources such as trityl chloride or carbon tetrachloride resulted in color changes to olive green, red, and grey,

respectively. When trityl chloride was used in NMR tube scale reactions, Gomberg's dimer was observed in the ^{1}H NMR spectrum of the reaction mixture. Very broad and paramagnetically shifted resonances prevented identification of any species, but the proposed products (**8-M**) are given in Equation 4.17.

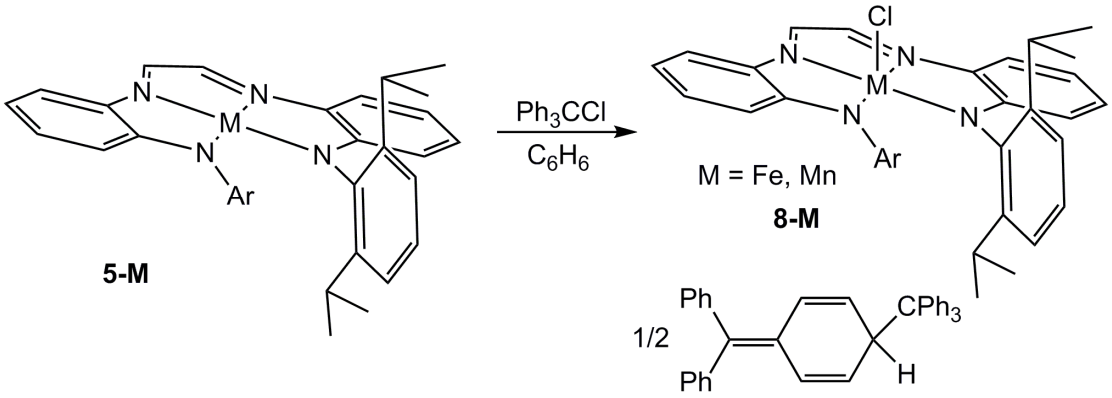

Equation 4.17.

2. O-atom transfer Reactions

Other efforts were directed towards substrates that would form multiple bonds with the metal. Crystal structures of 5-M (M = Cr, Mn) provided evidence for a metal center with enough space to bind incoming substrates despite the bulky 2,6-disubstituted aryl groups. In reactions with pyridine N-oxide, none of the compounds reacted, as no color change was observed even at elevated temperature. Treatment of **5-Fe** with pyridine N-oxide showed a shift in the diagnostic NMR signals of **5-Fe**, indicative of an interaction but no color change was observed suggesting nothing more than a complexation of the pyridine N-oxide. Subsequent heating resulted in color change to a dark grey solution and loss of ^{1}H NMR signals, indicating decomposition. Similar reactivity was explored with **5-Cr** and **5-Mn** with related preliminary results.

Initial calculations were performed to gain insights into the thermodynamics of metal oxo formation from **5-Mn** (Mn^{II}) and **8-Mn** (Mn^{III}) and the results are shown in Figure 4.19. The formation of a square pyramidal Mn^{IV}-oxo (**9-Mn**) by O-atom transfer is calculated to be endergonic by 5.5 kcal/mol and involves a spin state change from the sextet state of **5-Mn** to a quartet for **9-Mn**. Calculationally, the O-atom transfer from pyridine N-oxide to **8-Mn** is uphill by 18.5 kcal/mol, so reactivity with more oxophillic metals such as Cr, V, and Ti is being examined in hopes of more favorable thermodynamics.

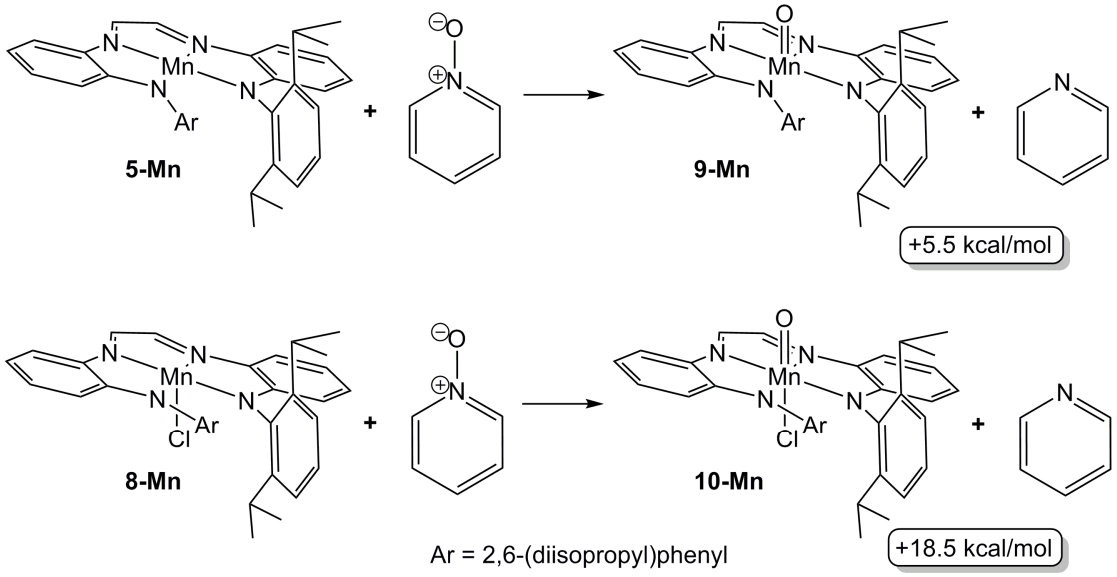

Figure 4.19. ΔG^{o} values for the reaction of pyridine N-oxide with **5-Mn** and **8-Mn**.

3. Reactions with pi-acceptor ligands

Carbonylation of **5-M** (M = Ti, Cr, Mn, Fe) in C_6D_6 showed no indication of reaction in the ^{1}H NMR or infrared spectrum. Addition of excess methyl isocyanide to a NMR tube of **5-Fe** afforded an immediate color change from green to grey before going back to green. The paramagnetically shifted ^{1}H NMR spectrum of **5-Fe** is replaced by a diamagnetic spectrum showing resonances corresponding to multiple

products. The IR spectrum of the crude reaction in C_6D_6 showed two new absorptions at 2150 cm^{-1} and 2094 cm^{-1} which may correspond to a bis-methylisocyanide adduct within the mixture.

III. Conclusions

Metal complexes, **5-M** (M = Ti, Cr, Mn, Fe), were synthesized bearing a new tetradentate redox non-innocent ligand. **5-Cr** showed an interesting electronic structure with bond distances indicative of ligand reduction. Alternatively, calculations support a high spin Cr(II) center antiferromagnetically coupled to an S=1 ligand. Cyclic voltammetry of **5-Mn** and **5-Cr** exhibited 2 ligand centered reductions for both compounds. **5-Mn** was unstable with respect to oxidation as a result of the labile d^5 metal center while **5-Cr** displayed three quasi reversible oxidations, two of which proposed as ligand based oxidations. Crystal structures showed that the apical positions of the four coordinate compounds are accessible to incoming ligands and may allow for group transfer reactivity. Initial reactivity studies showed that oxidations are possible with halide atom sources and O-atom transfer studies have not produced any promising results to date.

IV. Experimental

A. General Considerations

All manipulations were performed using either glovebox or high-vacuum techniques unless otherwise indicated. Hydrocarbon and ethereal solvents were dried over sodium and vacuum transferred from sodium benzophenone ketyl (3-4 mL tetraglyme/L were added to hydrocarbons). Benzene-d_6 was sequentially dried over

sodium and stored over sodium metal. All glassware was oven dried at 165 ^{o}C before use.

$Ti[N(TMS)_2]_2Cl(THF)_2$,[21] $Cr[N(TMS)_2]_2(THF)_2$,[22] $Mn[N(TMS)_2]_2(THF)$,[23] $Fe[N(TMS)_2]_2(THF)$,[24] $Co[N(TMS)_2]_2(THF)$,[25] $Cl_2Ti(TMEDA)_2$,[26] $Cl_2V(TMEDA)_2$,[27] $NiCl_2(DME)$,[28] $Ni[N(SiMe_3)(DIPP)]_2$[29] were prepared by literature procedures. ^{1}H and ^{13}C NMR spectra were obtained on Varian 300 MHz (Mercury), 400 MHz, and 500 MHz (INOVA) spectrometers. ^{1}H NMR and ^{13}C NMR shifts are referenced to benzene-d_6 (^{1}H, δ 7.16 ppm; ^{13}C 128.39 ppm), tetrahydrofuran-d_8 (^{1}H, δ 3.58 ppm; ^{13}C 67.21 ppm), and chloroform-d (^{1}H, δ 7.26 ppm; ^{13}C 77.16 ppm). Cyclic voltammograms were recorded in THF solution ~1 mM concentration using tetrabutylammonium perchlorate (0.1 M) as an electrolyte with a 3 mm glass-carbon working electrode, Pt-wire counter electrode, and Ag wire reference electrode. The cyclic voltammetry experiments were referenced to the ferrocene$^{0/+}$ redox couple at +0.683V.

B. Synthesis

*4-(N-2-(2,6-diisopropylphenylamine)phenylamino)pent-3-en-2-one (**2**).* In air, N-(2-aminophenyl)-2,6-diisopropylaniline (**1**) (700 mg, 2.60 mmol) was added to a solution of acetylacetone (1.04 g, 10.4 mmol) in 25 mL ethanol. A catalytic amount of p-toluenesulfonic acid was added. A dean stark trap filled with sieves was attached and the reaction was heated to reflux for 14 h. After cooling to room temperature the solvent was removed under vacuum. The oil was dissolved in methylene chloride and washed with saturated sodium bicarbonate. The organic layer was dried over Na_2SO_4 and solvent removed under vacuum leaving a red solid (550 mg, 1.57 mmol, 60%). ^{1}H

NMR ($CDCl_3$, 400 MHz, 295 K): δ 11.93 (s, 1H, -N*H*), 7.22 (m, 3H, dipp C-*H*), 7.03 (m, 2H, aryl C-*H*), 6.63 (t, J = 8 Hz, 1H, aryl C-*H*), 6.18 (d, J = 8 Hz, 1H, aryl C-*H*), 5.41 (s, 1H, halfnac C-*H*), 3.05 (sept, J = 7 Hz, 2H, -C*H*-$(CH_3)_2$), 2.12 (s, 3H, -CH_3), 1.92 (s, 3H, -CH_3), 1.15 (d, J = 7 Hz, 6H, -CH-(CH_3)$_2$), 1.10 (d, J = 7Hz, 6H, -CH-(CH_3)$_2$. ^{13}C {^{1}H} NMR ($CDCl_3$): δ 196.81, 163.28, 147.50, 144.54, 134.73, 128.47, 127.64, 123.98, 123.48, 117.29, 112.21, 97.57, 29.35, 28.53, 24.56, 23.20, 19.41.

*4-(N-2-(2,6-diisopropylphenylamine)phenylamino)-2-(N-2-(2,6-diisopropylphenylamine)phenylimino)-3-pentene (**3**).* A solution of triethyloxonium tetrafluoroborate (0.850 g, 4.48 mmol) in 7 mL dry CH_2Cl_2 was added slowly to a solution of **2** (1.57 g, 4.48 mmol) in 16 mL CH_2Cl_2 under argon at -78 ^{o}C. After warming slowly to room temperature the reaction was stirred for 30 min. N-(2-aminophenyl)-2,6-diisopropylaniline (**1**) (1.20 g, 4.48 mmol) was dissolved in 8 mL dry CH_2Cl_2 and added dropwise to the reaction mixture under argon. The reaction was heated to reflux overnight. Upon cooling, KOH (250 mg, 4.48 mmol) in 20 mL water was added and stirred vigorously for 15 min. The organic layer was separated and the aqueous layer was extracted with methylene chloride. The combined organic layers were dried over Na_2SO_4 and solvent removed under vacuum to give a thick red oil. The product was characterized by ^{1}H NMR spectroscopy and not isolated. ^{1}H NMR ($CDCl_3$, 400 MHz, 295 K): δ 7.19 (m, 6H, dipp C-*H*), 6.84 (m, 4H, aryl C-*H*), 6.63 (t, J = 8 Hz, 2H, aryl C-*H*), 6.15 (d, J = 8 Hz, 2H, aryl C-*H*), 5.49 (s, 2H, -N*H*), 5.06 (s, 1H, halfnac C-*H*), 3.08 (sept, J = 7 Hz, 4H, -C*H*-$(CH_3)_2$), 2.02 (s, 6H, -CH_3), 1.92 (s, 3H, -CH_3), 1.06 (m, 24H, -CH-(CH_3)$_2$).

*N,N'-Di-2-(2,6-diisopropylphenyhlamine)-phenylglyoxaldiimine (**4**)*. N-(2-aminophenyl)-2,6-diisopropylaniline (**1**) (4.7 g, 18 mmol) was dissolved in 60 mL MeOH. A 40 wt% glyoxal solution (1.3 g, 8.8 mmol) was dissolved in 2 mL MeOH and added dropwise. The solution turned orange and was stirred 12h after which an orange solid precipitated. The bright orange solid was collected by filtration and washed with cold MeOH (1.2 g, 2.2 mmol, 24%). ^{1}H NMR ($CDCl_3$, 400 MHz, 295 K): δ 8.65 (s, 2H, imine C-*H*), 7.31 (m, 6H, dipp C-*H*), 7.03 (m, 2H, arylC-*H*), 6.68 (m, 4H, aryl C-*H*), 6.21 (d, J = 8 Hz, 2H, arylC-*H*), 3.24 (sept, J = 7 Hz, 4H, -C*H*-$(CH_3)_2$), 1.17 (m, 24H, -CH_3). ^{13}C NMR ($CDCl_3$, 125 MHz, 295 K): δ 156.07, 148.07, 145.08, 135.43, 133.90, 130.04, 127.57, 123.97, 116.98, 116.44, 112.30, 28.50, 24.86, 23.31. ^{1}H NMR (C_6D_6, 400 MHz, 295 K): δ 8.48 (s, 2H, imine C-*H*), 7.31 (m, 6H, dipp C-*H*), 7.05 (s, 2H, -N*H*-), 6.92 (m, 4H, aryl C-*H*), 6.54 (t, J=8 Hz, 2H, aryl C-*H*), 6.37 (d, J = 8 Hz, ary lC-*H*), 3.46 (sept, J = 7 Hz, 4H, -C*H*-$(CH_3)_2$), 1.19 (d, J = 7 Hz, 12H, -CH_3), 1.14 (d, J=7 Hz, 12H, -CH_3). Anal. for $C_{38}H_{46}N_4$ (calc), C 81.68, H 8.30, N 10.03; (found) C 82.37, H 8.33, N 9.58.

*Iron N,N'-Di-2-(2,6-diisopropylphenyhlamide)-phenylglyoxaldiimine (**5-Fe**)*. To a 25 mL round bottom flask containing $Fe[N(TMS)_2]_2(THF)$ (116 mg, 0.259 mmol) and **4** (145 mg, 0.259 mmol) was added 12 mL freshly distilled C_6H_6. The reaction was warmed to room temperature and the dark olive green solution was stirred for 2 d. After this time all volatiles were removed under vacuum and the green solid was triturated 2x with additional benzene. Diethyl ether was added and the reaction was filtered and the filter cake was washed until the filtrate was colorless. The ether was removed and 10 mL pentane added. After cooling to -78 ^{o}C a dark green

solid (120 mg, 75%) was collected by filtration. A single crystal suitable for X-Ray diffraction was obtained by slow evaporation of a concentrated pentane solution. ^{1}H NMR (C_6D_6, 400 MHz, 295 K): δ 72.59 ($\nu_{1/2}$ = 186 Hz, 2H), 54.93 ($\nu_{1/2}$ = 284 Hz, 2H), 32.95 ($\nu_{1/2}$ = 160 Hz, 4H), 18.50 ($\nu_{1/2}$ = 660 Hz, 2H), 13.80 ($\nu_{1/2}$ = 200 Hz, 12H), 8.26 ($\nu_{1/2}$ = 290 Hz, 4H), -10.94 ($\nu_{1/2}$ = 134 Hz, 2H), -23.31 ($\nu_{1/2}$ = 1040 Hz, 12H), -33.32 ($\nu_{1/2}$ = 104 Hz, 2H). μ_{eff} (Evans, C_6D_6): 4.7 μ_B. Anal. for $C_{38}H_{44}N_4$ (calc), C 74.50, H 7.24, N 9.15; (found) C 66.52, H 7.03, N 7.04.

*Chromium N,N'-Di-2-(2,6-diisopropylphenyhlamide)-phenylglyoxaldiimine (**5-Cr**)***:** A 50 mL flask is charged with $Cr[N(TMS)_2]_2(THF)_2$ (400 mg, 0.774 mmol) and tetradentate ligand **4** (432 mg, 0.774 mmol), and 25 mL freshly distilled benzene was added. Upon warming to room temperate the solution becomes deep purple. After stirring overnight volatiles are removed under vacuum and the maroon solid was triturated with C_6H_6, filtered and washed until washes were colorless. Solvent was removed under vacuum, pentane added, cooled to -78 ^oC and filtered. A maroon solid (360 mg, 76%) was collected on the frit. A single crystal suitable for X-Ray diffraction was acquired by slow diffusion of pentane into a concentrated THF solution. ^{1}H NMR (C_6D_6, 400 MHz, 295 K): δ 77.97 ($\nu_{1/2}$ = 2600 Hz, 2H), 71.47 ($\nu_{1/2}$ = 1800 Hz, 2H), 20.92 ($\nu_{1/2}$ = 190 Hz, 2H), 18.07 ($\nu_{1/2}$ = 570 Hz, 2H), 6.78 ($\nu_{1/2}$ = 580 Hz, 2H), 4.71 ($\nu_{1/2}$ = 70 Hz, 2H), 4.20 ($\nu_{1/2}$ = 250 Hz, 12H), 2.85 ($\nu_{1/2}$ = 120 Hz, 6H), 1.78 ($\nu_{1/2}$ = 720 Hz, 10H), -1.38 ($\nu_{1/2}$ = 880 Hz, 2H). μ_{eff} (Evans, C_6D_6): 2.7 μ_B. Anal. for $C_{42}H_{52}CrN_4O$ (calc), C 74.09, H 7.70, N 8.23; (found) C 74.52, H 7.95, N 8.14.

*Manganese N,N'-Di-2-(2,6-diisopropylphenyhlamide)-phenylglyoxaldiimine (**5-Mn**)*. To a flask containing $Mn[N(TMS)_2]_2(THF)$ (104 mg, 0.232) and tetradentate ligand **4** (130 mg, 0.232 mmol) was added 20 mL benzene at -78 ^oC. The solution was warmed to room temperature and the dark green solution was stirred 12 h. Solvent was removed under vacuum and triturated with fresh benzene. Diethyl ether was added and the solution was filtered and any solids were washed until colorless. Diethyl ether was removed under vacuum and 10 mL fresh pentane added, cooled to -78 ^oC and filtered to give a dark green solid (85 mg, 60%). A single crystal suitable for X-Ray diffraction was obtained by slow diffusion of pentane into a concentrated diethyl ether solution. ^1H NMR (C_6D_6, 400 MHz, 295 K): δ 20.25 ($\nu_{1/2}$ = 600 Hz, 4H), 16.59 ($\nu_{1/2}$ = 600 Hz, 2H), 10.73 ($\nu_{1/2}$ = 2000 Hz, 36H), -17.82 ($\nu_{1/2}$ = 1600 Hz, 2H). μ_{eff} (Evans, C_6D_6): 5.4 μ_B. Anal. for $C_{42}H_{52}MnN_4O$ (calc), C 73.77, H 7.66, N 8.19; (found) C 72.48, H 7.65, N 7.85.

*Titanium N,N'-Di-2-(2,6-diisopropylphenyhlamide)-phenylglyoxaldiimine (**5-Ti**).* To a solution of tetradentate ligand **4** (300 mg, 0.54 mmol) in THF was added LiHMDS (180 mg, 1.1 mmol) at room temperature. The resulting dark green solution was stirred for 30 min at which time $TiCl_2(TMEDA)_2$ (189 mg, 0.54 mmol) was added. The green solution was stirred 10 h before solvent removed under vacuum. The dark green solid was triturated twice with fresh benzene. The ^1H NMR spectrum of the solid shows ~90% conversion to one diamagnetic product. ^1H NMR (C_6D_6, 400 MHz, 295 K): δ 7.16 (m, 6H, dippC-*H*), 6.76 (t, J=7 Hz, ArC-*H*), 6.70 (s, 2H, imineC-*H*), 6.63 (t, d=8Hz, 2H, ArC-*H*), 6.44 (d, J=8 Hz, ArC-*H*), 5.78 (d, J=8 Hz, 2H, ArC-*H*), 3.44 (sept, J=7 Hz, 2H, -C*H*-$(CH_3)_2$), 3.09 (sept, J=7 Hz, -C*H*-$(CH_3)_2$), 1.19 (d, J=7

Hz, 6H, -CH_3), 1.08 (d, J=7 Hz, 6H, -CH_3), 0.98 (d, J=7 Hz, 6H, -CH_3), 0.94 (d, J=7 Hz, 6H, -CH_3).

Chloro bis-(bis-trimethylsilylamide) titanium N,N'-Di-2-(2,6-diisopropylphenyhlamine)-phenylglyoxaldiimine (7). A J. Young NMR tube was charged with Ti[N(TMS)$_2$]$_2$Cl(THF) (30 mg, 0.062 mmol) and **4** (18 mg, 0.031 mmol). Benzene-d$_6$ (0.5 mL) was added and the solution instantly became dark orange. Within 15 minutes ^{1}H NMR confirmed formation of a new symmetric diamagnetic product in >90% purity. ^{1}H NMR (C_6D_6, 400 MHz, 295 K): δ 7.60 (m, 2H), 7.15 (m, 2H), 7.05 (m, 4H), 6.77 (m, 4H), 6.55 (s, 2H), 6.23 (m, 2H), 5.25 (s, 2H) 3.23 (sept, J = 7 Hz, 4H), 1.03 (d, J = 7 Hz, 12H), 0.88 (d, J = 7 Hz, 12H), 0.45 (s, 27H), 0.42 (s, 45H). ^{13}C NMR (C_6D_6, 125 MHz, 295 K): δ 147.48, 140.82, 139.72, 135.71, 127.37, 127.15, 124.32, 117.75, 113.62, 109.45, 28.57, 25.84, 24.19, 23.73, 6.66, 5.15.

C. Single Crystal X-Ray Diffraction Studies.

Upon isolation, the crystals were covered in polyisobutenes and placed under a 173 K N_2 stream on the goniometer head of a Siemens P4 SMART CCD area detector (graphite-monochromated MoK$_\alpha$ radiation, λ = 0.71073 Å). The structures were solved by direct methods (SHELXS). All non-hydrogen atoms were refined anisotropically unless stated, and hydrogen atoms were treated as idealized contributions (Riding model). Any deviation from this protocol will be noted for the individual descriptions below.

1. *5-Fe.* A green block (0.40 x 0.35 x 0.25 mm^3) of **5-Fe** was obtained from slow evaporation of a concentrated pentane solution. A total of 32629 reflections were

collected with 8690 determined to be symmetry independent (R_{int} = 0.0383). SQEEZE was applied to one disordered pentane solvent molecule.

2. *5-Mn*. A green block (0.20 x 0.15 x 0.10 mm^3) of **5-Mn** was obtained from slow evaporation of a concentrated diethyl ether solution. A total of 32418 reflections were collected with 16405 determined to be symmetry independent (R_{int} = 0.0383).

3. *5-Cr*. A dark red block (0.35 x 0.20 x 0.10 mm^3) of **5-Cr** was obtained from slow diffusion of pentane into a concentrated THF solution. A total of 71009 reflections were collected with 18259 determined to be symmetry independent (R_{int} = 0.0472).

REFERENCES

(1) Jacobsen, E. N.; Zhang, W.; Muci, A. R.; Ecker, J. R.; Deng, L. *J. Am. Chem. Soc.* **1991**, *113*, 7063–7064.

(2) Palucki, M.; Pospisil, P. J.; Zhang, W.; Jacobsen, E. N. *J. Am. Chem. Soc.* **1994**, *116*, 9333–9334.

(3) Yoon, T. P.; Jacobsen, E. N. *Science* **2003**, *299*, 1691–1693.

(4) Jacobsen, E. N.; Deng, L.; Furukawa, Y.; Martínez, L. E. *Tetrahedron* **1994**, *50*, 4323–4334.

(5) Lai, T.-S.; Che, C.-M.; Kwong, H.-L.; Peng, S.-M. *Chem. Commun.* **1997**, 2373–2374.

(6) Groves, J. T.; Nemo, T. E. *J. Am. Chem. Soc.* **1983**, *105*, 5786–5791.

(7) Groves, J. T.; Takahashi, T. *J. Am. Chem. Soc.* **1983**, *105*, 2073–2074.

(8) Groves, J. T.; Nemo, T. E.; Myers, R. S. *J. Am. Chem. Soc.* **1979**, *101*, 1032–1033.

(9) Chanda, A.; Shan, X.; Chakrabarti, M.; Ellis, W. C.; Popescu, D. L.; Tiago de Oliveira, F.; Wang, D.; Que, L.; Collins, T. J.; Münck, E.; Bominaar, E. L. *Inorg. Chem.* **2008**, *47*, 3669–3678.

(10) Kundu, S.; Thompson, J. V. K.; Ryabov, A. D.; Collins, T. J. *J. Am. Chem. Soc.* **2011**, *133*, 18546–18549.

(11) Ghosh, M.; Singh, K. K.; Panda, C.; Weitz, A.; Hendrich, M. P.; Collins, T. J.; Dhar, B. B.; Sen Gupta, S. *J. Am. Chem. Soc.* **2014**.

(12) Bain, G. A.; Berry, J. F. *J. Chem. Educ.* **2008**, *85*, 532.

(13) Perumareddi, J. R. *J. Phys. Chem.* **1967**, *71*, 3155–3165.

(14) Ghosh, M.; Sproules, S.; Weyhermüller, T.; Wieghardt, K. *Inorg. Chem.* **2008**, *47*, 5963–5970.

(15) Muresan, N.; Weyhermüller, T.; Wieghardt, K. *Dalton Trans.* **2007**, 4390–4398.

(16) Gardiner, M. G.; Hanson, G. R.; Henderson, M. J.; Lee, F. C.; Raston, C. L. *Inorg. Chem.* **1994**, *33*, 2456–2461.

(17) Rijnberg, E.; Richter, B.; Thiele, K.-H.; Boersma, J.; Veldman, N.; Spek, A. L.; van Koten, G. *Inorg. Chem.* **1998**, *37*, 56–63.

(18) Condon, E. *Phys. Rev.* **1926**, *28*, 1182–1201.

(19) Allen J. Bard; Faulkner, L., R. *Electrochemical Methods: Fundamentals and Applications*; Second.; John Wiley & Sons, Inc.: University of Texas at Austin, 2001.

(20) Taube, H. *Chem. Rev.* **1952**, *50*, 69–126.

(21) Scoles, L.; Gambarotta, S. *Inorganica Chim. Acta* **1995**, *235*, 375–380.

(22) Horvath, B.; Strutz, J.; Horvath, E. G. *Z. Für Anorg. Allg. Chem.* **1979**, *457*, 38–50.

(23) Horvath, B.; Moeseler, R.; Horvath, E. G. *Z. F□r Anorg. Allg. Chem.* **1979**, *450*, 165–177.

(24) Olmstead, M. M.; Power, P. P.; Shoner, S. C. *Inorg. Chem.* **1991**, *30*, 2547–2551.

(25) Bryan, A. M.; Long, G. J.; Grandjean, F.; Power, P. P. *Inorg. Chem.* **2013**, *52*, 12152–12160.

(26) Edema, J. J. H.; Duchateau, R.; Gambarotta, S.; Hynes, R.; Gabe, E. *Inorg. Chem.* **1991**, *30*, 154–156.

(27) Edema, J. J. H.; Stauthamer, W.; Van Bolhuis, F.; Gambarotta, S.; Smeets, W. J. J.; Spek, A. L. *Inorg. Chem.* **1990**, *29*, 1302–1306.

(28) Ward, L. G. L.; Pipal, J. R. In *Inorganic Syntheses*; Cotton, F. A., Ed.; John Wiley & Sons, Inc.: Hoboken, NJ, USA, 1972; Vol. 13, pp. 154–164.

(29) Lipschutz, M. I.; Tilley, T. D. *Chem. Commun.* **2012**, *48*, 7146–7148.